Using atmospheric pressure tendency to optimise battery charging in off-grid hybrid wind-diesel systems for telecoms

Shane Phelan

B.Eng in Electronic Engineering, M.Eng Telecommunications Engineering

A Dissertation submitted in fulfilment of the
requirements for the award of Doctor of Philosophy

to

Dublin City University

School of Electronic Engineering

Supervisors: Dr. Stephen Daniels, Dr. Conor McAardle

January 19, 2014

Declaration

I hereby certify that this material, which I now submit for assessment on the programme of study leading to the award of PhD is entirely my own work, that I have exercised reasonable care to ensure that the work is original, and does not to the best of my knowledge breach any law of copyright, and has not been taken from the work of others save and to the extent that such work has been cited and acknowledged within the text of my work.

Signed: .....

Student ID: 52080621

Date: January 19, 2014

Contents

Abstract

Off grid telecom base stations in developing nations are powered by diesel generators. They are typically oversized and run at a fraction of their rated load for most of their lifetime. Operating these generators at partial load is inefficient and over time physically damages the engine. A hybrid configuration, which is the combination of multiple energy sources, uses a battery bank which powers the telecoms load for a portion of the time. The generator only operates when the battery bank needs to be charged. Adding a wind turbine further reduces the generator run hours and saves fuel. The generator is oblivious to the current wind conditions which lead to simultaneous generator-wind power production. As the batteries become charged by the generator, the wind turbine controller is forced to dump surplus power as heat through a resistive load.

This dissertation details how the relationship between barometric pressure and wind speed can be used to add an additional layer of sophistication to the battery charger. A numerical model of the system is developed to test the different battery charging configurations. This work demonstrates that if the battery charger is aware of upcoming wind conditions it will provide modest fuel savings and reduce generator run hours in small scale hybrid energy systems. The contribution from this work provides insight into the power being wasted in small scale hybrid systems with storage and how they can operate more efficiently when the charging mechanism is aware of upcoming wind conditions. The system will operate more efficiency if the diesel generator is disengaged during periods of moderate to high wind power production. The methodology proposed in this dissertation ensures that this is the case, especially during periods of high wind power production.

Acknowledgements

I would like to thank all those who I worked with from the Energy and Design lab, in particular my supervisor Dr. Stephen Daniels, co-supervisor Dr. Conor McArdle, Paula Meehan who spent many an hour proofreading my work and Jie Yang who helped me develop several monitoring systems.

Also, I would like to thank my girlfriend Sharon McEneaney for her support and patience though out the duration of this work and beyond. A big thank you to my parents Sean and Geraldine who without their support I would never have made it this far.

I would like to thank Cinergy for providing access to their hybrid energy systems and telecommunications sites which provided much of the data for this study. I would like to thank all the Cinergy team, Andrew Griffin, Kealan Delaney, Mark Perrem, Fergal Mcloughlin and Anthony Donoghue who were all extremely generous with their time, help and suggestions. The author is also thankful for the financial support from both Cinergy and the Irish Research Council for Science, Engineering and Technology (IRCSET) for jointly funding this research.

List of Figures

List of Tables

List of Notations

I_2C Inter-Integrated Circuit

Ah Amp Hours

ANN Artificial Neural Network

BTS Base Transceiver Station

COE Cost of Electricity

CT Current Transformer

DAQ Data Acquisition

GSMA Global System for Mobile Communications Association

HOMER Hybrid Optimization Model for Electric Renewables

HSRES Hybrid System with Renewable Energy Sources

kVA Kilo Volt-Ampere

kW Kilo Watt

kWp Kilo-Watt Peak

LAN Local Area Network

MPPT Maximum Power Point Tracking

NWP Numeric Weather Predictors

OECD Organisation for Economic Co-operation and Development

OPEX Operational Expenditure

PEM Proton Exchange Membrane

PVGIS Photovoltaic Geographical Information System

RPM Revolutions per Minute

SLI Starting Lighting Ignition

UPS Uninterruptible Power Supply

VPL Visual Programming Language

VPN Virtual Private Network

VRLA Valve Regulated Lead Acid

List of peer reviewed publications

- Shane Phelan, Paula Meehan, and Stephen Daniels. Using Atmospheric Pressure Tendency to Optimise Battery Charging in Off-Grid Hybrid Wind-Diesel Systems for Telecoms. *Energies*, 3052–3071, 2013, doi:10.3390/en6063052.
- S Phelan, P Meehan, S Krishnamurthy, and S Daniels. Smart energy management for off-grid hybrid sites in telecoms. In *Symposium on ICT and Energy Efficiency and Workshop on Information Theory and Security (CIICT 2012)*, pages 15–21, Stevenage, UK, July 2012, doi:10.1049/cp.2012.1855. Institution of Engineering and Technology.
- J. Yang, S. Phelan, P. Meehan, and S. Daniels. A distributed real time sensor network for enhancing energy efficiency through ICT. In *Symposium on ICT and Energy Efficiency and Workshop on Information Theory and Security (CIICT 2012)*, pages 8–14, Stevenage, UK, July 2012, doi:10.1049/cp.2012.1854. Institution of Engineering and Technology.
- P. Meehan and S. Phelan. Temporal and frequency analysis of power signatures for common household appliances. In *Symposium on ICT and Energy Efficiency and Workshop on Information Theory and Security (CIICT 2012)CT*, pages 22–27, Dublin, July 2012, doi:10.1049/cp.2012.1856. Institution of Engineering and Technology.

List of contributions

- Shane Phelan and Stephen Daniels. Monitoring and Control of Remote Hybrid Energy Installations. In *Presentation of work at Rince Research Day*, 2013.
- Shane Phelan and Stephen Daniels. Smart Energy Management for Off-Grid Hybrid Sites in Telecoms. In *Poster presented at Symposium on ICT and Energy Efficiency and Workshop on Information Theory and Security (CIICT 2012)*, 2012.
- Shane Phelan and Stephen Daniels. Changes in Energy and how we and Systems React. In *Presentation of work at Rince Research Day*, 2012.
- Shane Phelan and Stephen Daniels. Renewable Energy Monitoring & Control. In *Poster presentation at Faculty Research Day*, 2011.
- Shane Phelan and Stephen Daniels. Remote Renewable Energy Monitoring and Control. In *Poster presentation of work at Cinergy Meetings, headquarters and events*, 2011.
- Shane Phelan. Energy & Design Lab. *Science Spin*, pages 32–33, November 2010.

Chapter 1

Introduction

1.1 Introduction

There are over 600,000 off-grid telecoms base stations distributed throughout the world [5] with 118,000 in India alone [13]. Each base station houses at least one set of base transceiver station (BTS) equipment which contains the power systems, cooling, radio frequency (RF) conversion and signal processing equipment required to communicate with mobile phones. This equipment can consume up to five kW of power depending on the location and importance of the site in the network [4]. Virtually all of these base stations are being powered by a pair of AC diesel generators running alternately at partial load 24 hours a day. Partial load operation is a consequence of over-dimensioning of diesel generators which is a persistent problem for powering telecom sites. This occurs where generators are sized to cope with the peak power of a site which will generally occur a small number of times in a given year [14]. The remainder of the time the generator will run at partial load, which is highly inefficient [15] as the generator is optimised to run at its rated load. The fuel consumption of these sites costs mobile phone operators hundreds of millions of dollars every year [5] and with the number of sites continuously increasing and the price of diesel on an upward trend, these costs will only increase. A hybrid energy system (HES) can be seen as one type of configuration which provides a fuel saving alternative to a diesel generator running continuously.

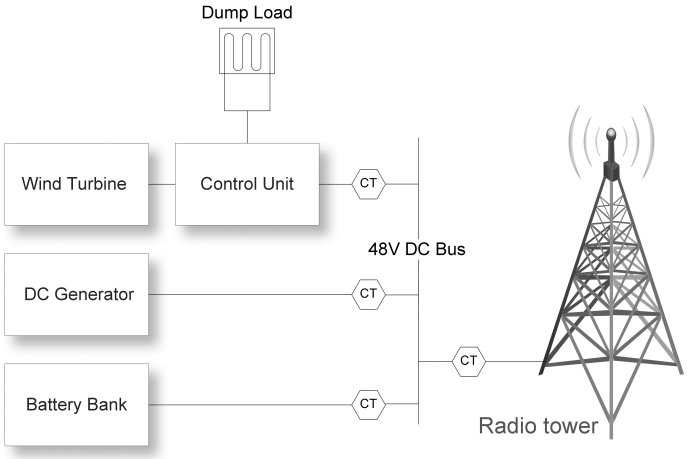

Figure 1.1: Off grid HSRES with current transducer (CT) measurement points

In this context, a HES can be described as an un-interruptible power supply (UPS) with two or more sources of power as demonstrated in Figure 1.1. In its simplest form, a diesel generator, a battery bank and the load are connected together in parallel. The diesel generator only operates when the batteries need to be charged, reducing the number of hours the generator is running. This process saves fuel as the generator is more heavily loaded [16] when charging the batteries and providing power to the load, therefore increasing the efficiency. Generators are most efficient at their rated load and this efficiency decreases linearly as the load decreases. This is in contrast to the traditional case [5] where the generator is powering the load only. The fuel consumption of a hybrid system in its 'simple form' can be reduced further [17, 18, 19] with the addition of a wind turbine or solar photovoltaic (PV) panels. It has been suggested [20] that defining this type of configuration as a hybrid system with renewable energy sources (HSRES) is more appropriate for this type of application. Depending on the location, the use of PV or wind must be selected and sized [21, 22, 23] correctly to account for seasonal lulls [24] in power production.

Designing a hybrid PV-diesel can be approached from several perspectives in terms of peak power, panel area, cell efficiency and the number of days of energy storage which the system can provide without sunlight. Often a compromise in features is the most financially attractive option with, a portion of the power being supplied by PV and a backup time ranging from a few

hours to as much as a day [20] or more [25]. The use of a diesel generator in conjunction with a PV array can be used to reduce the upfront costs while taking care to choose the optimal tilt angle for the installation [26]. The diesel generator is also useful for supplementing the lower power contributions from the panels as a result of seasonal variations in the climate [27]. Wind turbines are also prone to seasonal change but to a lesser extent than solar based systems.

Hybrid wind-diesel systems come in several forms which vary as a result of the type of load or weather patterns imposed on the equipment. Larger deployments are often based on synchronous hybrid configurations with an AC bus but without a battery bank [28]. These applications tend to provide power to remote villages [29] or islands [30] which have no access to the grid. With synchronous systems the battery bank is not there to act as a 'buffer' to smooth out variations in the load and wind. As a result there are significant gains to be made from control system optimisations [31] which anticipate [32] variations in both the wind supply and the load. The complementary nature [27] of wind and solar has encouraged the addition of solar PV as a supplemental power source for many systems [17, 20, 18, 19]. The use of hydrogen as a supplemental [33] and eventually primary [34] power source for HSRES applications has seen a surge in research activity [35, 36, 37]. A physical hybrid wind-diesel test platform [38] was used to gather system performance data on a telecoms base station in Ireland. Throughout the testing period data was acquired describing current flows, fuel usage, temperatures, voltages, power dumped and cumulative power for all of the components in the structure. These measurements allowed a clear picture of the internal operation of the HSRES to be established. This data formed the basis of a hybrid system model used to simulate the operation of the equipment. This rich source of data added a large level of sophistication to the model which is not available in conventional models described in literature.

Figure 1.2 demonstrates the efficiency of the generated power and the distribution of its consumption in a wind-diesel system. This information is based on information available in the literature and these parameters were observed to be optimistic based on analysing the performance of the hybrid system.

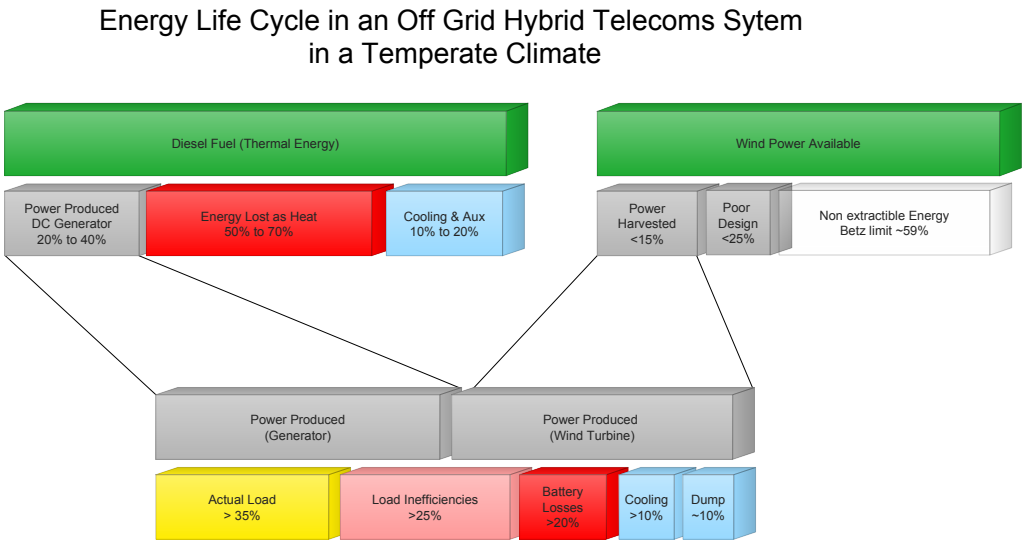

Figure 1.2: Overview of power wasted in a Hybrid Energy System from experience of working with these systems

Diesel generator efficiency plateaus at approximately 43% [15, P.34] but this is for utility scale machines, smaller generators tend to have a lower efficiency [39]. The low efficiency in combustion machines is as a result of the heat lost by the engine, vibrations, noise and the power required by the cooling equipment to remove the heat. The areas of engine and wind turbine efficiency are well understood and there are not any prospects for improving these parameters within the scope of this work. Looking at how the power is used after it has been generated by either the generator or wind turbine, there is scope for improvements in this instance. A large level of power is wasted in the telecommunications equipment which process the telephony information and this aspect is under extensive research [39, 13, 5, 4, 40]. Lead acid battery efficiency is now as high as 90% [41] but it is generally not commercially viable in this application to purchase battery banks of this quality. An efficiency of approximately 80% is more common for battery banks used in telecoms applications [42, 43]. The power consumed by forced air cooling in a warm climate is generally approximately ten percent [44] of the total power consumption. The use of refrigerant based air conditioning has a power consumption that is significantly higher [5]. Telecoms companies have expressed concern [45] with base transceiver station (BTS) equipment being exposed to higher ambient

temperatures and as a result new equipment has been designed [46] to tolerate a broader temperature range. This will facilitate the broader adoption of forced air cooling which cannot cool as effectively as air conditioning. Given this trend and taking into account the load limitations of the HSRES, the ten percent cooling load was chosen. The rest of the power is lost by the wind turbine dumping power when there is insufficient capacity in the battery bank to store the power supplied to it.

The research proposal is to improve the system efficiency by attempting to predict when the wind turbine will provide power to the system. This information would allow the generator controller to ensure that the battery bank has sufficient capacity to store the power. Any excess power which cannot be stored is dissipated as heat by the wind controller and this has been shown to account for up to eight percent of the energy produced by the wind turbine. Wind prediction is extremely important for the commercial wind power industry in terms of unit commitment and unit dispatch [47]. Unit commitment is difficult for wind energy as the electricity markets require energy producers to detail how much energy they plan to produce on a given day. This request is usually at least one or two days before the unit is actually dispatched [48] which is where the next problem lies. Wind energy is regarded as being "non-dispatchable" due to its varying nature and its inability to ramp up production if needed. Wind power can be curtailed if absolutely necessary to preserve the stability of the grid but this activity is not ideal for the wind farm operators who are trying to maximise the return for its investors. To ensure that the unit commitment is accurate, wind farm operators have a variety of meteorological tools available to them to predict wind speed and power with a good level of accuracy for periods up to five days. These prediction techniques are discussed in detail in Chapter four.

HSRES installations are less sensitive to fluctuations in wind power output as they are not connected to the grid and have a battery bank to balance out the power variations. When low levels of wind power are being produced the diesel generator will make up for the shortfall in the wind power in the same way as thermal generation makes up for shortfalls in large scale grid systems. When excess wind power is being produced, as is the case when the battery

bank is fully charged, small wind turbines will dump or divert power through resistive loads. This work uses an accessible wind prediction methodology to anticipate periods of potentially high wind speed to reduce the occurrences where wind power is being diverted and wasted. The method, described in detail in Chapter four, uses the relationship between barometric pressure and wind speed to predict the magnitude of the wind power approximately six hours in advance. This allows the system controller to alter the battery charging regime to ensure there is enough capacity in the battery bank to store the additional power produced by the wind turbine. Depending on the system configuration, controller modifications and knowledge of upcoming wind conditions, it is possible to reduce the amount of power wasted by the wind turbine.

Field testing HSRES installations is expensive in terms of fuel and physical equipment costs. Prior to field testing it is useful to create a software model to establish the viability of different controller and equipment configurations. A numerical software model was constructed as part of this work using a Simulink®-based platform which simulated each component in the system. The construction of this model along with the algorithms describing the performance of each component is discussed in detail in Chapter five. The model uses barometric pressure data as an input and uses the prediction methodology in Chapter four to anticipate the upcoming wind power from the turbine.

1.2 Research Objectives

Research Goals

- Become familiar with the state of the art of hybrid energy systems
- Identify information to be acquired and build monitoring systems to capture this data
- Analyse and interpret the data acquired from the hybrid systems
- Observe the areas of power wastage in the system and how the system can be improved with reference to the current literature
- Design a numerical model of a hybrid system using the acquired data as

a basis for the design of the model

- Propose a wind prediction methodology to reduce the amount of power that is wasted by the wind turbine in the hybrid system
- Integrate the wind prediction methodology into the numerical model and establish whether the knowledge of wind conditions can improve the efficiency of the system

1.3 Thesis Organisation

Chapter two of this thesis introduces the concept of hybrid systems for telecoms applications. All of the major components of a base station and its different configurations are discussed to provide background and motivation for design decisions made throughout this work. Two dominant renewable energy sources are also discussed in the context of secondary power sources to telecoms base stations.

Chapter three covers the experimental set-up of the system and sensors which remotely acquired the data from different locations around the world. The use of different types of sensors is covered along with some of their installation configurations. A number of case studies are included with initial results describing the data acquired.

Chapter four discusses the prediction of power output for the secondary power sources introduced in Chapter two. Solar, not being the primary focus of this work, is briefly introduced with a more in-depth review of current wind prediction techniques. The approach to wind prediction in this work is examined along with justification for the design and configuration decisions made while constructing the methodology. Results demonstrating the methodology and how it should be integrated into a working hybrid system are included.

Chapter five describes the process of constructing a numerical model for simulating the operation of a hybrid system using performance profiles from the data acquired during the case studies. This hybrid model is then complemented with the addition of the wind prediction methodology introduced in Chapter four. The results of combining the two are presented to demonstrate

the positive aspects of using wind prediction for small scale hybrid systems.

Chapter six draws a conclusion to the current work, describing the contributions from each major section, along with proposed future work which would build upon the research completed to date.

Chapter 2

Hybrid Systems for Telecoms

2.1 Introduction

As outlined in Chapter one, A HSRES contains several core components which are commonly utilised in the construction of both hybrid and conventional telecoms base stations. Storage technologies are discussed in greater detail as they are the most sensitive components in the system and most of the control decisions are influenced by their electrical/chemical limitations. Existing power for off-grid base stations is commonly supplied by dual AC based diesel generators which run alternatively to each other [49]. The decision to use this type of configuration is primarily motivated by the lower upfront operational expenditure (OPEX) costs as a trade off against the higher running costs.

The HSRES used in this research (component layout in Figure 1.1, pictured in Figure 2.1) consists of a 5.8 kW Fortis Montana wind turbine, six kW DC diesel generator, 400 Ah battery bank and DC load (two kilowatt temporary test load) which is all connected together on a common 48 VDC bus. The wind turbine was mounted on top of a heavily loaded 35 meter lattice telecoms tower. The diesel generator, equipped with a DC alternator, charges the battery bank when the voltage falls below a specific set-point. The wind turbine and generator are both connected in parallel to the DC bus so when the generator is running the wind turbine will also simultaneously contribute power to the battery bank. This type of configuration is not typical for hybrid

energy installations but it allows more efficient generator performance by removing the need for rectifiers, transfer switches or inverter-chargers. AC based systems need these additional components to convert back to DC to charge the batteries, connect to other AC sources and connect to DC telecoms loads. These two types of configurations are compared in table 2.1.

Component selection and system architecture configurations for off grid systems are complex and this discussion should allow the reader to understand the justification for design decisions made though out this work. Component descriptions also go into detail on their performance limitations which influence their operational characteristics which are measured and eventually simulated in later chapters. This chapter discusses the selection of components in a HSRES and details the different configurations of multiple energy sources and loads.

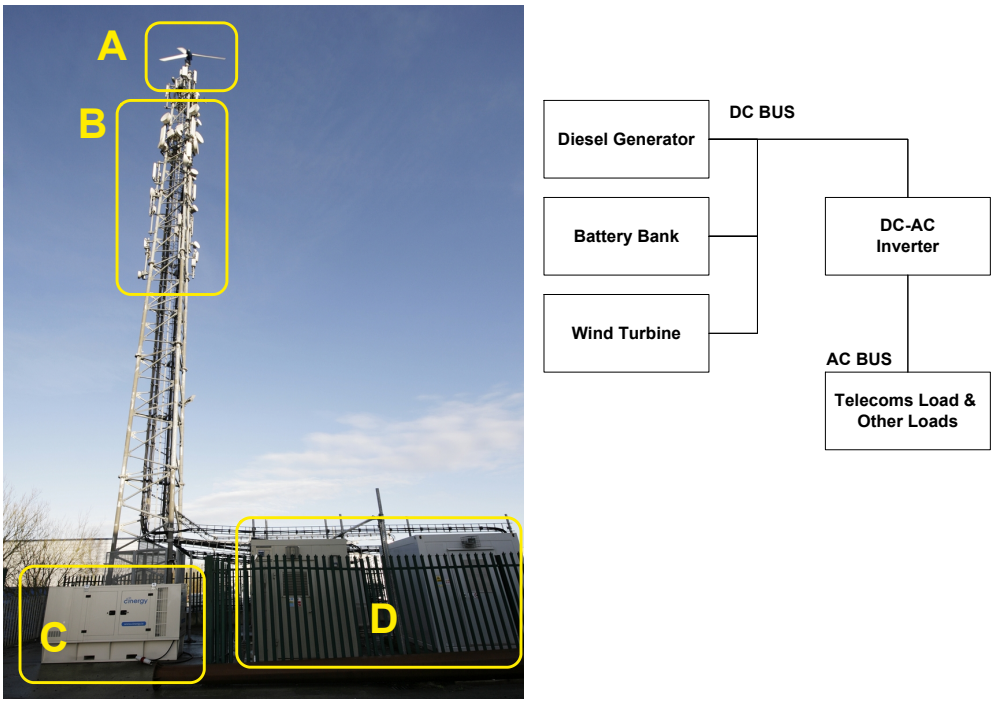

Figure 2.1: Test HSRES based on a telecoms site in Carlow, Ireland. 5.8kW Fortis wind turbine (A); Telecoms GSM antennae (B); Hybrid Generator including battery bank and DC diesel generator (C); Telecoms housing for base station equipment (D)

2.2 Primary power supply

This section details the different types of primary electrical sources which provide power to the system which comprises of a single operator telecoms base station. The majority of base stations are powered by either diesel generators on site or grid power. In locations where the grid is unreliable, the site will have a backup generator to power the site during outages. A small but growing portion of telecoms sites receive contributions from renewable energy sources to reduce fuel consumption. Occasionally base stations receive the majority of their power from renewable energy sources but it costs more to over size the renewable source. A suitable balance must be found between the sizing of the renewable energy source and the diesel generator.

2.2.1 AC diesel generator

AC diesel generators are currently the standard primary power supply for remote off-grid telecoms base stations. They also provide standby support for base stations which are connected to unreliable power grids. In standby applications the generator initiates operation when the controller detects grid failure. Studies undertaken by the Global System for Mobile Communications Association (GSMA) estimates that there are over 600,000 sites operating in an off-grid configuration [50]. These generator sets are typically described by their:

- kilo Volt-Ampere (kVA) rating
- engine revolutions per minute (RPM)
- single or three phase output

A generators' size is always specified in apparent power, measured in (kVA), as this allows them to be sized correctly for supplying loads with different power factors. Power factor is the ratio of apparent power in kVA to real power in kilowatts (kW). Purely resistive loads have current-voltage waveforms which are 'in phase' giving a power factor of close to one. Capacitive or inductive

loads have current-voltage waveforms which are 'out of phase' giving a power factor less than one [15].

The rotation speed of the crankshaft in RPM determines the power of the engine of an AC generator when comparing machines of similar weight and size. There are also specific speeds for different bus frequencies as the rotation speed must be proportional to the number of poles in the alternator to give a specific line frequency output. For example, a generator operating a 50 Hz AC bus could have a speed of 1500 RPM while a similarly sized generator operating with a 60 Hz bus would have a speed of 1800 RPM. The RPM of a generator is an important factor as while a higher RPM will give more power it will also produce more noise. Noise pollution is an important consideration when the generators are running in remote regions with no other sources of noise. Diesel generators can produce in excess of 90 dB at one meter decreasing to 64 dB at 20 meters [15]. Additionally the higher the engine speed, the faster the components wear out leading to a shorter operating life [25]. For the purposes of this work all references to AC generators will be those which are less than 30 kVA in size, a rotational frequency of 1500 RPM (50 Hz) and a three phase power output. Not all AC generators have a constant RPM and often utilise a gearbox to ensure the continuity of the shaft frequency to the alternator which provides the power to the AC bus.

2.2.2 DC diesel generator

In the context of this work the DC generators discussed will charge a battery bank whenever its voltage drops below a certain specified level. DC generators are similar to their AC counterparts with the main difference being their voltage and current output ranges. Telecoms applications operate within a low voltage range (12 V to 72 V) to protect employees working with the equipment. This voltage range (multiple of 12) is chosen as it matches the voltage of the backup batteries in the BTS equipment. The lower voltages result in higher current telecoms equipment (20 A - 200 A) which require more attention to cable sizes and run distances to limit power loss. As the voltage output range of the generator is quite low in comparison to mains, a drop of one VDC across

AC Generator	DC Generator
Rectifier needed to convert 240 V to -48 VDC	Already operates at -48 VDC and can be connected directly to equipment
Bi-Directional inverter needed to charge battery bank	Generator connected directly to battery bank
Can supply AC loads directly	Inverter needed for AC loads
Transfer switch needed to connect to AC bus	Can connect directly to DC bus
Market price of generator lower due to high volumes	Rarity of DC generators and expensive internal components result in higher prices

Table 2.1: Difference between AC and DC generators for hybrid installations

a component can have a significant effect unless thicker cable is used. Large diameter cable has lower resistance and consequently a lower voltage drop and is the best choice for connecting DC generators to battery banks.

AC generators have a fixed RPM as they must maintain the correct mains frequency for the equipment but DC generators do not have this requirement. Their RPM will change throughout a charging cycle, as the power requirement to charge the battery bank decreases towards the end of the cycle which will reduce noise pollution and fuel consumption. Table 2.1 compares some of the factors which need to be taken into account when using AC or DC generators for hybrid installations. DC generators will consume less fuel as the DC power does not need to be rectified to power the load or charge the batteries. Throughout this work, it was found to be the case, that AC generators are less expensive due to their higher market penetration.

2.2.3 Electricity grid

The power grid is the cheapest source of energy for supplying base stations with an Organisation for Economic Co-operation and Development (OECD) average of $0.156/kWh [51]. Grid reliability varies significantly in different regions with system uptime factors that can range from 100% in Germany [52] compared to the rolling blackouts [53] which are a frequent occurrence

in India. This compares to prices from diesel generators which can have a fuel cost starting at \$0.60/L of fuel [54] before even taking into account the capital costs for purchasing the generator. Fuel costs are even higher for sites in extremely remote locations which are not easily reached by land and even higher for sites which only have helicopter access.

Despite these costs, the requirement for backup diesel generators on remote sites is often unavoidable even on sites located in developed nations. Nigeria has a total of 24,252 telecoms sites with over 48% of theses sites powered by the electricity grid. Many of these sites are powered by an unreliable grid with more than 81% of these locations suffering outages in excess of six hours a day [49]. The costs of having and maintaining a backup generator are seen as a hidden cost when connecting to a grid with poor reliability. This is in addition to premature battery maintenance/failure from using battery cells, designed for infrequent backups, on a daily basis for grid outages.

2.3 Storage methods

In general a HES will have a storage component if a generator is going to switch off for periods of time or if excess power from renewable energy sources is to be captured.

2.3.1 Charging lead acid battery banks

A battery is an energy storage device that consists of electrochemical cells that undergoes oxidation/reduction (Redox) reactions as a means of discharging/charging. Each cell contains a cathode where reduction takes place (the loss of electrons) and an anode where oxidation takes place (gaining an electron) during a discharge cycle. This Redox reaction operates in reverse during a charging cycle. This reaction is not perfect and imbalances in the chemical concentration between the electrolyte solution and the surface of the electrode results in polarization losses. Another important factor which strongly affects the performance of a cell during charging or discharging is the internal resis-

tance of the cell [9, Chapter 2.1]. This resistance is a sum of the following components of a cell in addition to cable losses connecting the cell to an active system:

- ionic resistance of the electrolyte
- electronic resistances of the active mass
- current collectors
- electrical tabs of both electrodes
- contact resistance between the actives mass and current collector

As a cell is charged the specific gravity of the electrolyte increases linearly and measuring its density is the most accurate method of establishing cell charge levels. The traditional techniques for measuring this density is with a hydrometer or refractometer, but this is not recommended during active charge/discharge cycles. An alternative method is proposed which senses the density in real-time using optical fibres. This would provide a much more accurate way of knowing battery status instead of relying on voltage alone [55]. Voltage sensing is the least expensive method for estimating battery status but this has been shown to be misleading as the voltage will be different depending on the size of the load [56].

The capacity of a battery bank is measured in Amp hours (Ah) and this can be converted to kWh by multiplying the nominal voltage by the Ah value. The battery bank size referred to frequently throughout this work, is 400 Ah which is approximately 20 kWh at 48 V. As a lead acid battery's capacity increases the number of cells in the battery decreases to keep the sizes of the modules manageable. A 400 Ah battery bank at 48 V typically consists of 24 modules at two volts connected in series to give a total nominal voltage of 48 V. It is possible to get cells with a higher voltage but the amount of lead in the battery means it can only be lifted with a forklift which makes manufacturing and transportation more difficult.

The charge rate or 'C' rate represents the amount of current required to charge or discharge a battery bank in one hour. Such a rate (1C) is extremely high and it is more common to use a fraction of this rate to determine battery

operation. Battery banks are conventionally specified with a capacity at a 0.1 C rate, which for a 400 Ah battery bank would be ten hours at 40 Amps. As the C rate increases, the losses in the battery bank also increase leading to an apparent reduction in capacity in the battery bank. As described before, these losses are a combination of I^2R losses (losses given off as heat) from the internal resistance of the battery bank along with polarization losses which increase linearly as the operating current rises [9, Chapter 2.2]. This loss in capacity can be seen below in Figure 2.2.

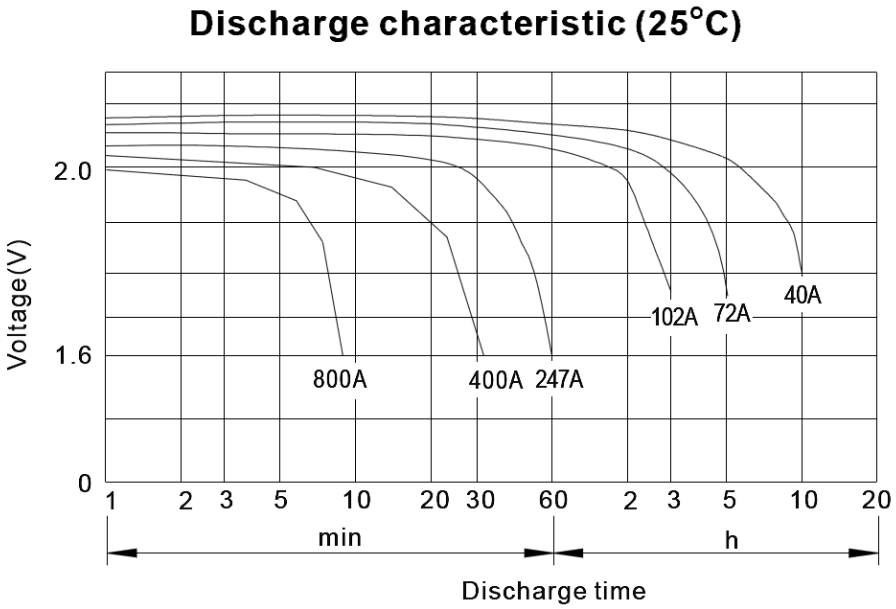

Figure 2.2: Loss in capacity with increase of current beyond rating for 400 Ah Battery bank [1]

Lead acid batteries are the most popular technology for telecoms applications due to their comparative low cost to other storage technologies. Large battery banks are expensive and there is a large price differential between different manufacturers and types of technology. Battery bank pricing highly representative of the idiom "you get what you pay for" as lower prices lead to compromises in quality and longevity [57].

Battery bank storage temperatures are also very important as it has a direct effect on their life time. The ideal charging temperature range is between 0°C and 40°C [58]. Maintaining such range is often difficult in applications with high ambient temperatures or high cycling currents. Temperature changes

must also be taken into account by the battery charger as lower temperatures cause an apparent decrease in capacity while higher temperatures result in an apparent increase in capacity [9, Chapter 3.10]. If changes in temperature are not taken into account the charger will overcharge the batteries in low temperature scenarios and undercharge the bank in higher temperatures.

Overcharging the batteries will cause gassing and evaporation of electrolyte which exposes the plates to air resulting in sulfation. Undercharging prevents some of the material deposited on the plates during discharge from being dissolved back into the electrolyte which also leads to sulfation. Sulfation occurs in varying degrees during normal battery operation but extremes in temperature tend to greatly accelerate the process and prematurely reduce the lifetime of the battery bank.

Gassing is common in lead acid batteries when charging at high voltages which are typically experienced towards the end of a charging cycle or equalisation charge. Generally this gas recombines into the battery electrolyte but if pressure builds up a valve releases the gas. This loss of gas is replaced in flooded lead acid batteries by topping them up with distilled water every three months [9]. The electrolyte in sealed batteries cannot be topped up and they are fitted with an emergency valve that opens if excess gas builds up inside. When this gas vents it cannot be replaced leading to the cell eventually drying out. As a result care must taken with sealed batteries to avoid the higher voltages which cause gassing.

Lead acid batteries under active load require a two stage charging regime in order to reach full capacity. The first stage, known as the 'bulk mode', charges the battery bank with a constant current until a specified voltage is reached. This voltage varies between different battery technologies but the battery bank is at approximately 70% of its capacity at the end of this stage. Once the specified voltage has been reached the charger then switches to 'absorption mode' where a fixed voltage is maintained until the end of the cycle as seen in Figure 2.4. Temperature will have an effect on the voltage of the cell so the charger must take this into account. If the fixed voltage is too low there will eventually be irreversible sulfation caused on the active material while if it is too high it will induce premature corrosion on the positive grid [59] inside

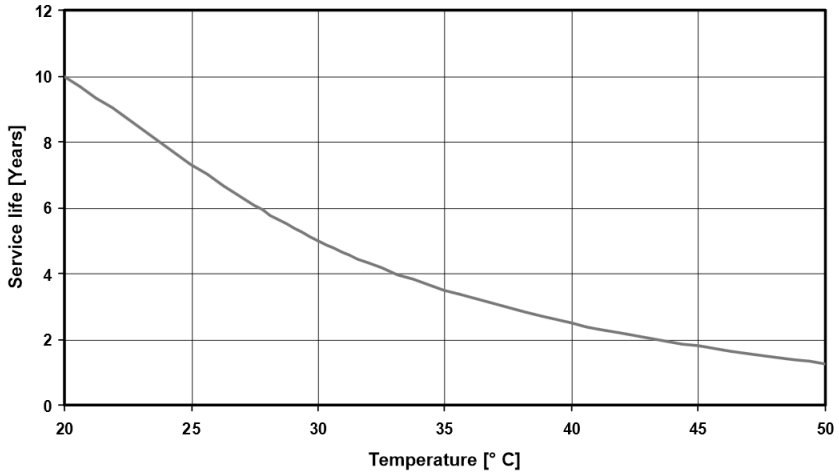

Figure 2.3: Effects of temperature on expected battery bank lifetime [2]

the battery cell. Temperature compensation in the charger will dynamically change the final voltage for absorption mode which is essential as the battery bank will always increase in temperature during a charge cycle. This increase is caused by its inefficiencies; the largest being as a result of the internal resistance of the battery cell.

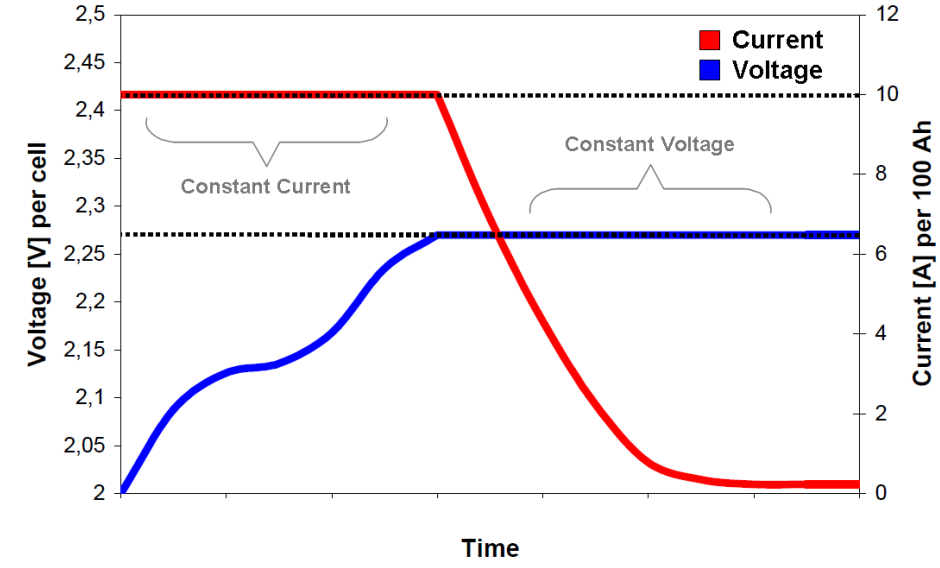

Figure 2.4: Two stage charging for stationary lead acid batteries [3]

The hybrid energy system used in this work uses a partial-state-of-charge (PSoC) cycling regime is used which keeps the battery bank between 40% and 80% state-of-charge (SoC). PSoC cycling is a relatively new term used

to describe the type of conditions which battery banks in hybrid electric cars experience throughout their operating life [9]. This SoC range is preferable for maintaining physical battery life compared to a battery bank that is fully discharged on a frequent basis. PSoC cycling requires occasional equalisation charges to reduce sulfation on the battery plates [9], discussions with the manufacturer [1] indicated that this process should occur at least once a month. Despite these charging criteria, the battery bank would not be expected to last longer than five years due to the intensity of the cycling they are subjected to. It is possible to increase the battery life further by reducing the number of transients [60] induced on the battery bank by fluctuations in the wind turbine or solar output. These fluctuations are known as "micro cycles" where the battery bank undergoes a large degree of small charge/discharge cycles without being either completely charged or discharged.

2.3.2 Gel battery bank

Gel-based Valve Regulated Lead Acid (VRLA) batteries are the dominant technology used for UPS and telecom backup applications [61]. This type of battery technology is designed to be float charged for its operating life. Float charging involves maintaining the batteries at a constant voltage between 2.2 and 2.3 V per cell which for a 48 V battery bank is 52.8 to 55.2 V [9, Chapter 17.26]. Unlike deep cycle batteries, gel batteries are not designed to undergo frequent cycling. In telecoms base station applications they are installed in parallel with BTS equipment to allow the electronics 'ride through' any short term interruptions to the power supply. These batteries should not be used for hybrid applications as the frequent cycling, deep discharging and high currents would cause them to degrade rapidly. The amount of cycles they can tolerate is similar to starting, lighting and ignition (SLI) automotive batteries with 200 - 700 cycles [9, Chapter 15.10] being a common range depending on depth of discharge.

2.3.3 Flooded lead acid battery

Flooded lead acid batteries are the oldest member of the lead acid family. They are a financially attractive storage option in telecoms applications where weight and size are not an issue. They have the lowest energy density [9, Chapter 15.10] with 25 Wh/kg but they have the ability to tolerate high charge/discharge currents due to their thick lead plates. These batteries are not sealed and need to be periodically topped up with distilled water to replace any electrolyte lost due to gassing. The frequency of gassing means the batteries must also be stored in a well ventilated enclosure to avoid any build up of explosive concentrations of hydrogen.

With proper maintenance this battery technology can endure between 1500 and 3000 cycles depending on depth of discharge and average storage temperatures. It has been observed that the charging efficiency for flooded lead acid cells decreases dramatically [41] as the batteries become charged. This factor has significant implications for applications where the state of charge is to be maintained at a level higher than 80%.

2.3.4 Absorbed glass mat

Absorbed glass mat (AGM) is similar to Gel battery technology in many ways in that they are completely sealed and only vent when there is an excessive pressure build up due to overcharging. Unlike Gel batteries, the AGM electrolyte is soaked into a highly porous glass matt fibrous material though which oxygen can pass from the positive to negative electrodes during charging [62]. Their sealed construction allows them to be installed horizontally into racks which saves considerable amounts of space and facilitates easy access to their electrodes. As AGM batteries are a relatively new technology, care must be taken when attaching them to battery chargers which have been configured for cell voltages that correspond to flooded lead acid cells.

Vision CL 400 Ah AGM batteries, which have been used in the test systems for this work, are rated for a charging voltage range of 2.35 to 2.45 V per cell or 56.4 to 58.8 V nominal voltage [1]. In comparison, flooded lead acid batteries

from Rolls are rated for charging to 2.5 V per cell or 60 V nominal voltage, with scope to go as high as 2.67 V per cell or 64.1 V nominal for equalisation charging [63]. These voltages would cause excessive gassing in an AGM battery causing the mats to dry out and become sulphated, this situation cannot be reversed as it is not possible to add distilled water to these cells.

2.3.5 Lithium ion battery technology

Lithium ion (Li-ion) battery technology and its variants are currently leading modern storage technology. They have significant advantages over lead acid batteries which can be seen in the summary table 2.2. The higher energy density (see table 2.2) of Li-ion battery cells would allow the weight and size of a battery backup system for a telecoms base station to be dramatically reduced. They are also less sensitive [9, Chapter 26.47] to repeated discharges in excess of 80% than lead acid cells whose life is dramatically reduced with deep discharging. The ability of the Li-ion battery technology to tolerate high temperatures in excess of 60°C [9, Chapter 26.66] with only a minor effect on battery lifetime [64] offers huge potential to reduce or remove battery cooling requirements in regions with high ambient temperatures.

The primary differences between lead acid and Li-ion battery technology can be seen in table 2.2. There are two major barriers to wide scale adoption of Li-ion batteries in telecoms applications. Primarily, the cost of the cells remains prohibitive at more than three times the cost [64] of lead acid cells with the same capacity. Secondly, Li-ion batteries continue to be affected with safety issues which manifest themselves in the form of heat or fire when the cells are deeply discharged, though the on-board circuitry in each cell should prevent this. Lithium is highly reactive and can combine with oxygen leading to the possibility of the battery catching fire [65].

-	Lithium Ion Battery Bank	Lead Acid Battery Bank
Energy Density	200 Wh/kg	35 Wh/kg
Rated Cycles	500 - 4000+	500 - 1,500+
Operating Temp	-20 to 50°C	-20 to 40°C
Cost	600€/kWh	200€/kWh
Cell Voltage	1.5 V	2.0 V

Table 2.2: Difference between Lithium Ion and Lead Acid battery banks, [9, Chapter 15.10, 26.47, 26.56]

2.3.6 Fuel cells including hydrogen and zinc bromine technologies

A fuel cell is similar to a battery in that it uses a chemical reaction to create electricity. A fuel cell achieves this by selectively mixing two chemicals which are stored in separate tanks. Fuel cells have recently shown promise as an eventual viable alternative to traditional battery technologies. There are a few main types undergoing active research for telecoms applications. Research into hydrogen proton exchange membrane (PEM) based technologies has been particularly active [34, 66, 67, 33] for supplemental and primary power supply applications for telecoms applications. Some test systems have additional complexity with the ability to produce and store hydrogen using electrolyzer units which is then used by the PEM to produce power [68, 67].

The main barriers preventing large scale adoption of this technology in telecoms are; PEM production costs and the difficulty of delivering hydrogen refill tanks to remote site locations. A flow battery is an unpressurised system which uses pumps to move electrolyte though a PEM cell. The electrolyte flows continuously while the voltage at the electrodes of the PEM dictates whether the fluid is storing energy or not. Flow batteries such as vanadium redox [69] and zinc bromine based technologies have both seen commercial deployments in recent years. Zinc bromine flow batteries have seen commercial deployments for telecoms applications with many advantages over conventional lead acid battery technologies. The main advantages over lead acid batteries is their ability to tolerate a large number of cycles (approximately 10,000) and a large temperature range which makes them suitable for outdoor applications [70].

Zinc bromine technology is not without its own issues as practical conversations with Redflow [71] indicated that zinc bromine batteries must be periodically discharged to zero percent. This process prevents material building up on the electrodes in a similar fashion to sulfation in lead acid batteries. Discharging the battery storage to zero percent in a hybrid telecoms system would lead to a system outage in DC based equipment as the zinc bromine batteries would be sole source of battery backup. This problem could be alleviated with the addition of a second battery bank allowing one bank to discharge completely while engaging the second bank. As the cost of fuel cells drops further they will continue to become more attractive as the primary storage technology for telecoms applications.

2.4 Conversion equipment

The type of conversion equipment needed depends on the HSRES configuration and whether the primary power sources is AC or DC.

2.4.1 DC-AC and bi-directional inverters

An inverter is a solid state device which converts DC power into AC power with varying degrees of quality. Cheap low quality inverters provide outputs in the form of a square wave or modified square wave with large amounts of harmonic distortion. These types of inverters are best suited to resistive AC loads and non sensitive equipment. A pure sine wave inverter is needed to produce a higher quality sine wave with low harmonic distortion and this is the type of unit used throughout this work. While the majority of the loads in a BTS are supplied by -48 VDC, there are also AC loads in the system such as lighting, aircraft beacons, monitoring equipment, computers and cooling equipment. The inverter converts the DC battery bank voltage to supply these loads. Inverters are extremely popular in the marine industry as they have been used for decades to provide power to electronic equipment during periods when boat engines are not running. Care must be taken when sizing inverters to power telecoms loads as they operate differently to marine loads.

While marine loads are periodic, in that the inverter is unloaded when the engine is running, a telecoms load is constant and can be close to the rating of the inverter.

For hybrid systems with an AC bus, with an AC generator and battery bank, a bi-directional inverter is a useful addition. When the diesel generator is running it powers the load and charges the battery bank through the inverter/charger. When the diesel generator is disengaged the power will flow from the batteries though the inverter to the AC bus. Some inverter/chargers can also provide a load shaving [72] feature where the batteries can assist the generator to supply loads in excess of its rating. This is a useful feature as it allows the generator to be undersized and operate efficiently at its rated load for longer periods of time.

Grid-tie inverters are designed to synchronise with the power grid and operate within a very specific set of voltage and frequency parameters. They are designed to suspend power exports to the grid during events such as over/under voltage, over/under frequency and blackouts. These restrictions ensure that the grid operator can maintain grid stability and personnel safety. This type of inverter is appropriate in small scale (under six kW single phase, ten kW three phase [73]) applications where power generated from wind/solar or other resources needs to be exported onto the grid. Depending on the agreement with the power provider, users may be able to sell the power exported to the grid.

2.4.2 Rectifiers

Rectifiers are a set of electronics that convert AC power into DC power which, in telecoms applications, is used to charge backup batteries and provide power to the transmitter loads. Rectifiers are critical components and are sometimes prone to failure so steps are taken to improve system reliability. There are multiple rectifiers installed in every base station and they adopt an N+1 configuration. An example of this is if the DC load for a telecoms site is specified to be four kW and each rectifier is rated at one kW, four rectifiers would be sufficient for the load.

To adopt the N + 1 configuration there would be an additional rectifier installed giving a total of 5. If one of the rectifiers were to fail a notification would be sent to the operator and the remaining four would be able to power the load. This gives the operator a chance to swap out the faulty rectifier while maintaining system uptime. While more rectifiers could be used to create higher levels of redundancy, it is important to keep the rectifiers loaded as their efficiency can vary. A rectifier's efficiency can range from 82% when loaded to 10% of its rating up to 93% when loaded to 70% of its rating [4].

2.4.3 DC-DC Converters

DC-DC converters switch DC voltage to a either a higher or lower level depending on the application. They are most commonly used in mobile phones where sensitive components need a fixed voltage whilst being supplied by a varying battery voltage. A similar problem can occur with telecoms BTS equipment when it is connected to a varying voltage source such is the case with a hybrid system. The problem can manifest itself with control gear which has been configured to operate within a narrow voltage range, outside of this range it will trigger low voltage alarms on the operators management system. This problem can be solved with the addition of a large DC-DC converter which can accept 30 to 60 VDC on its input from the generation equipment while outputting -48 VDC to the BTS equipment.

2.5 Types of loads

2.5.1 BTS equipment and antennae

As described in the introduction there are two types of base stations on telecoms networks; those which exist on the periphery that only handle communications for their own cell; and those which are stationed on the core network. A cell is a circular region surrounding a telecoms tower which can range in size depending on the type of communication frequency. These cells are placed beside each other with a certain degree of overlap to ensure continuity of service

when moving from cell to cell. If a peripheral base station were to experience an outage then only the cell within its area of coverage would be affected. On the other hand if a base station on the core network were to suffer an outage, multiple cells would be affected as any peripheral base stations downstream of the core base station would be affected. As a result of this risk, these types of sites are very well protected with multiple levels of redundancy. In addition to their primary power source they use batteries for short term outages and diesel generators for longer term events. As the equipment on these sites is handling more traffic than peripheral nodes, the power consumption is significantly higher.

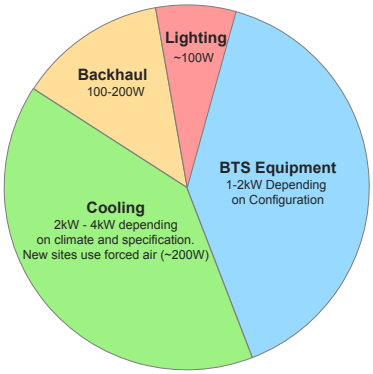

Figure 2.5: Peripheral node BTS power consumption distribution [4, 5]

The hybrid systems discussed during this work are designed to supply power to telecoms sites consuming up to two kW of power continuously such as the peripheral nodes with power consumption similar to that described in Figure 2.5. These sites provide coverage for a single cell for an individual telecoms operator with a point to point link back to the core network. The average power consumption of these types of sites in Ireland was found to be approximately 1.2 kW [38] but in developing nations with larger towers, bigger cell sizes and an air conditioning load, the average power consumption is higher. The main factors affecting this increase are the air conditioning which can add between two and four kW to the peak load and the power consumption of the BTS equipment for extended transmission range.

2.5.2 Air conditioning

Cooling is a major power consumption component of BTS sites located in warm climates such as Africa and the middle east with up to half (see Figure 2.5) of the power consumed by cooling. This power consumption is as a result of using compressor based cooling solutions (air conditioning) which can double the power consumption of an entire telecommunications network in some cases [74]. There are alternatives to air conditioning such as open ventilation, forced fan cooling and heat exchangers which can reduce the cooling load by more than ten percent [44] but at the expense of a higher ambient enclosure temperature. These alternatives are only viable if the equipment can tolerate [46] the higher temperatures which the equipment will be exposed to.

The use of solar panels can be used effectively to provide shade for the generation equipment and battery bank. Shading the equipment from direct sunlight prevents the enclosures from being heated beyond ambient temperatures which reduces the cooling load for both the battery bank and generator.

2.6 Secondary power sources

2.6.1 Wind turbines for telecoms sites

Wind turbines offer a viable and cost effective source of renewable energy to supplement the power requirements of off-grid telecom base stations. Given the load requirements of peripheral nodes the use of micro wind turbines, which provide power between one and ten kW depending on their size, are the most suitable for meeting this demand.

The most important factor when considering a wind turbine for any site is the average wind speed for the location. The wind speed is measured in meters per second (m/s) and sites with an average of five m/s or less are seen as non-viable for small wind turbines [75]. Turbines in poor locations (regions with an average wind speed less than five m/s) will produce power but the payback period is longer than the install life of the turbine itself. One way

of improving the performance of the wind turbine at a site is to increase the height of the turbine monopole. The change in wind speed with respect to height or wind shear can be seen in Figure 2.6. It is an important factor for commercial wind turbine design as the rotor and nacelle must be engineered to cope with the fatigue in scenarios where there can a difference of up to 20% between the wind speed at the top and bottom of the rotor [76]. Shear analysis is also a useful way of estimating the average wind speeds, at different hub heights, above a location where the anemometer recordings have been taken at ten meters (a common height for meteorological stations). The use of sheer analysis in the early stages of site evaluation should not be relied upon alone as it is vulnerable to anemometer errors [77], seasonal variations [78] and different wind directions. Figure 2.6 demonstrates the difference as height increases between two different data sources for the same location at Dublin City University from Met Eireann [79] (2km away in Dublin airport) and the Sustainable Energy Authority Ireland (SEAI)[80] which is a large scale wind map of the area. The equation used for calculating the wind sheer can be found below where V_{ref} is the known wind speed and reference height Z_{ref} can be used to find wind speed V(z) at a height above the ground z with roughness length Z_o:

$$V(z) = V_{ref} \frac{In\frac{z}{Z_o}}{In\frac{Z_{ref}}{Z_o}} \tag{2.1}$$

There are a number of buildings and trees in the vicinity of these wind measurements so the area can be classified as rough terrain. This classification determines the roughness length which affects wind speed of the region around the wind turbine. This parameter must be taken into account when comparing different terrain such as the calm open sea which would have a very short roughness length [81, P.44]. This would compare favourably against the centre of a city with tall buildings which would have a very long roughness length. When plotting the graph in Figure 2.6, the location was classified as rough terrain with a calculation based on smooth terrain included as a reference.

Knowing the average load of the site is important when identifying a suitable turbine size. The ratio of the potential power output from a power plant to

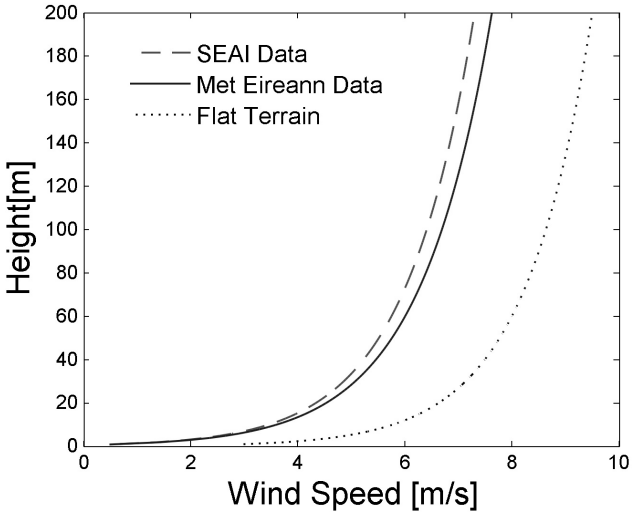

Figure 2.6: Localised wind shear comparing two data sources for a location in rough terrain compared with smooth terrain using equation 2.1

its actual power output is known as capacity factor. Commercial power plants (gas and coal in particular) have capacity factors higher than 90% while wind farms have a capacity factor as high as 30% for offshore deployments, but this can be as low as 20% on land [82] depending on the quality of the site. If the average load for a base station is 1.2 kW then a six kW wind turbine operating with a capacity factor of 20% would be seen as a good match to the load. Under sizing the turbine will result in additional generator run hours to supply the load while over sizing the turbine will result in additional costs and excess power which cannot always be stored.

The wind turbine controller used in this work, annotated in Figure 2.7, is connected to the cable from the permanent magnet generator driven by the turbine blades. This cable is attached to the box at point 'E' and the wires are then connected to the brake switch at point 'D'. The brake switch allows the turbine to be manually shut down during periods of maintenance or malfunction. It functions by creating a short circuit across the three phases which puts a massive load on the motor causing it to stop. The turbine cable provides three phase AC with rapidly varying amplitude and frequency that must be rectified into DC to charge the battery bank. The turbine power is converted from AC to DC by two three phase rectifiers at point 'C' which are

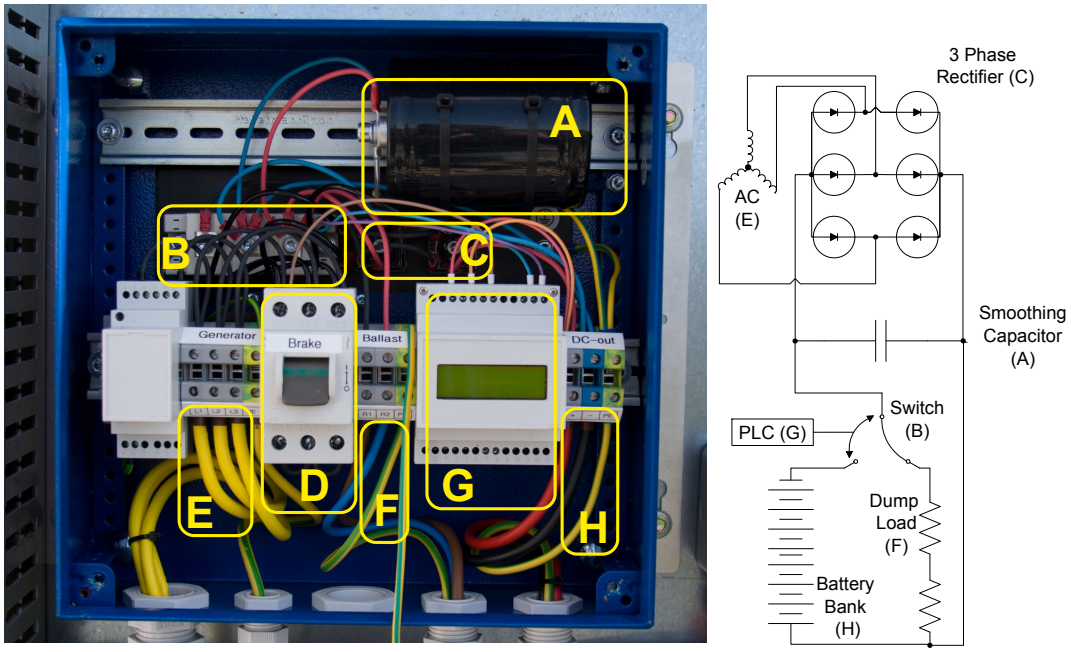

Figure 2.7: Wind controller with diversion load and battery charger for rectifying wild AC into 48 VDC. Smoothing resistor (A); solid state switch (B); three phase rectifiers (C); short circuit brake (D); three phase turbine cabling (E); diversion load output (F); PLC Controller (G); charger output (H)

then connected to the solid state two way switch at point 'B'.

The switch is managed by the micro-controller, with display, at point 'G' which continuously analyses the output DC voltage at point 'H'. If the controller deems the output voltage to be too high it begins switching some of the power to the dump load that has cabling exiting the controller enclosure at point 'F'. On the other hand if the voltage is below the cut off threshold for charging the batteries all of the power exits though point 'H'. The power will still have a certain level of 'ripple' as a diode bridge is not able to create a smooth DC voltage by itself. A large capacitor is added at point 'A' to smooth out the voltage ripple on the DC output. This capacitor is only connected to the portion of the switch that is connected to the batteries, there is no need to have clean DC power going into the dump load. The controller is configured to charge the battery bank to a maximum of 56.4V which corresponds to ~2.35 V for each cell in the battery bank (24 in total). This value is in the conservative range of cut off voltages for a battery bank undergoing active cycles which is

recommended to prevent gassing in AGM battery banks [1].

As the voltage of the battery bank approaches 56.4 V the turbine controller will begin to dump power through its resistor banks to dissipate the excess power. It achieves this diversion using Pulse Width Modulation (PWM) switching where a duty cycle of 0% allows all the power to the battery bank up to a level of 100% where all of the power is being dumped into the resistor bank and dissipated as heat. The resistor bank must be capable of dissipating the full power output from the wind turbine for extended periods if necessary as it would damage the turbine to switch it off in high wind speeds.

2.6.2 Solar panels

Solar panels offer a valuable, reliable and abundant source of energy for installations in locations with adequate solar irradiation. Similar to average wind speed being important to turbine performance, the yearly sum of global irradiation falling per square meter is critical when evaluating the performance of a solar based system. As was the case with the wind turbine section, these descriptions will focus on solar installations which are suitable for supplying power to peripheral nodes in telecoms applications.

There are numerous different solar technologies undergoing active research to improve their efficiency but the technology of choice in the telecoms industry is currently silicon based cells. These technologies can be categorised into poly-crystalline (poly-Si) and mono-crystalline (mono-Si) silicon cells. Poly-Si cells are independently verified to have module efficiencies beyond 20% while mono-Si cells have efficiencies beyond 25% [83]. Solar panels usually have a warranty of 20/25 years but studies have shown that the panel lifetime extends far beyond this time-scale [84].

Figure 2.8 from the Photovoltaic Geographical Information System (PVGIS) demonstrates the variation in solar irradiation, measured in W/m^2 or cumulatively in kWh/m^2, for optimally-inclined solar panels across Europe and into Africa. It can be seen that the amount of energy produced by a solar installation in northern Europe would produce half the power of an equivalently sized system in southern Europe. A single 140 W solar panel, of area one m^2,

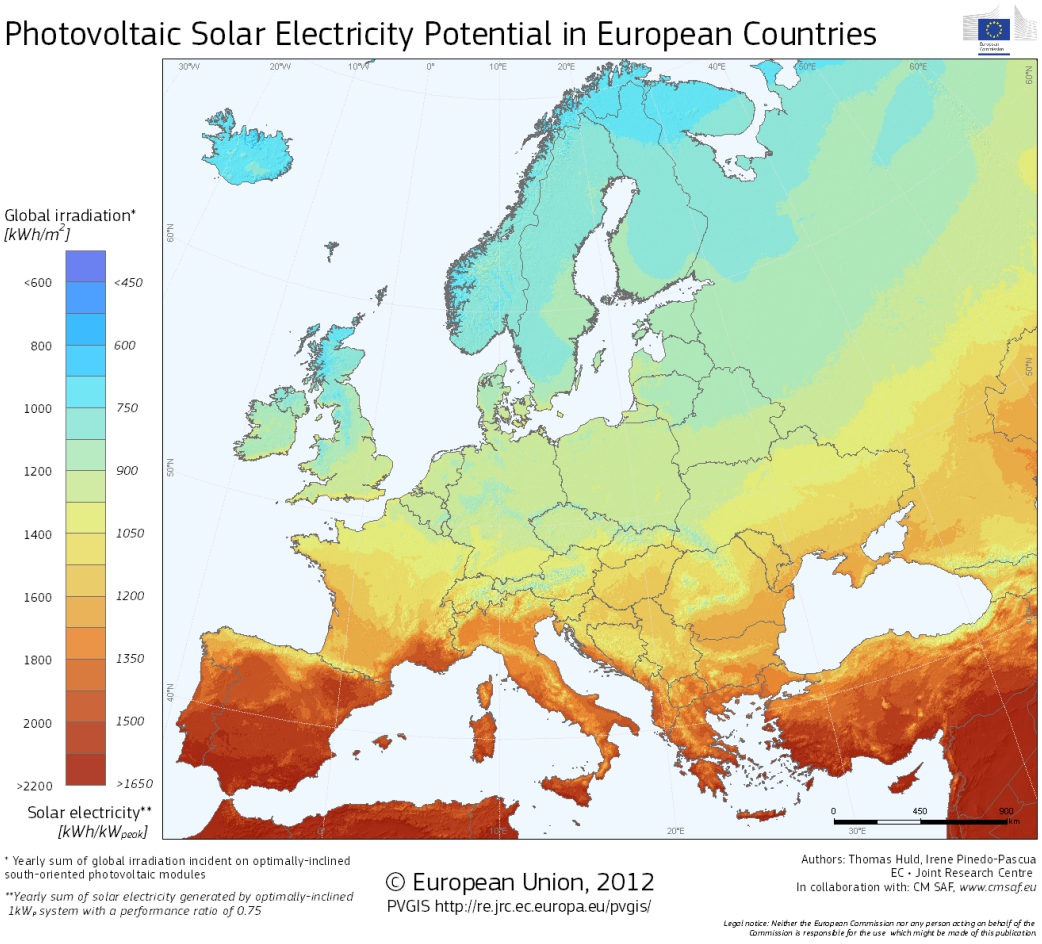

Figure 2.8: PV solar potential in kWh and for a one kW peak system in EU countries [6]

14% efficiency, would produce at most 0.168 kWh in central Germany while the same panel could produce 0.308 kWh in southern Spain. These are ideal numbers and it is unlikely that the solar panel will reach its potential power output for a number of reasons:

- Maximum power point
- Inverter efficiency
- Power losses in the cabling

The performance of a solar cell can be observed by looking at its IV curve which plots the short circuit current against voltage as seen in Figure 2.9.

This curve is useful for highlighting the power production of solar cells when they are operating at their maximum power point. The maximum power point is where the peak power of the solar cell is produced at the "knee" of the curve. It is not always possible for certain system configurations to operate at this point as the voltage is much higher than what the battery bank can tolerate.

If the solar panel, represented by the IV curve in Figure 2.9, was connected to a 12 VDC battery system it would be limited to the voltage range of the battery. The battery would need to be connected to the solar panel with a charge controller to protect the battery. Like the controller for the wind turbine discussed earlier, it restricts the voltage range of the battery to protect it. The controller, in the simplest case, will disconnect the load from the battery when the voltage drops to 11 VDC to prevent the battery from being too deeply discharged. On the opposite end of the scale as the battery becomes fully charged, the controller will begin to implement PWM charging to restrict the high cut off voltage to 14 VDC.

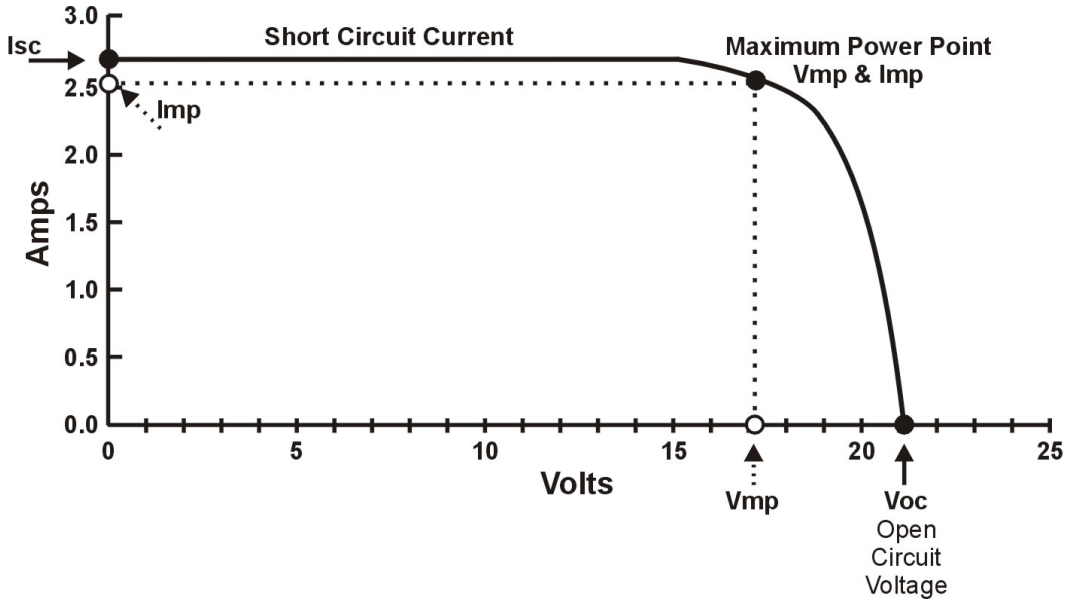

Figure 2.9: IV curve for evaluating the performance of solar cells [7]

Looking back to the curve in Figure 2.9, the maximum power point is at 17 VDC with a current of 2.7 ADC giving a maximum power of almost 46 W. Given that the voltage of the 12 VDC system is limited to 14 VDC at full charge, this means that the maximum power is limited to 39 W or a loss of

15%. This problem can be rectified with the use of a maximum power point tracking (MPPT) charge controller. This type of device maintains the solar panel at its maximum power point while stepping down the voltage to the appropriate level to charge the battery correctly. In this way a 48V solar cell can maintain its maximum power point of 68 VDC while stepping down the voltage to 56 VDC which is suitable for charging AGM batteries. When designing this type of system, it must be considered whether the additional expense of buying an MPPT based controller is justified for the 15% increase in power.

A 6.16 kW peak (kWp) system is proposed, with a financial quotation as seen in appendix Figure A.7, as an example to demonstrate the affect of location on the return of the system. This installation would comprise of 44 PV modules with the area of each being one m^2 with the efficiency of each panel is 14% giving 140 W of power at its maximum power point. The solar irradiation map in Figure 2.8 provides guideline kWh values for an optimally inclined one kWp system with a performance ratio of 0.75. This ratio was formulated with a combination of losses due to temperature, reflectance effects, cabling and inverter losses [85].

Continuing with the location in southern Spain, discussed previously, a one kWp system could potentially produce up to 1,650 kWh of power in a typical year. The 6.16 kWp system would produce up to 10,164 kWh when the one kWp system is scaled up to that size. Diesel fuel contains approximately ten kWh/Litre of thermal energy and a diesel generator is up to 30% efficient at converting this thermal energy to electrical energy. This implies that if the addition of solar panels is to offset the cost of diesel fuel then for every three kWh of power produced from solar a litre of fuel will be saved. Taking into account a fuel cost of \$0.60/L [54] and given that the 6.16 kWp system costs \$22,300 it will take at least 11 years for this system to break even.

2.7 Summary

This chapter has discussed the operational characteristics of the core components used in the construction and powering of telecoms base stations. The primary power sources section included different types of diesel generators and the power grid as the principal contributors of energy to telecoms sites. Hybrid off-grid sites often supplement the primary power source with a renewable energy resource such as wind or solar as discussed in secondary power sources. The telecoms equipment is a -48 VDC based system which comprises of a mix of components with different voltage requirements.

The operation of battery banks, current technologies and emerging alternatives are discussed in the storage methods section. The vulnerability of battery banks to damage and their importance to the reliable operation of the system positions them as one of the core discussion topics in this chapter.

The conversion equipment section details how components with different voltage ranges can be connected together effectively. The type of loads found on a telecoms site dictate the equipment configuration needed to cater for these loads. Integration of renewable energy sources requires a battery bank to store power during periods of excess power or generator operation and power the load at all other times.

Chapter 3

Remote monitoring of HSRES experimental set-up

3.1 Introduction

Remote monitoring of renewable energy installations is of particular importance to this work as it allows sophisticated performance data of equipment to be collected and analysed. This section details the broad range of components which were measured throughout the course of this work. This data was acquired in a number of different locations ranging from on site measurements in Dublin City University to other regions in southern Ireland, Wales, Egypt, Ghana and as far away as Fiji in the pacific.

The primary form of bulk data acquisition was though the use of an Advantech UNO-2173A [86] industrial computer and data acquisition (DAQ) equipment. The industrial computer was programmed using LabVIEW™ which enabled rapid system prototyping along with the ability to modify the system remotely to rectify any software errors. The industrial pc was connected to a Labjack U6 DAQ [87] which had a large number of inputs to accommodate the range of sensors installed on the HSRES.

This chapter discusses the sensors and techniques used to remotely acquire the data used throughout this work. The data forms the basis of design criteria for

selecting charging regimes, controller settings and modelling configurations. Specific example applications are provided describing how the sensors were deployed, how they acquired the data and some provisional results from these applications. The data is essential to provide a template for constructing the characteristic equations that represent each component in the software model. The software model, described later in Chapter five, simulates the operation of the physical HSRES system. An overview of the monitoring approaches used in this work and their overlaps can be seen in Figure 3.1.

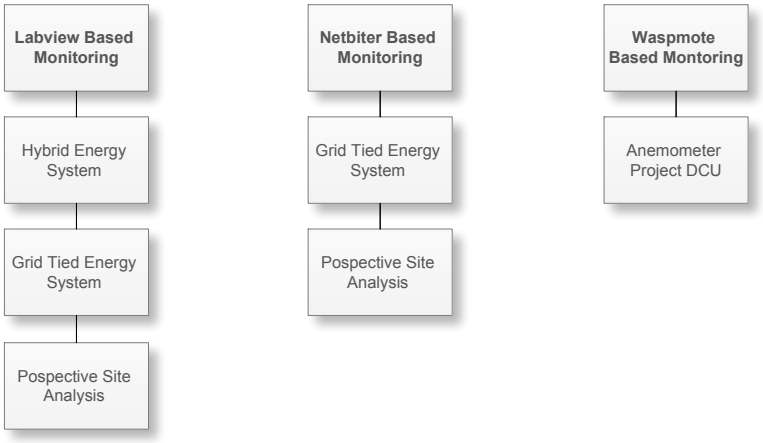

Figure 3.1: Flow of different monitoring approaches and the technologies used in each application

3.2 Network and communication

Several different technologies were used for communications with the remote monitoring equipment. The bulk of the communication took place over cellular mobile networks as a wired connection was not available in any of the locations. The system with the largest amount of sensors was the off-grid hybrid test system which had more than 20 data variables under measurement. The safest way to connect the remote systems to the central server was though a virtual private network (VPN) which used cellular modems from Digi®. The purpose of a VPN is to securely expand a local area network (LAN) through a public network.

In this case it allows remote nodes to appear on the same network with the central server despite the fact that the nodes could be thousands of miles away on a wireless telecommunications network. The system used a gateway router was connected to the internet. This router was connected to the central server and any other computers that needed to connect directly to the remote nodes. Each remote node was connected to a cellular modem with Ethernet connection which allowed the DAQ to send data back to the central server.

Once systems have undergone testing and are deemed reliable, there is no need to monitor every parameter on a frequent basis as is the case with HSRES prototypes. Reliability of the systems was verified when stable battery charge times were established for a given load. When monitoring this equipment on a long term basis, with a low number of sensors and a low data rate, the Netbiter® monitoring system was used. In its most basic form the DAQ connects to its own cloud servers via its own cellular connection or optionally through Ethernet over a remote node within the VPN mentioned previously. This has advantages (higher reliability, quick deployment) and disadvantages (less data granularity with one hour v.s. one sec and data point costs) but it was sufficient for low frequency measurements taken on an hourly basis. It is based on ARM® technology with analog inputs, digital outputs and a dedicated Modbus® connection [88]. Modbus® is a protocol that enables reliable master/slave communications to multiple devices sharing the same 2/4 wire bus [89]. The Modbus® connection was the most suitable component as it allowed up to ten devices (Netbiter® limitation) to be connected to the same port with unique addresses.

The second form of monitoring technique was based in Dublin City University where five anemometers with wind speed, direction, temperature and solar irradiation were measured. The development was based on a technology called Waspmote [90] from Libelium® and in essence the Waspmotes are an industrial version of the Arduino™ electronics platform. There were five waspmote nodes and a base station deployed in the installation. Each remote node had a set of environmental sensors which communicated its readings back to the base station every minute. The base station, which contained its own database, synchronised with the laboratory server to provide near real time environmental

data from all the nodes. The nodes were programmed [91] to connect to the base station using a point to point wireless ZigBee connection as opposed to the mesh network that is sometimes implemented with ZigBee.

Comparing the Netbiter and Waspmote systems, the Netbiter system is not suited to large data sets. While it is capable of handling large data sets, the price of storing these data points is prohibitively expensive. The default amount of data storage for the Netbiter system is 50,000 data points which are used up rapidly in high frequency applications. The Waspmote system on the other hand has no such limitation as the data is being acquired directly and is then stored in the database. High frequency data acquisition is feasible with this system as there are no real storage limitations other than the size of the machine on which the database is stored. It was for this reason that the Waspmote system was chosen for the anemometer application.

3.3 Electrical sensing and applications

This section outlines the electrical sensors used to measure power, current and voltage on both AC and DC circuits. There are several different techniques for measuring either AC or DC currents. One technique is to put a power resistor, known as a shunt, with a tiny but known resistance in series with the load. The shunt is always rated for a specific current range and a known voltage drop for that range. An example of this would be a shunt designed to measure current with a range of zero to 150 ADC and a voltage drop of zero to 50 mV. Shunts allow sensitive equipment to measure high currents without any risk of damaging the sensor inputs. Figure 3.2 shows a set of 150 A 50 mV shunts at point 'A' with a larger 300 A 50 mV shunt at point 'C'. The larger shunt is there to accommodate the potentially large currents that may occur if the wind turbine and generator were to simultaneously produce their maximum power output into the battery bank.

Current transformers (CTs) are another type of sensor used for measuring current. Traditionally associated with measuring AC current, there are also current transducers which are capable of measuring DC current. CTs have

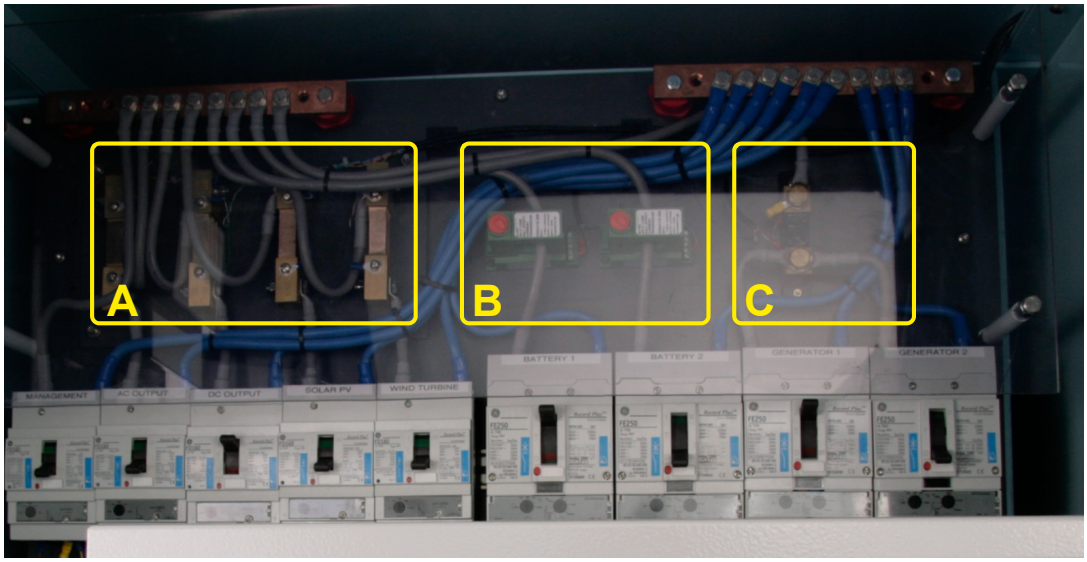

Figure 3.2: Current shunts measuring up to 150 ADC (A), up to 300 ADC (C) and current transformers (CTs) with split cores (B)

several advantages over shunts in that they do not need to be inserted in series with the circuit. The CT is a ring shaped sensor with a magnetic core that has a hole in its centre and the power cable goes though this hole. The current flowing through the cable induces an alternating magnetic field in the coil which is wrapped around the magnetic core and this current is proportional to the load current. AC CTs have a ratio rating between the load and induced current. An example would be a ratio of 100:5 which means if 100 A was flowing in the primary (load) then five A would be flowing in the secondary (CT output). Care must be taken when installing CTs onto a live cables as open circuit connector voltages can fluctuate into the kV range which can be potentially fatal. CTs measuring DC current will often have either a voltage (0 - 5 V) or current (4 - 20 mA) output which is a common input range for measurement DAQs. This type of sensor can be seen in Figure 3.2 at point 'B' where there are two DC CTs in the centre of the Figure. The CTs were useful for this application as they were superior for measuring bi-directional currents to the battery bank and auxiliary connection. Additionally these sensors were equipped with split cores which allowed them to be added or removed from a system without having to disconnect heavy gauge DC cabling with a core size larger than 11mm^2.

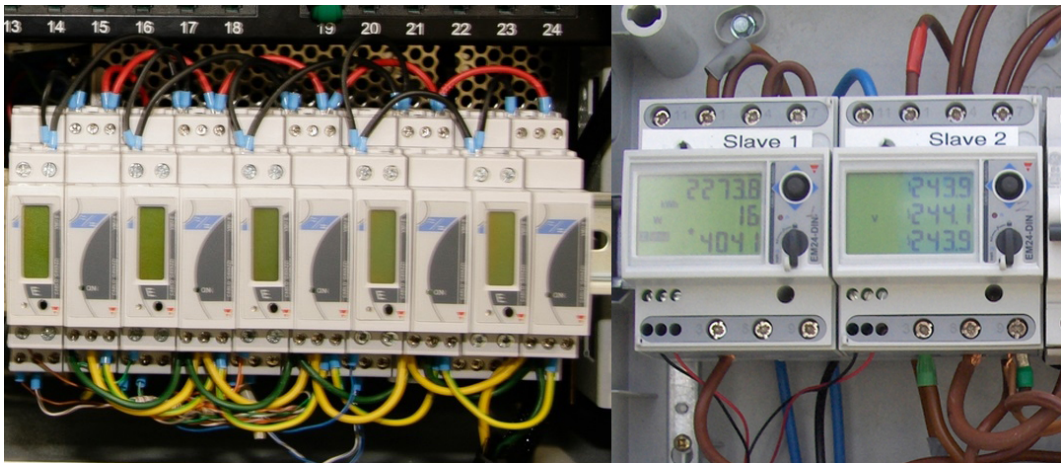

Figure 3.3: Modbus®-based DC Power (Left) and AC Power (Right) sensors

Voltage sensors use a potential divider that steps down the voltage to the level which is low enough to be safely read by a DAQ and also are optically isolated for safety with an opto-isolator. This type of isolation transfers electrical signals from optically within the chip from its input to its output. Voltage transducers were used in this work to step the DC voltage from a 30 - 60 VDC range down to a more manageable zero to ten VDC range. These transducers were later replaced with more modern Modbus® sensors as can be seen in Figure 3.3 which were able to measure both voltage and current simultaneously with multiple inputs. For systems with an AC bus, three phase Modbus®-based power sensors were used to monitor the following values:

- voltage (V)
- current (kWH)
- power factor
- grid power imported (kWh)
- grid power exported (kWh)
- phase one cumulative power (kWh)
- phase two cumulative power (kWh)
- phase three cumulative power (kWh)

These sensors were very useful as they were capable of measuring each of the phases independently which allowed a number of power sources and loads to

be measured simultaneously. As the sensors store the cumulative power (kWh) values for each phase, it allows the system to be remotely monitored with a very low data acquisition rate (hourly) while maintaining an accurate account of the power consumption over time.

The main component of this work is a DC based UPS designed to power remote telecoms base stations which were located in regions with no power grid. The base system consists of a 5.8kW wind turbine, 400Ah battery bank, 6kW DC generator and a 5kW inverter as can be seen in Figure 3.4.

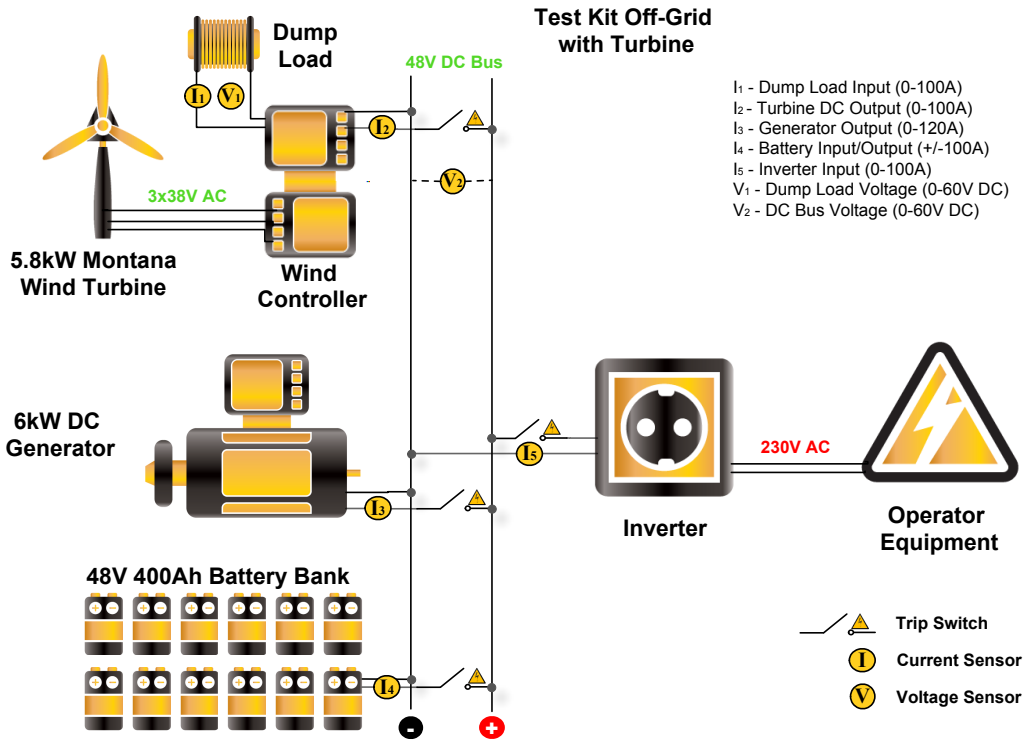

Figure 3.4: High Level Wiring Diagram of off-grid HSRES designed as part of this work

The system operates with a common DC bus so the voltage only needs to be measured at one point. There will be small voltage differences (less than one percent) due to the length of cable runs between devices but this does not make much of a difference overall. The first current measurement point (I_1) is located at the dump load for the wind turbine. The dump load is used to dissipate power in the event that the battery bank does not have sufficient

capacity to store the power generated. The type of current flowing is pulse width modulated (PWM) with one portion going to the batteries and the other to the dump load. As the battery bank becomes full, the duty cycle of the PWM current is dynamically altered resulting in greater proportions of dumped power. Measuring the PWM current results in less accurate current readings [92] especially at low current levels below two amps. As a result of low level inaccuracies and noise, a floor of one ADC was introduced to remove the fluctuations. The high current measurements will be an average of the PWM power which is measured using a 150A 50mV shunt connected to a voltage converter which steps up the 50mV shunt voltage to a ±10V range. The measurement points can be seen in Figure 3.5.

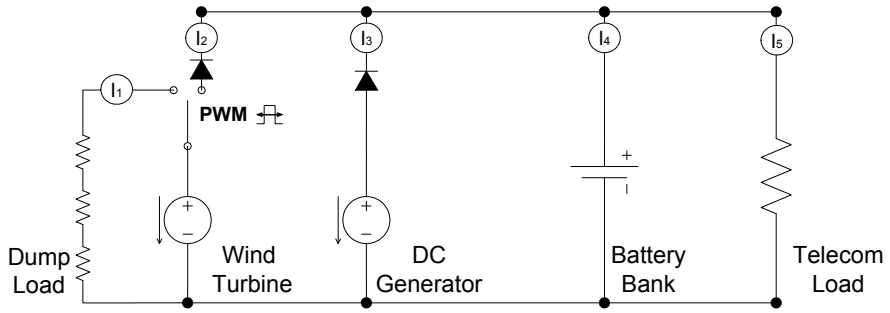

Figure 3.5: Simple schematic of hybrid system demonstrating current measurement points

The second monitoring point (I_2) measures the amount of current generated from the wind turbine onto the DC bus. This current is measured in the same way as (I_1) and would be an inverted version of the dumped current. The generator current (I_3) and the inverter current (I_5) are also measured in the same way. The battery current (I_4) is calculated from the sum of the current sinks and sources. The equation used for this calculation is:

$$I_4 = I_5 - (I_2 + I_3) \tag{3.1}$$

The battery current is positive when supplying power to the load and it is negative when storing power whether that power be from the wind turbine, generator or both. These calculations were carried out immediately after ac-

quisition using LabVIEW^{TM}(see Figure A.1 and Figure A.2 in the appendix) which was operating with a Labjack^{TM}U6 data acquisition device inside the generator enclosure. The monitoring system stored the data in a local database which was periodically synchronised with a central server. The system was internet enabled with a GPRS modem which allowed it to be accessed remotely. This facilitated programming alterations to be made where necessary and access to the latest data. This data was used for several purposes which included mechanical optimisation to the physical system and also observation of the system performance. The electrical operation during a typical charging cycle can be seen in Figure 3.6.

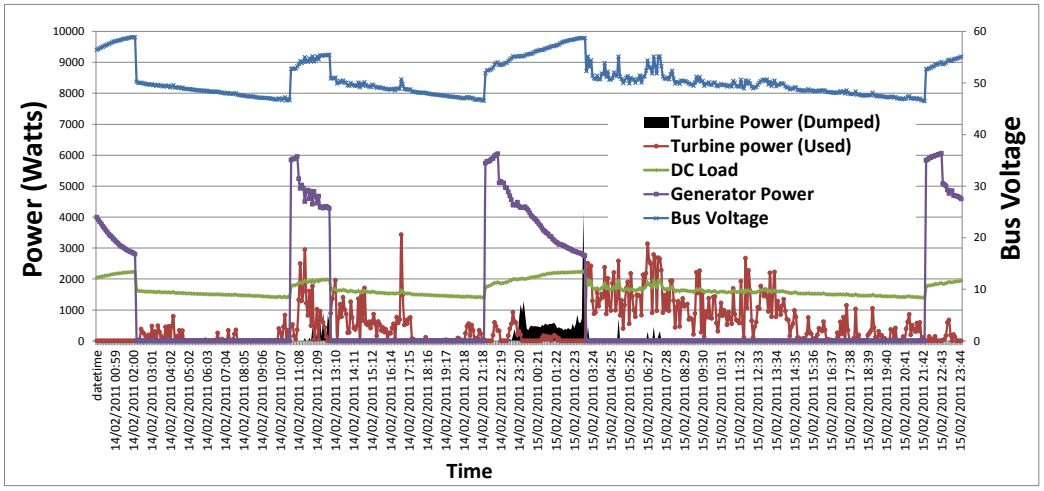

Figure 3.6: 48 hour HSRES operation where excess wind power is being dumped which can be seen on the 14/02/2011 at 12:09 and at 22:19 to 02:23

The data from the HSRES for two days operation can be seen in Figure 3.6. This data shows almost four generator cycles which are supplemented by wind power. During this period a total of 25 kWh of wind power was generated. Of that number, 22 kWh was used by the system while three kW (12%) was dumped as heat (see the solid colour in Figure 3.6 and also in Figure 3.7). This power was dumped by the wind turbine controller as the bus voltage had exceeded the controllers maximum voltage level and this voltage level is always reached in the final stages of a charging cycle.

The graph in Figure 3.7, which highlights the amount of power dumped, power flow from the generator and wind turbine, demonstrates the flow of wind power when the generator is charging the batteries. During the act of charging the

battery bank, the generator engages at a low 'cut in' voltage and disengages at a higher 'cut out' voltage which is referred to as a generator cycle. During a cycle the generator operates in two modes, the first mode is constant current (CC) mode. CC mode charges the battery bank with the highest current that the generator can provide until a specified voltage is reached. This can be seen in the 'Total Generator Power' graph within Figure 3.7 at times 11 hours and 22 hours where the power is maintained at six kW for a period of time. The generator then switches to constant voltage (CV) mode where it maintains a fixed voltage until the battery bank reaches the cut out voltage.

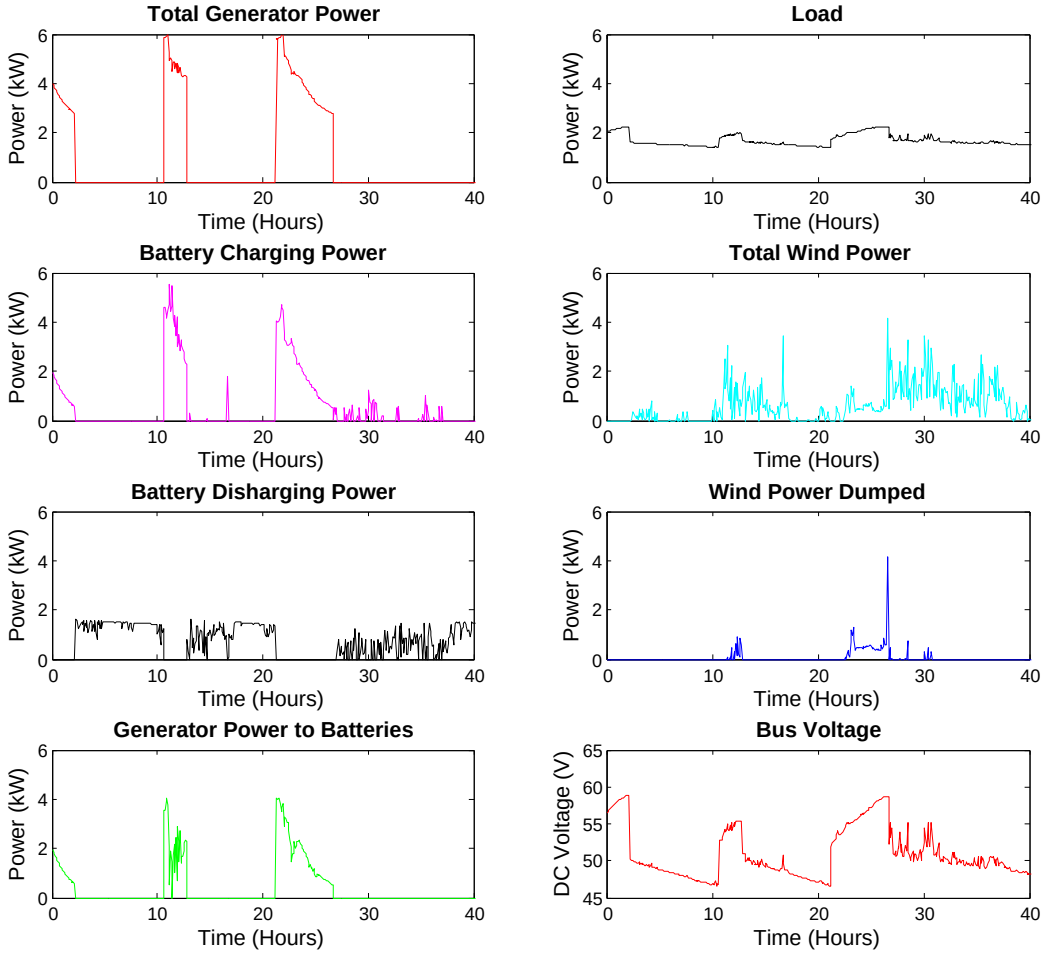

Figure 3.7: Simultaneous energy flow in each of the components in the test HSRES

As the battery bank voltage rises, the power flowing into it, from the generator, will trail off over time. The generator controller is configured to charge

the battery bank using two-stage charging as the three-stage configuration is not economical in a cycling environment [9]. As the battery bank becomes charged, its ability to accept power is diminished [9] which causes the voltage to rise and forces the wind turbine controller to dump power. This power diversion is evident in the 'Wind Power Dumped' graph within Figure 3.7 during the generator charge cycles. Throughout the charge cycle, the voltage of the battery bank is rising as the power is stored. This is evident in the first generator cycle in Figure 3.7 where power is dumped towards the end of the generator cycle where the bus voltage is highest. The second cycle occurs during a much windier period and so the voltage rises faster causing more energy to be dumped.

3.3.1 Grid-tied scenario

Another variation of the HSRES is a configuration where an on grid telecoms site is simultaneously powered with a wind turbine and the grid. The wind turbine, the telecoms load and the grid all share a common AC bus. The wind turbine will contribute to the load and is supplemented with grid power where necessary. When the wind turbine is producing power in excess of the load, the power is exported to the grid as seen in Figure 3.8. This behaviour was not modelled as part of this work. All of the parameters were measured with two energy sensors which were connected via Modbus® directly to a cellular modem. This modem was connected to a central server as a virtual COM port through which the Modbus® values were acquired by LabVIEW™. This implementation was not 100% reliable and was later changed to the cloud based data acquisition device based on the Netbiter® platform.

The monitoring of the base station in the grid-tied scenario is less complicated than the off-grid version as there are less components. The system has a higher reliability as there are less components and hence less potential points of failure. Even if the wind turbine and all the controller electronics fail the load will continue to be supplied from the grid. If any one component fails in an off-grid configuration the system will only remain operational for a period of hours in the best case scenario. The parameters that were monitored are :

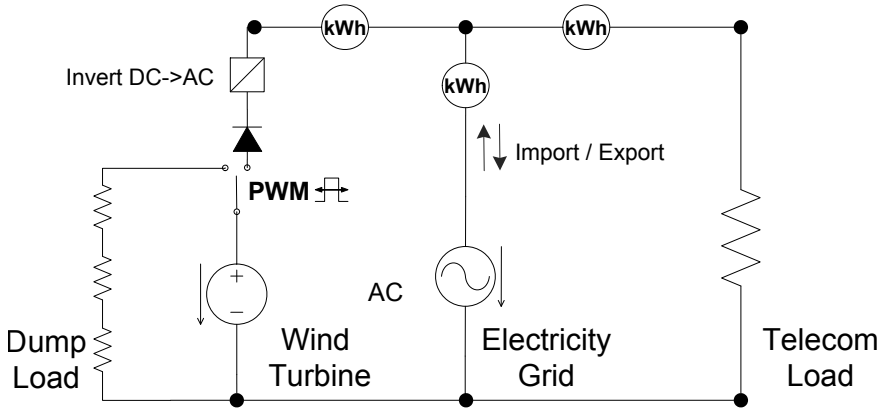

Figure 3.8: Schematic of grid-tied HSRES

- grid power imported (kWh)
- grid power exported (kWh)
- telecoms load (kWh)
- wind turbine power generated (kWH)
- wind turbine instantaneous power (kW)

These measurements were taken on an hourly basis (instantaneous value were recorded every ten minutes). The average instantaneous power values could be taken from the kWh measurements by calculating their rate of change. The purpose of these measurements was to provide a source of telecoms load data. A sample of hourly data from a grid tied telecoms site with 5.8 kW wind turbine can be seen in Figure 3.9.

Instances where the wind turbine power exceeds the telecoms load in Figure 3.9, the power is exported to the power grid. This data ranges from May to October and does not contain any of the wind power extremes which are more frequent during the winter months when the wind turbine will provide its maximum power.

3.3.2 Site analysis prior to deployment scenario

Before the deployment of a HSRES to a telecoms site, the site first needs to be monitored for a period of time to establish its suitability. In its simplest

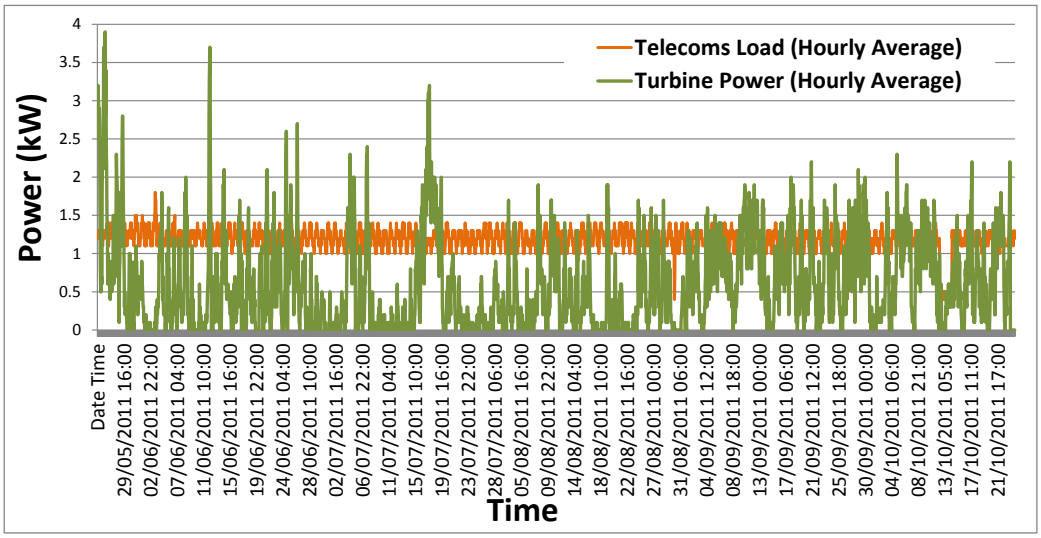

Figure 3.9: Grid tied site data with wind power and fluctuating telecoms load

form, only the power consumption of the site was measured with more complex versions measuring temperature, generator fuel tank level, solar radiation and other parameters. This allowed unseen spikes in the load, such as equipment air conditioning, to be identified. Prospective site monitoring took place at sites in the UK, Ireland, Egypt and Ghana.

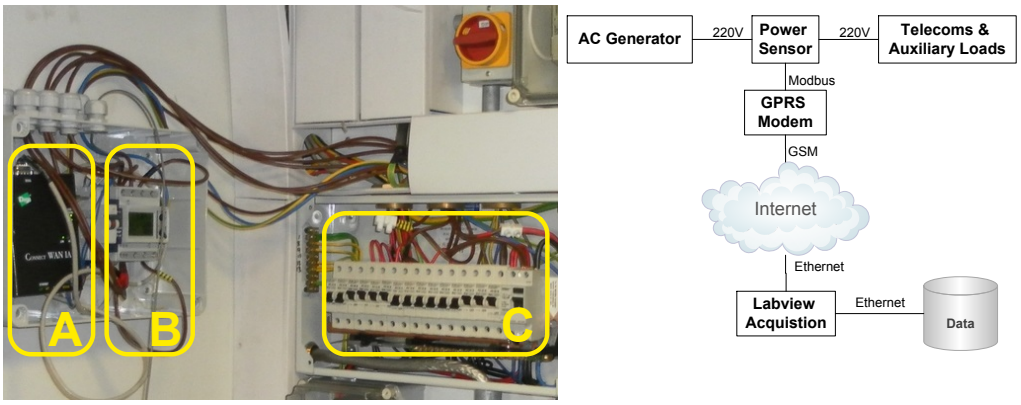

Figure 3.10: Site monitoring undergoing installation with Modbus®-enabled cellular modem (A), three phase power meter (B) which is connected in series to the BTS power lines (C) and overview of the system

The first versions of these monitoring systems were LabVIEW™ based as it allowed working prototypes to be developed and deployed quickly (see Figure

A.3 and Figure A.4 in the appendix). They could also be reconfigured easily to ensure compatibility between different sites and operators when needed. Eventually these products migrated to a cloud based monitoring platform. The initial iteration of the monitoring system was comprised of a GPRS modem and Modbus-based power meter. This system can be seen in the Figure 3.10.

The sensor was constantly polled from the central server to obtain its latest instantaneous and cumulative power values for each phase of the power supply. This type of set-up was suited to initial analysis but as the number of sites undergoing monitoring increased it became necessary to find a 'set and forget' configuration. The Netbiter® technology described earlier in this chapter was deemed suitable for this application. The initial deployment for this data acquisition set-up was in Ghana, Africa. This enclosure, internal electronics and sensors can be seen in Figure 3.11 before it was deployed and in Figure A.6 during deployment.

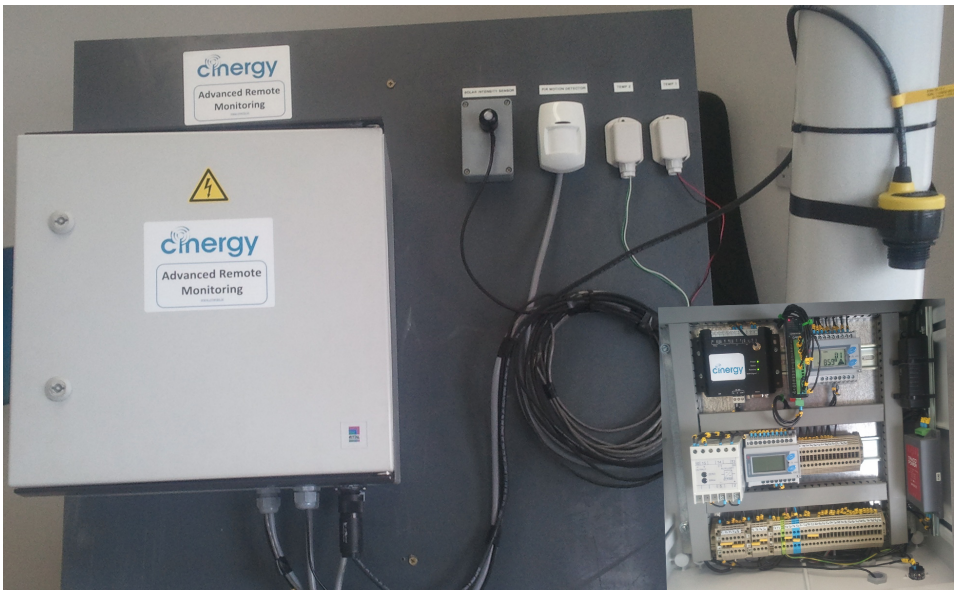

Figure 3.11: Netbiter®-based site monitoring enclosure electronics and sensors before deployment

As this was an African telecommunications site, additional sensors such as solar radiation and temperature were also monitored along with fuel in the tank which was measured with an EchoPod DL14 ultrasonic depth sensor. This sensor periodically sends out ultrasonic pulses from the top of the tank

to the fuel. The time taken for the pulse to be transmitted and received allows the distance to be calculated by the sensor. The most notable findings of this monitoring were the types of loads that the generator was being subjected to on the site. The existing oversized generator was supplying three phase power to energize the site but as is often the case with these systems, the load was not balanced across all three phases. One phase could be supplying 300 W of power with another drawing more than 700 W. Phase imbalance does not physically damage the engine, compared to the damage being done by under-loading the oversized generator, but it does result in a reduction in the effectiveness of line voltage regulation [15].

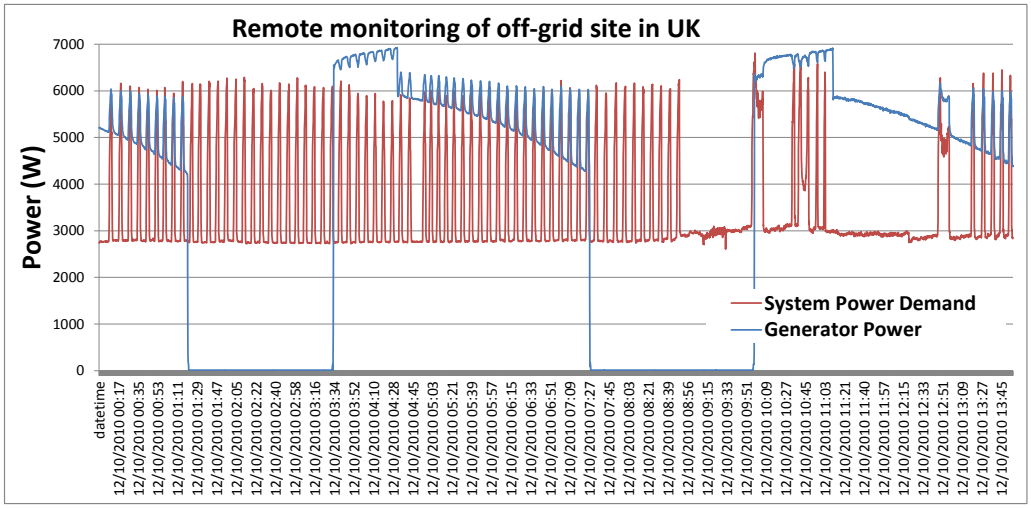

Figure 3.12: A 12 hour sample of site monitoring data

An example of some site data, acquired from a remote telecoms site in the UK, can be seen in Figure 3.12. This data shows the power consumed by the load and the power being produced by the generator. The generator is attempting to charge a battery bank and supply the load at the same time. It is incapable of carrying out this task and at times (see the final stages of the graph in Figure 3.12), the load is consuming more than the generator is supplying. Looking at the first eight and last five air conditioning cycles (spikes between three and six kW) it can be seen that the load partially exceeds the generator power. This implies that the load is discharging the batteries during a charging cycle to make up for the power deficit. A minimum load of three kW can be observed from the graph in Figure 3.12, this is the DC load which

is powering the transmitters. The power spikes represent the air conditioning which is coming on to cool the enclosure. The power consumption from this type of site would be deemed unsuitable for the generator, especially with air conditioning equipment in place. The main factor which makes this site unsuitable is how often the generator is running in this case as it is initiating every three hours. On an appropriately sized site the target would be to have the generator off for eight or more hours to save enough fuel to justify the hybrid configuration.

3.4 Temperature sensing

Temperature sensors (LM35CZ) were used for acquiring data in several locations in both the generator enclosures, electronics enclosures and outdoor temperatures. The LM35CZ [93] is a precision integrated-circuit temperature sensor with a supply voltage (4.5 - 5.5 VDC), output voltage (10 mV/°C) and temperature range (0 - 90°C) and was suited for the environmental conditions experienced by the equipment. Temperature sensing was useful for establishing that a cooling system optimisation was needed. After examination of the data that can be seen in Figure 3.13, the generator cooling system stops air flow at the end of a charging cycle.

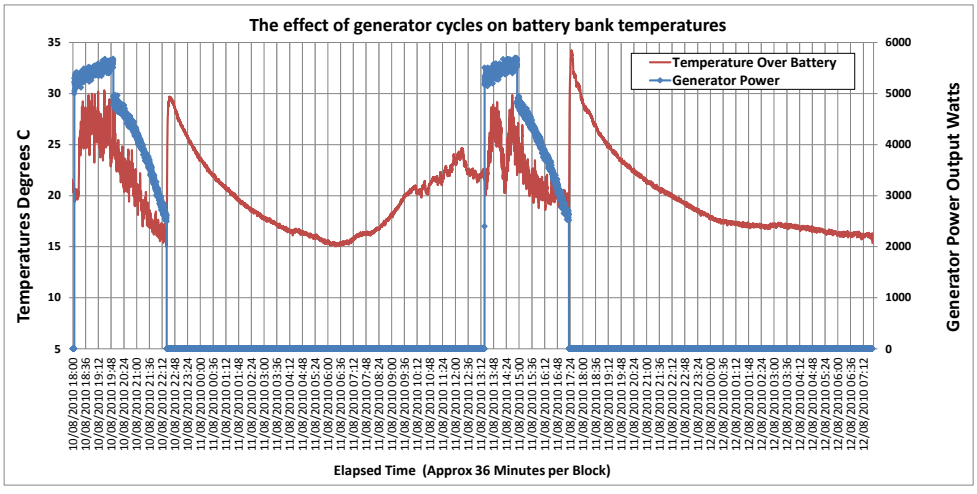

Figure 3.13: Effects on battery bank temperature from a charging cycle

This data shows two generator cycles and the battery bank temperature. The

battery bank is located in the same enclosure as the generator so its temperature will rise due to heat from the engine and also from heat dissipated in the battery bank itself. The ideal temperature for nominal battery bank operation is 20° C (See Figure 2.3 discussed previously) where higher temperatures rapidly degrade the health of the battery. While the average temperature of the data over two days is almost 20 degrees, the battery bank temperature spikes as high as 34° C at the end of a charging cycle. The reason for this spike in temperature is that the generator enclosure is actively cooled by an array of fans while the generator is running. When the generator turns off, the fans also turn off causing the residual heat in the engine and battery bank to heat up the enclosure. The solution to this problem was to configure the generator controller to continue running the fans for a period of time after the generator turned off.

3.5 Solar irradiation

Solar irradiation was acquired in this work to establish the viability of using solar panels instead of wind in certain locations, to analyse how the intensity of the sun affected the temperature inside the generator enclosure and to investigate if there was a correlation between barometric pressure and solar irradiation. It was measured with a sensor [94] known as a Pyranometer in Watts per meter squared (W/m^2). The output range of the sensor is zero VDC when it is dark (0 W/m^2) to 2.5 VDC when there is a solar intensity of 1100 W/m^2. The solar irradiation values can be measured cumulatively or using instantaneous values. This system used instantaneous values as the sample rate was high enough (12 seconds) to allow the information to be interpolated when up-scaling the data.

The sensor was placed horizontally so that the solar values recorded will only take into account solar irradiation falling per m^2 on the horizontal plane. To record the precise value, the sensor needs to be tilted to the optimal angle to take into account the different elevations of the sun throughout the seasons. The difference between the horizontal and optimum tilt solar irradiation measurements is approximately 20% [6].

3.6 Wind speed and direction

Wind speed and direction information was monitored to compare the performance of five different locations on the Dublin City University campus. The primary goal was to use the information from the highest performing anemometer (located at the most exposed location in the university) as a data input for the numerical model detailed in Chapter five. The wind speed and direction sensors are comprised of a reed switch and circular resistor array respectively. The anemometer has a single reed switch with a magnet attached to the rotating cup mechanism which closes the reed switch on each revolution. This gives a pulsed output which is proportional to the speed of the wind. Measuring pulses from a reed switch can lead to a significant source of error as the switch tends to 'bounce' as the magnet passes over it. The switch should only close once but the sensitivity of the DAQ may register multiple closures incorrectly. This system uses a frequency to voltage converter chip instead. This device will convert the incoming pulses into a voltage which is proportional to the frequency of the input. The sensor does not have the bandwidth to measure the high frequency pulses that result from switch bouncing. This limitation filters out the unwanted high frequency signals. The Waspmote can then easily measure the voltage with an analogue input as opposed to trying to count the pulses and avoid the bouncing issues encountered with a digital input.

Figure 3.14: Base-station and the five anemometers deployed across the Dublin City University campus

From left to right, in Figure 3.14, the set of five anemometers are located on the physics building, library, concert hall, research block and on the sports building. The base station beside the anemometer on the physics building receives the data from the other surrounding nodes.

Initial testing, graphing and simulations used hourly wind data supplied by

Met Éireann. This data was sufficient initially but eventually higher frequency data over a longer time period was needed for the model. The laboratory constructed, programmed and deployed a wireless remote monitoring network for five anemometers around the university campus. This installation provides real-time wind speed, direction, pressure, solar and temperature data for the HSRES model described in Chapter five. Each unit records the sensor data every one second, averages the data to a 12s interval and this data is transmitted in bulk every one minute to the central base station. This base station is synchronised to the main lab database every ten minutes to ensure data integrity. The five different locations and deployment configurations can be seen in Figure 3.15.

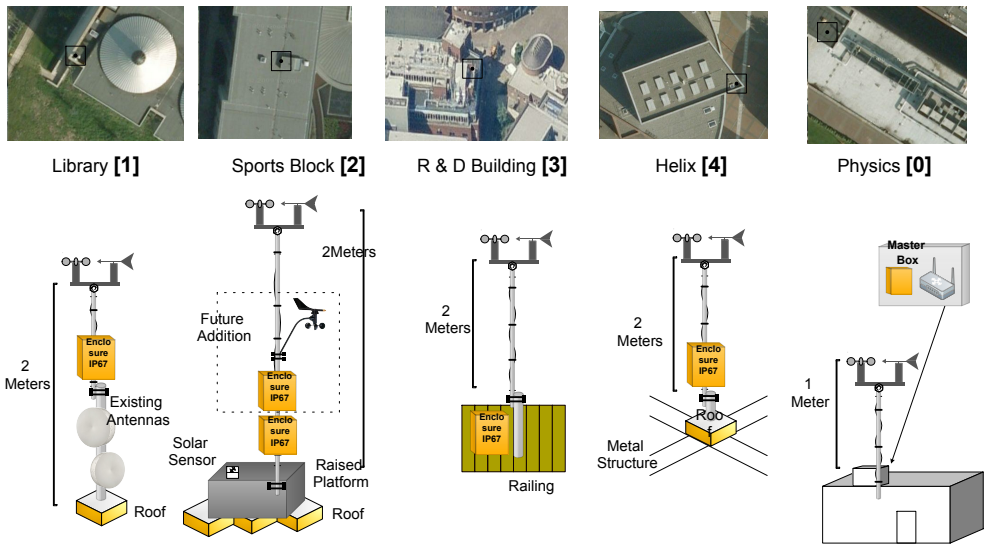

Figure 3.15: Dublin City University anemometer locations

Despite a choosing a lower sampling rate of 12s (averages) there are over five million data points so far available for processing which would prove to be a useful problem for statistical analysis. The construction of the units allowed us to learn from the development of a wireless Zigbee network, sensors, enclosures and mounting. The average wind speeds for the prospective deployment of a commercial wind turbine in the university will also be established after analysing the data. There has been some provisional analysis done on these speeds with the average wind speed for the best location found to be 3.9 m/s and a prevailing wind from a south easterly direction at a height of ten meters.

Provisional wind rose calculations for Dublin City University can be seen in Figure 3.16. This wind data was acquired from February 2012 until November 2012.

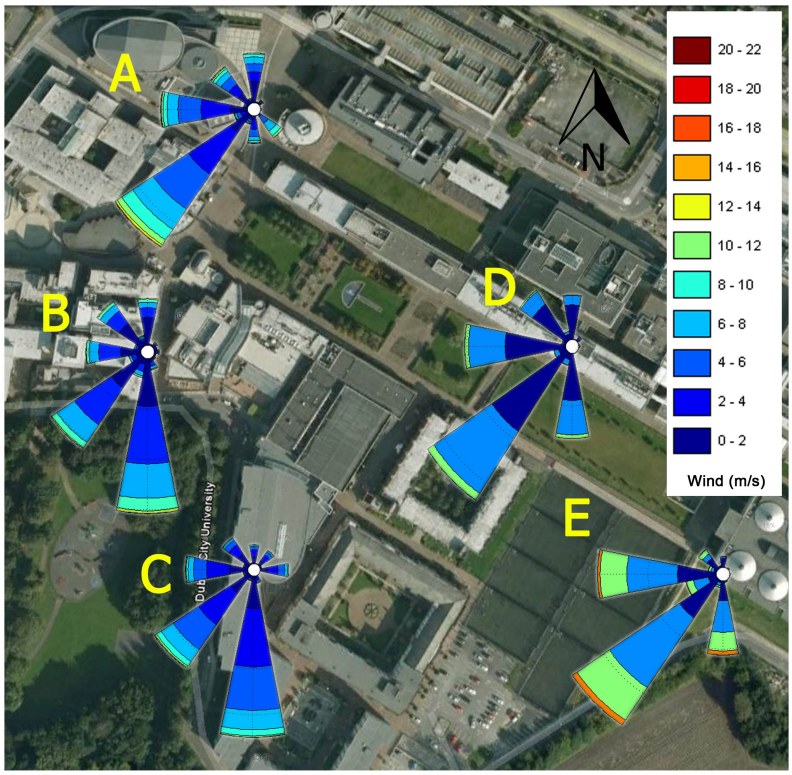

Figure 3.16: Dublin City University wind rose for the first two months of deployment at the five anemometer locations with satellite imagery from Google Maps

Wind rose calculations allow a visual representation of the distribution of wind speed and direction data simultaneously. The magnitude of the sectors highlight the dominant wind directions while the distribution of wind speeds can be seen in the colour codes within each section. Looking at the five locations in Figure 3.16 it can be seen from the sector magnitudes that the prevailing wind is from the south west. Anemometers at location A, D and E reflect this wind direction while B, C do not. These two locations are skewed by their proximity to large trees in a park adjacent to the university and also a higher density in buildings in that area. The anemometer at point E is the most exposed point in the university to the prevailing wind and the colour distribution in the sectors indicate that this location receives higher

wind speeds than the other locations.

3.7 Barometric pressure

The barometric pressure was measured to provide a source of data for the verification of the wind prediction methodology in Chapter four and the numerical model in Chapter five. This system was constructed with a BMP-085 [95] pressure sensor and Arduino™ board with Ethernet Shield as can be seen in Figure 3.17. Arduino™ is a platform upon which users can build on existing content in the public domain. The code for communicating with different sensors is publicly available and it allows a system to be deployed very quickly. The pressure sensor has a resolution of one millibar (mb) which is lower than the pressure data available from the meteorological office which was observed to be a higher resolution when acquired by the lab. This level of accuracy and cost is unnecessary as the methodology proposed in this work is attempting to identify between large changes in barometric pressure and resulting wind velocity.

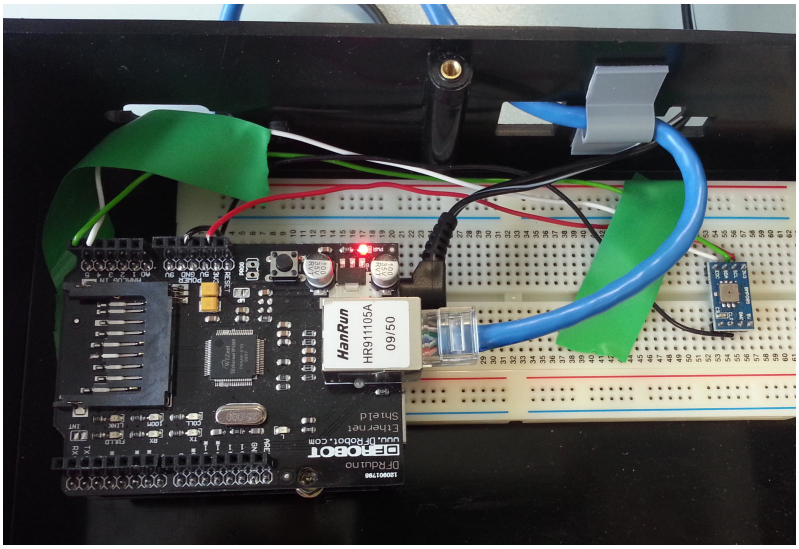

Figure 3.17: BMP085 pressure sensor with Arduino™ based communications

The Arduino™ communicates with the pressure sensor via inter-integrated circuit (I_2C) which is a common communication protocol for chip to chip com-

munications. The Arduino™ board acquires the barometric pressure reading every ten minutes and arranges [91] it into a packet suitable for transmission. The lab server was configured to accept these packets and it automatically stores them in a database once the packet has been received. The pressure readings also need to be corrected for altitude as the uncorrected pressure readings in the university are slightly lower than sea level measurements due to its higher altitude. In this case Dublin City University was found to be approximately 56 meters above sea level including the height of the building it is mounted in. This shifted the pressure measurements positively as pressure decreases with height. The system would still work even if the pressure sensor was not corrected for altitude as it is measuring differences.

3.8 Fuel flow rate

The fuel consumption of the generator was measured using a Fluidwell® fuel flow meter which is a Modbus®-based sensor which is configured to make a differential measurement between the inflow and return fuel lines from a diesel generator. As can be seen in Figure 3.18 the flow meter (B) is connected to the fuel lines (C) and is being used in conjunction with a DC power sensor (A) which will also allow simultaneous measurement of the current and voltage. The sensors were then connected to a common two wire bus which was wired to a Digi® modem with Ethernet to serial interface. This allowed the data to be acquired a safe distance away from the noise and fumes emitted from the enclosed test space which was housing the DC generator.

Diesel generator specifications will often provide a fuel consumption graph which details how the fuel usage varies as the engine moves from an unloaded to a fully loaded state. This specification cannot be completely relied upon as different physical and control configurations would change the fuel consumption profile. Some of the factors which may affect the fuel consumption are altitude, fuel temperature, fuel type, cooling type and the exhaust design [96]. The process of taking these additional factors into account is called generator 'Derating'.

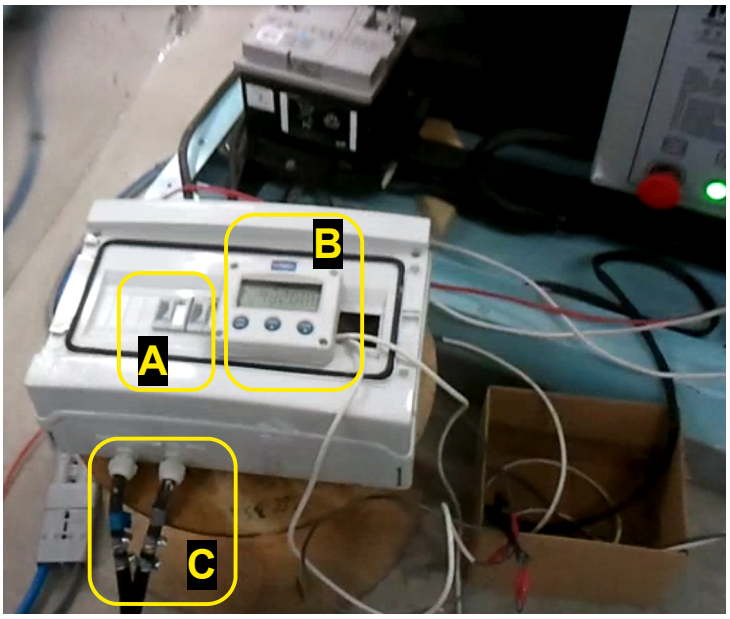

Figure 3.18: Differential fuel consumption measurement using Fluidwell flow meter (B), current and voltage measurement (A) and fuel lines (C)

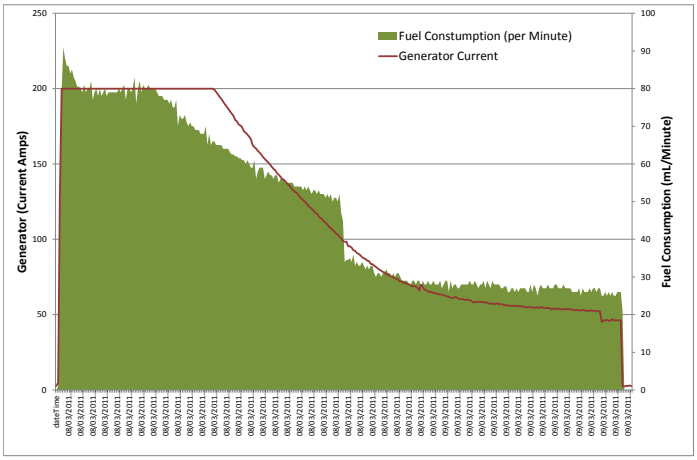

Figure 3.19: Fuel testing graph with current (A) vs fuel consumption (mL/min) for off grid hybrid test system

The off grid hybrid test system was operated in a hybrid configuration so that it could be established how much fuel was consumed per day for different loads. The engine is operating most efficiently when it is running at its rated load [15]. During a product development cycle it also needs to be established how much fuel a new generator was consuming for different battery bank charging regimes. Diesel engines have an incoming and return fuel line so the flow rate

of both lines has to be measured with the difference being the actual fuel consumption. A typical current vs fuel graph can be seen in Figure 3.19. This graphs shows how the fuel consumption decreases as the current decreases. The sudden drop in fuel consumption half way though the cycle is where the engine switches to a lower RPM to finish out the cycle. This fuel graph was very useful for the subsequent development of the generator model as it allowed accurate fuel consumption for a given current to be calculated in real time. This parameter is important for calculating the fuel savings for different control algorithms.

3.9 Summary

This chapter describes the implementation of the different systems used in remotely acquiring all the data used throughout this work. These acquisition systems are described individually along with more detailed information about deployments with these units. Some of the data acquired from these applications is discussed and analysed which gives a better understanding as to how the hybrid systems operate. The data acquired by these sensors is used as a basis for predicting wind speed in Chapter four and modelling the hybrid systems in Chapter five.

Chapter 4

Prediction of wind speed and solar insolation

This chapter discusses short term prediction of incoming renewable energy resources with the intent to reduce generator run time. In particular this chapter looks at wind prediction focusing on barometric pressure changes as a means of making that prediction.

4.1 Introduction

This method will avoid the generator turning on and consuming fuel when a weather system containing higher than average wind speeds is anticipated. This method uses the rate of change of barometric pressure to estimate short term wind conditions and optimise generator dispatch time. There is also scope for savings to be made with the prediction of solar insolation in hybrid systems with battery banks. While wind turbines must dump excess power through resistive loads, solar cells can be switched on and off repeatedly without any risk of damage to the cells. In this way instead of diverting power the solar panel harvests less power over time but this still constitutes a waste of power. If the periods of time where the solar cell has been switched off by the controller can be avoided by ensuring that there is sufficient capacity in the battery bank then an energy saving can be made.

The wind prediction methodology is implemented in the hybrid model described in Chapter five. In this case wind speed and barometric pressure data are used in conjunction with a numerical model of a HSRES to save fuel and reduce emissions.

4.2 Prediction of wind speed

This section details the environmental factors which cause wind speed and the changes in other variables which cause the formation/destruction of weather systems. The different approaches to predicting wind speed are discussed along with the feasibility of integrating them into this work. The section then focuses upon using barometric pressure as a wind prediction mechanism with a detailed discussion on how this can be used to optimise generator operation.

4.2.1 Sources of wind and continental air movements

A pressure difference between two regions will cause air to flow, in the form of wind. Heating the air due to a temperature increase from the sun or movement across warm surfaces, such as the oceans, will cause the gas to expand and also cause airflow. This work focuses on the air flow that occurs due to pressure gradients inside low pressure systems moving across the sea and continental land masses. The pressure gradient describes the change in barometric pressure levels around a high or low system. This gradient is represented with isobars, typically placed at four millibar (mb) intervals, connect regions with the same pressure. The higher the proximity of these lines to each other, the higher the pressure gradient and larger subsequent wind speeds [97, P.183]. The 'Coriolis effect' affects the earth's wind flow as a result of the planet's rotation which causes rotational wind movement within these areas of differing pressure. Anti-clockwise air movements are a characteristic of low pressure regions known as cyclones and clockwise air movements are high pressure systems knowns as anti-cyclones.

As depressions move (see Figure 4.1) from one region to another, the baromet-

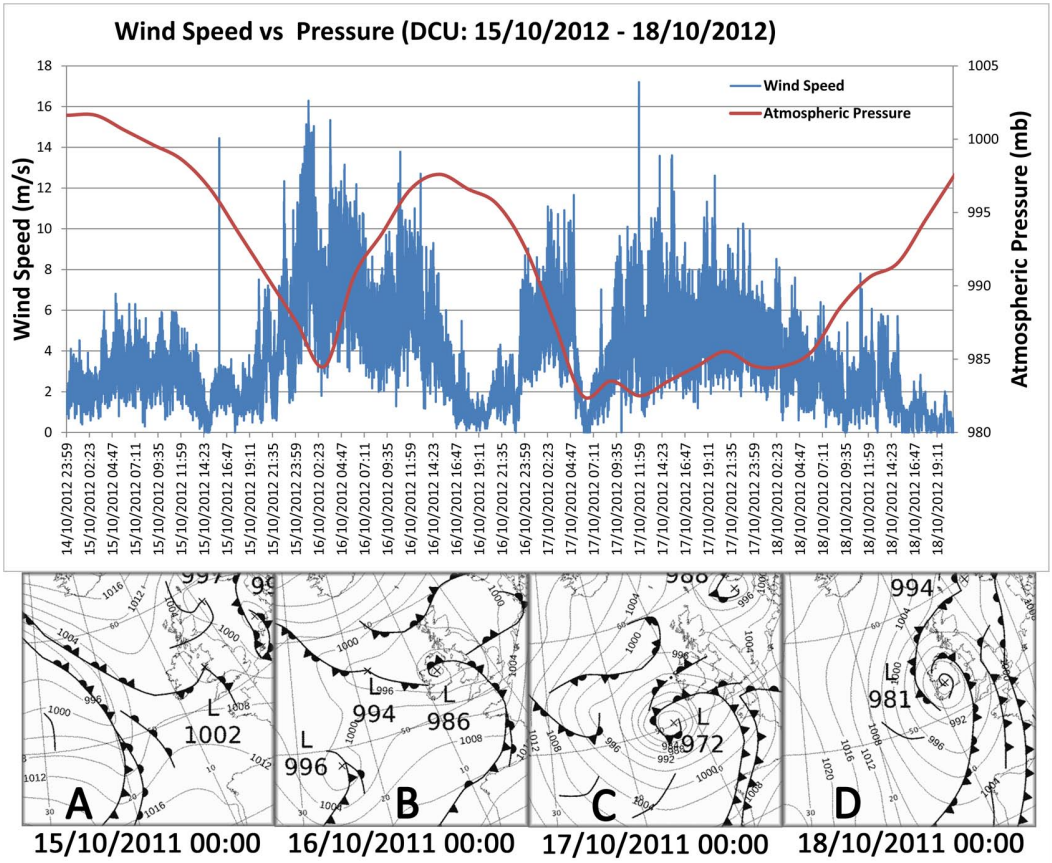

Figure 4.1: 72 hours of cyclonic activity with wind speed, barometric pressure and synoptic charts

ric pressure changes, within a certain range when measured at fixed points. This range typically varies 950 - 1030 mb with extremes outside this range in extreme weather conditions such as hurricanes [98]. Figure 4.1 was constructed with barometric pressure and wind data acquired in Dublin City University in addition to four days of historical weather charts [99] from the same time period. The chart's cover an area of $6{\times}10^6 km^2$ including western Europe, southern Iceland and a large portion of the Atlantic ocean. Chart A in Figure 4.1, recorded on the 15th October 2011, which only creates a 'gentle breeze' on the Beaufort scale [100], demonstrates the low wind speeds that are evident when the isobars are largely spaced. Over the next 24 hours this low pressure system deepened with a decrease in pressure from 1004 mb on chart A to 986 mb on chart B. This deepening pressure system also caused an equivalent in-

crease in gradient wind speeds ('near gale' or greater than 17 m/s) as a result of closely spaced isobars and the eye of the depression located close to the measurement location in Dublin City University.

During the day on the 16th this pressure system dissipated but another low pressure system, approaching from the Atlantic, deepened further as it approached the southern Irish coast. Between the evening of the 16th on chart B and the early morning of the 17th on chart C the pressure decreased again with higher than average wind speeds but lower than the previous day as the eye of the depression was located several hundred kilometres off the Irish coast. By the 18th on chart D the depression had swung northwards over Ireland but by this stage the strength of the cyclone was weakening and the isobar spacing broadening. As the cyclones approach the measurement location the decrease in pressure and corresponding increase in wind speeds can be seen in the graph of locally recorded information in Figure 4.1.

4.2.2 Rationale for wind prediction and current techniques

The growing installed capacity of wind power has led to an increased focus on forecasting techniques which increase the reliability of integrating it into the national power grid. The variable nature of wind means that its power can fluctuate significantly over relatively short time scales. These fluctuations can occur over a matter of seconds with large gusts of wind but these sudden variations tend to be smoothed out by the wind turbine which will take time to respond due to its size. Over longer time frames measured in hours and days the wind speed can vary dramatically due to approaching weather systems or diurnal wind variations where the wind speed varies during the day/night due to varying landmass temperatures.

This behaviour requires a certain amount of spinning reserve on the grid where thermal generators can immediately begin supplying power to the grid during sudden lulls in wind power. Accurate forecasting reduces the amount of spinning reserve required to accommodate the uncertain levels of wind power onto the grid which reduces costs and allows a greater wind penetration overall

[101]. The cost of spinning reserve can be reduced further with the integration of large scale storage into the power grid [102] which can manage both under and over production of wind power. The time scale for wind forecasting is divided into four levels [10] and an example of their uses in commercial wind forecasting:

- Very short term: From few seconds to 30 minutes ahead.
- Short Term: From 30 minutes to six hours ahead.
- Medium Term: From six hours to one day ahead.
- Long Term: From one day to one week ahead.

Each of the timescales facilitate the decision making process of the day ahead electricity markets. This allows operators to commit to generating a certain amount of power while incurring penalties or increased market prices if they fail to meet their targets. In the case of off-grid hybrid systems, the time scale is limited by the number of hours of backup offered by the battery bank. While a backup period of 24 hours is recommended [20] as the optimal cost and storage level for an off-grid HSRES, operators may choose lower storage levels (8 to 12 hours) to reduce capital expenditure which leads to lower upfront costs. This reduces the time available for predicting wind power before the generator is forced to initialise charging. Lower storage levels increase the risk of a system outage as there is less time available to deploy a repair team to the site if a generator has broken down. Table 4.1 outlines the different forecasting methods which are the current state of the art of weather forecasting.

The persistence forecasting method is based on the principle that the wind speed now is going to be very similar in the future. If the average wind speed now P(t) is seven m/s then in 30 minutes time P(t+k) it is likely to be close to seven m/s. As the time period increases the accuracy decreases and which explains why this method is limited to short term forecasting [10]. This method was developed by meteorologists as a tool to complement numeric weather predictors (NWP). The long computation time and poor short term accuracy of NWP meant that this method was proven to be more effective over very short-term prediction windows [103]. Persistence forecasting would not be suitable for the control algorithm that was implemented as the system

Forecasting Method	**Subclass**	**Examples**	**Remarks**
Persistence Method/Naive Predictor	-	*P(t + k)=P(t)*	-Benchmark approach -Very accurate for very-short and short term
Physical Approach	Numeric Weather Predictors (NWP)	-Global Forecasting System -MM5 -Prediktor -HIRLAM, etc.	-Use of meteorological data such as wind speed and direction, pressure, temperature, humidity, terrain structure etc. -Accurate for long term
Statistical Approaches	Artificial Neural Network	-Feed-foreward -Recurrent -Multilayer Perceptron -Radial Basis Function -ADALINE, etc.	-Accurate for short-term -Their hybrid structures useful for medium to long term forecasts -Usually, outperform timeseries models
	Time-series Models	-ARX -ARMA -ARIMA -Grey Predictors -Linear Predictors -Exponential Smoothing, etc.	-Accurate for short-term -Some very good time-series models supersede NN structures.
Some New Techniques	-	-Spatial Correlation -Fuzzy Logic -Wavelet Transform -Ensemble Predictions -Entropy based training, etc.	-Spatial correlation is good for short term -Entropy based training of model improves performance. -Considering non-Gaussian error pdf improves accuracy
Hybrid Structures	-	-NWP+NN -ANN + Fuzzy Logic = ANFIS -Spatial Correlation + NN -NWP + timeseries	-ANFIS is very good for very-short term forecast. -NWP + NN structures are very accurate for medium and long-term foecasts

Table 4.1: Wind speed and power forecasting methods [10]

needs to know if there is going to be a change in the wind speed. For the purposes of this work the control system does not need to know precise wind

speeds like the algorithms in the literature attempt to achieve. Instead the system needs to know what volume of wind to expect to ensure that there is sufficient capacity to store the excess energy.

The physical approach to predicting wind speed and weather patterns in general using NWP is the standard tool used by meteorological departments [10]. As briefly described in table 4.1 this technique uses large sets of meteorological data which is integrated into sophisticated weather models to make a prediction. The processing of this data requires vast computing power and with the processing power of a supercomputer, a 'run' typically takes up to six hours [10]. High end supercomputers tend to consume multiple MW of power which means that the energy cost of a single 'run' would consume more energy than the algorithm would save in the system lifetime. This restricts this type of prediction to medium to long term predictions which are relatively accurate up to five days in advance. This type of weather prediction is useful for commercial wind farms which can use the information to enhance dispatch control decisions [104]. This information would improve the control regime in a HSRES but issues such as the resolution of the predictions (terrain is typically divided into a grid with blocks of $15km^2$ or larger [10]), local terrain and cost of accessing the data would need to be resolved. Research has shown that by combining NWP approaches with other prediction methods with local data can improve the local forecast [105].

Statistical forecasting requires the use of historical weather patterns as training data for different algorithms. The amount of training data required can range from as little as 24 hours using neural networks to as high as 28 months in some cases using Markov models [106]. Artificial Neural networks (ANN) are accurate forecasting tools for wind prediction [107], especially when combined (Hybrid Structures) with some of the new techniques such as fuzzy logic [10, 108, 109, 110]. An ANN based forecasting system would potentially offer a suitable platform to enhance the control system algorithm. ANN's have already been used to predict short-term wind speeds in an off grid hybrid context [111] with the ability to match variable loads with simultaneous turbine and fuel cell outputs. The main issues with ANN processing are that it is seen as a 'black box' approach where interactions between neurons are difficult to

quantify. Many implementations are continuously retraining themselves with new data and this could be seen as a liability by commercial users who prioritise reliability over price.

4.2.3 Barometric pressure

The method proposed here keeps track of this pressure gradient using a barometric sensor as the pressure systems in the region move above it. Pressure gradients have been used recently to predict [112] wind speed using hidden Markov models (HMMs) to identify cross dependencies between barometric pressure and wind speed. Barometric pressure has also been found to be the most important variable when predicting step ahead wind speed using data mining methods with NBTree as the prediction model [113]. NBTree is a hybrid model combining the use of data clustering techniques with Naïve Bayes classification. Their motivations are analogous to those in this work in that they are striving to provide a solution to users who were frustrated with the use of black-box-like expressions that do not explain the relationship between input and output. The relationship between the data input and output in this work is intended to be much clearer than black-box type methods. Using a barometric pressure differential over a three hour period the pressure gradient is monitored and applied to a marine meteorological scale [11] as seen in table 4.2. An example of this would be, if a barometric pressure gradient of three mb in three hours was measured then the likelihood of wind with speeds approaching ten m/s occurring in the short term (30 min to six hours) is very high. This was observed to be the case at the measurement location used in this study and can be seen occurring in Figure 4.1.

The pressure differentials have been focused into three categories as demonstrated in table 4.3. Pressure changes are generally small and the majority of changes, over a three hour period, are less than two mb as can be seen in the pressure gradient instances element of Figure 4.2. Pressure changes between two to three mb and higher are less frequent but more significant in terms of the amount of wind recorded in the hours following the pressure changes. It can be seen in the wind recorded six hours after pressure changes section of

Tendency over 3 Hours (mb)	**Marine Forecast Term**	**Approaching Weather**
<0.1 mb	Steady	Calm
0.1 - 1.5 mb	Rising (or Falling) Slowly	Light Breeze
1.6 - 3.5 mb	Rising (or Falling)	Strong Breeze
3.6 - 6 mb	Rising (or Falling) Quickly	Gale
>6 mb	Rising (or Falling) Rapidly	Storm

Table 4.2: Marine forecasting terminology for barometric pressure tendency [11]

Figure 4.2, small changes in pressure result in a higher occurrence of low wind speeds.

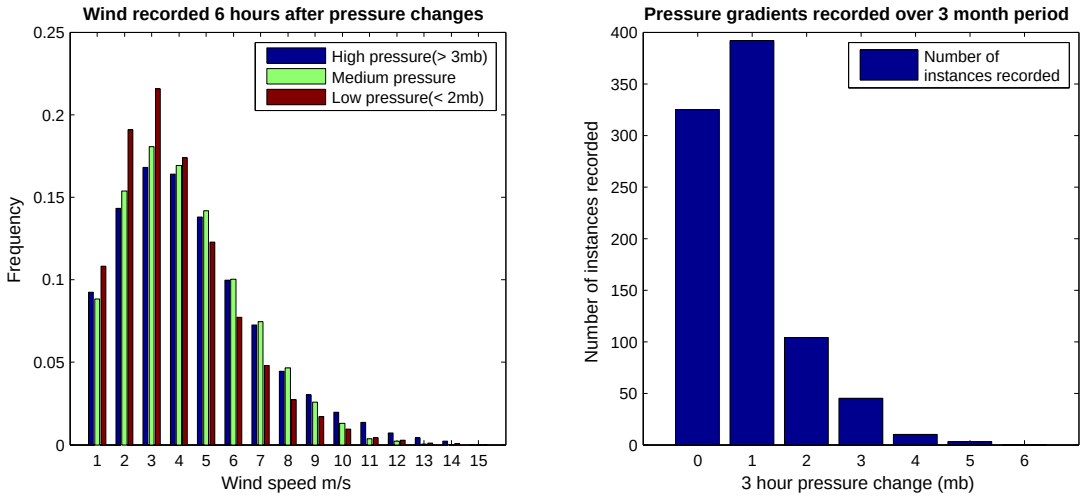

Figure 4.2: Normalised wind speeds recorded after pressure changes and how many of these changes that occur in a three month period

A period of time with low pressure changes over a three hour time frame can be seen in Figure 4.3. This graph shows the wind speeds in m/s recorded by an anemometer, the barometric pressure and the generator signal as described in table 4.3. This graph demonstrates that when the barometric pressure is stable the wind speed during this period is low in terms of its potential for power generation. Through out this period, the generator will receive a signal of '3' which causes it to remain in its default charging configuration. A single data point sends a signal of '2' to the generator during this period as a result of an isolated pressure drop that does not persist in subsequent pressure recordings.

Tendency after 3h	Wind Speed Expected	Suitability for 1.2 kW Load	Charger Response & Signal	Expected kWh from wind
< 2 mb	< 5m/s	Cannot sustain load	Charge (3)	< 5 kWh
$\geqslant 2$ AND < 3 mb	5m/s to 10m/s	Can sustain load and periodically charge battery bank	CC Mode (2)	~ 10 kWh
$\geqslant 3$ mb	> 10m/s	Can sustain load and charge battery bank	Inhibit charging (1)	> 20 kWh

Table 4.3: Table describing relationship between expected wind speed, charging signal for 1.2 kW average load and approximate power generation for subsequent 12 hours from a 5.8 kW Fortis Montana wind turbine

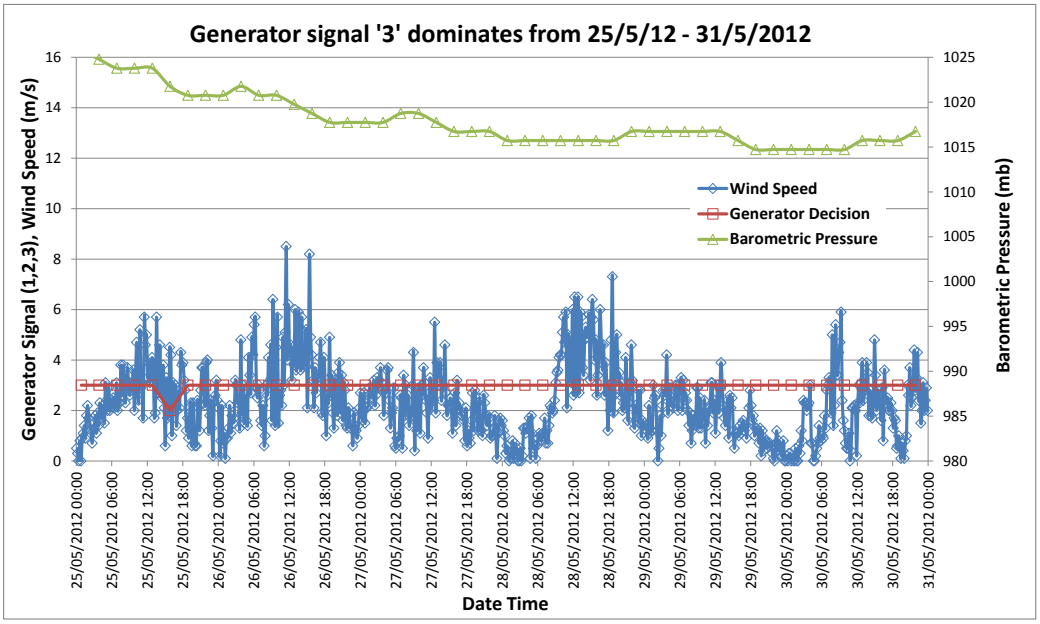

Figure 4.3: An example of instances where pressure changes of less than 2mb over three hours which sends signal '3' to the generator

It can be observed that pressure changes between two and three mb demonstrate relatively higher wind speeds between five and eight m/s. This type of activity, with pressure changes between two and three mb per hour, can be seen in Figure 4.4. During this time the barometric pressure falls from

1016 mb to 1004 mb which results in a sustained signal '2' being sent to the generator to ensure it remains in CC charging mode. This ensures there is capacity in the batteries to accept the power produced from the subsequently higher wind speeds which can be seen to occur from the pressure drop. It has been discussed previously that increases in barometric pressure generally do not translate into higher wind speeds. This can be seen to be the case as the pressure increases again in the second half of the period in Figure 4.4. In this period, if the increasing pressure was not ignored, it would have resulted in a signal '2' being sent to the generator which would have impeded its charging but with no gain as the wind speed was decreasing.

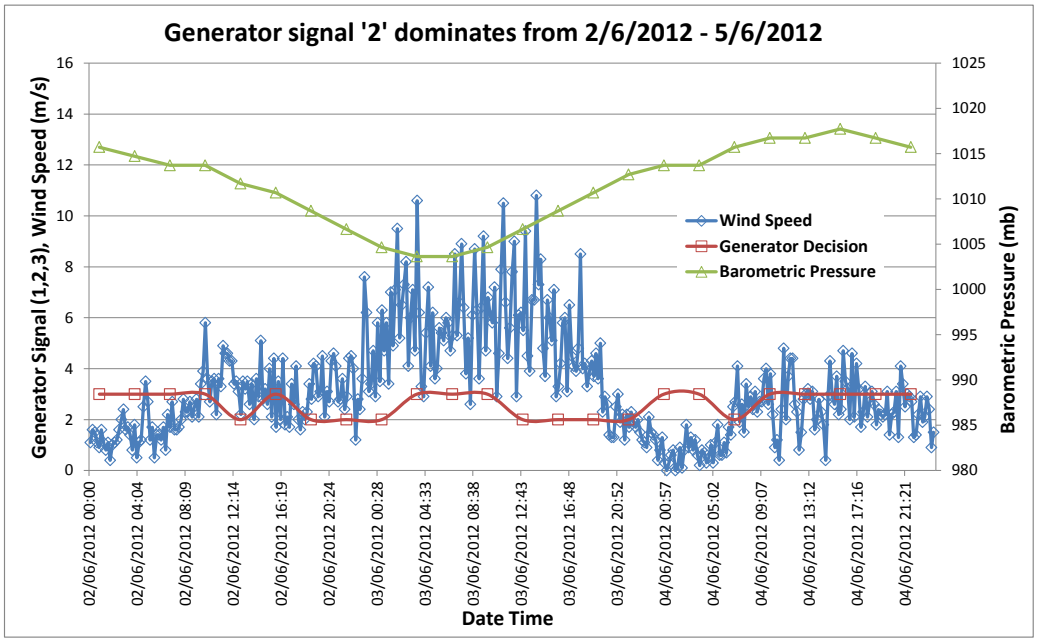

Figure 4.4: Pressure changes greater than 2 mb and less than 3 mb over three hours which sends signal '2' to the generator

Pressure changes of three mb and higher show comparatively higher wind speeds between nine and 14 m/s which is the region that produces significant amounts of wind power. While the wind speed distribution beyond nine m/s appears low it must be remembered that every time the wind speed doubles, the power increases by a factor of eight [81]. A period of time with barometric pressure changes greater than three mb over three hour intervals can be seen in Figure 4.5. The barometric pressure is initially stable but this quickly drops

leading to a very substantial increase in wind speed. As the wind speed begins to rise the generator has already received a signal of '1' from the controller which causes it to immediately shut down. Despite a dramatic increase in pressure, this fails to translate into a substantial increase in wind speed as is the case when there is an equivalent decrease in pressure.

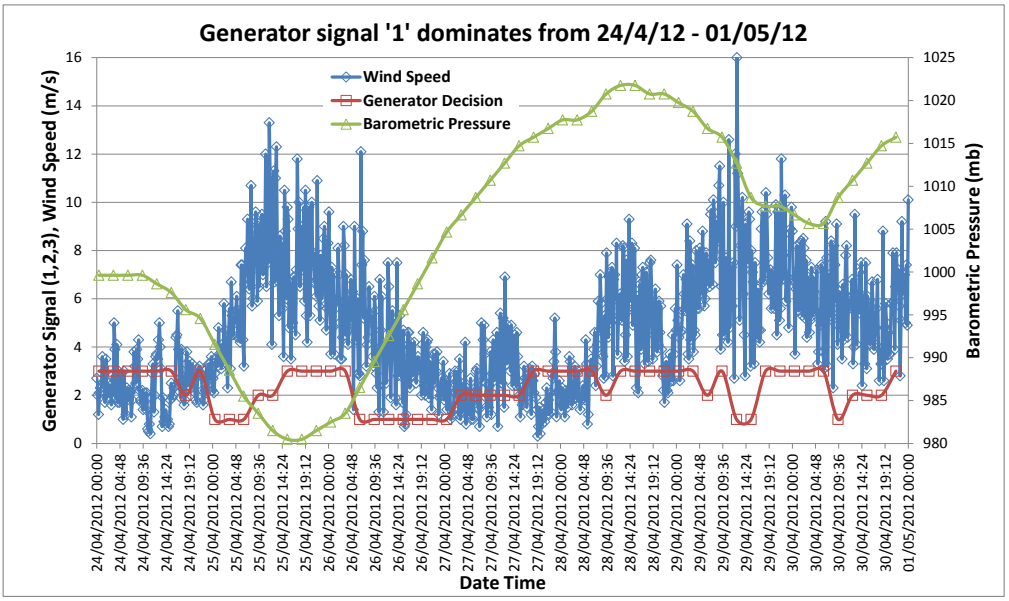

Figure 4.5: Pressure changes greater than 3 mb which sends signal '1' to the generator

The decisions in table 4.3, chosen heuristically, are made for an average load level of 1.2 kW and a wind turbine power profile which is skewed towards higher wind speeds for its rated load. The constraints in the table would be modified for different site locations, load types and contributions from renewable energy components. Larger or more efficient wind turbines will produce more power in low wind speeds would allow for more aggressive charging signals as there is a higher likelihood of their power output meeting the load. Similarly, a lower load is more likely to be supplied by a turbines power output in low wind speeds so the generator could be stopped earlier. The wind speed and barometric pressure data was acquired on the east coast of Ireland in Dublin City University as described in [91].

4.3 Summary

The meteorological reasoning behind the formation of weather systems and the resulting wind speeds is introduced while focusing on the changes in barometric pressure. A review of literature on existing wind and weather prediction techniques is carried out for different forecast methods with a brief discussion on their suitability for this work.

The discussion goes into more detail describing the barometric pressure technique used in this work and what control decisions are made from the patterns analysed. The three control decisions are investigated with emphasis on the barometric pressure changes required to trigger them. This technique is implemented and simulated in the model described in Chapter five.

Chapter 5

Modelling Hybrid Energy Systems

This chapter combines the components of a HSRES discussed in Chapter two, the performance profiles of these components from data acquired in Chapter three and the wind prediction methodology introduced in Chapter four. The combination of these elements aims to attain a fuel saving by simulating a numerical HSRES model using Simulink® which is optimised to anticipate and react to future wind conditions.

5.1 Introduction

Previous chapters have focused on the acquisition and characterisation of data from each component in a HSRES apart from the battery bank. This information acquired from the physical HSRES test system formed the basis of a numerical model which was used to simulate different HSRES configuration settings. The model uses the individual performance profiles derived from the data acquired from the remote monitoring equipment installed on the physical test system. Modelling different HSRES configurations is the quickest and most cost effective technique for testing different components and establishing how they operate together.

The real world testing of a hybrid generation system costs a great deal in terms of time and financial burden. The power production profile from a wind turbine or an array of solar cells must be designed in conjunction with appropriate controller charging algorithms to suit the battery bank. The number of hours or days of autonomy, maximum charge/discharge current, temperature tolerances, cell voltage and battery bank type, need to be chosen before deployment. The size of the battery bank generally determines the type of generator in terms of its power rating as larger battery banks can accept larger amounts of current in addition to the load which also must be powered. The simultaneous performance of all these components operating together must be analysed so that the charging regime can be finalised before deployment.

While this testing is necessary in the commercial market before deployment, a computer model is sufficient for testing different control mechanisms to allow technicians to get a better starting point for component settings. There are several simulation packages used to model hybrid systems in this research area. For example Simulink® [29] and the Hybrid Optimization Model for Electric Renewables (HOMER) [114] are a popular choice for researchers in this area.

5.2 Modelling hybrid systems

There are two simulation platforms which feature prominently in the small scale HSRES area. Each of the platforms have strengths and weaknesses which are highlighted in this section along with the reasoning for choosing one for this work. Both platforms use a visual programming language (VPL) in that the code is 'block diagram based' rather than 'text based'. This allows the user to use icons and boxes to visualise the data (or in this case power) flow during simulations.

5.2.1 Modelling using HOMER

HOMER is a modelling environment with pre-existing component models for different sized generators, solar panels, wind turbines, fuel cells, hydro, utility

grid, a wide range of different loads and storage methods [115]. These components can be connected together in a block diagram on an AC or DC bus where their performance can be evaluated. This software allows a user to get a system model running quickly with a high degree of accuracy as its library of components come with suitable pre-set profiles and data outputs. It does not allow the low level control system modifications and accommodation of real time wind/pressure data into the model as is described in this work. It is very accessible software in that it does not require the user to have in-depth knowledge of the low level operations of the systems which they are simulating.

HOMER is useful for carrying out financial analysis for prospective hybrid systems with detailed costings for each of the components, fuel and maintenance [116, 117]. It has been used to provide a state of the art review of hybrid energy systems where it was highlighted that despite their fuel savings the high costs are impeding their development [35]. It is seen as an entry level configuration tool by the GSMA [118] with a focus on system evaluation [33] and economics with the ability to simulate hybrid power systems for telecoms sites [42, 119, 43]. Despite having a different load profile, the design of hybrid systems for small isolated villages [19] has many design similarities to telecoms systems in terms of the types of loads and storage requirements.

5.2.2 Modelling using Simulink

Simulink® is a powerful modelling tool which can be used to construct programs with coded block diagrams. This approach requires a more in-depth, low level and technical understanding of the system than is the case with HOMER. This allows for a tailored model which can be built to solve for the operational characteristics of each component. It is more flexible in terms of the types of calculations that can be performed and how it can integrate easily with dynamic data sources which would be changing in real time.

Simulink® has been used as the basis for a multitude of small scale hybrid wind-diesel models. It was used to simulate a hybrid wind-diesel system with two generators with the ability to start each generator economically based on the size of the load and the power contribution from the wind turbine

[120]. The addition of the wind turbine led to a marked reduction in the COE with the economic dispatch of generators reducing the cost further. Economic dispatch of generators is the process of deploying different generators to suit the load requirements at different times. An example might be small loads during the night time powered by a small generator with large peak loads in the daytime supplied by a much larger generator. Some models attempt to maximise the amount of power extracted from the wind turbine while at the same time maintaining power quality which is important for grid based systems [121, 122]. These systems, implemented through modelling, the provision of wind power to an active grid without the need for storage.

Additionally, hybrid system configurations are very useful when powering remote villages which are cut off from the central grid, an application which shares common traits with the simulation methods in this work [29, 32, 123]. Simulink®-based models have become popular in the area of hydrogen fuel cell research where fuel cells and electrolyzers are being integrated into hybrid systems [124] as a means of either replacing the battery bank, diesel generator or sometimes both. Trends in hybrid deployments have indicated that as costs become lower, these systems will gain more traction as viable solutions for powering off grid sites [125]. This is of particular importance to solar based hybrid systems which have high initial costs but are still viable for powering hybrid sites as demonstrated in several models [126, 127, 128]. Simulink® was chosen as the simulation platform for this work to allow custom refinements to be made to the generator control system.

5.3 Model components

This section details the characteristic equations and configuration settings of each of the components in the hybrid system. Some of the features in the code are discussed in terms of how the components perform their calculations and how they integrate into the overall model. The equations for each component were found by applying a polynomial fit to the source data in Matlab. The range of the polynomial fit function can vary from a fourth to tenth degree polynomial with higher degree polynomials usually providing a better approx-

imation to the data. Better approximations are not always possible as it is affected by the number of points in the source data.

5.3.1 Wind Turbine

The wind turbine controller used in the physical system is designed for charging a 48 VDC battery bank and is rated to operate with a 5.8 kW Fortis Montana wind turbine. The turbine supplies three phase 'wild' AC which varies in frequency/amplitude depending on the wind speed and this is rectified to charge the battery bank. The charger is configured to deliver power to the battery bank while the voltage is below 56.4 V. Typically a battery bank based on AGM technology should be charged up to 58 VDC but this charger is configured for a conservative voltage level to reduce the risk of overcharging. As the voltage of the battery bank approaches 56.4 VDC the controller will begin to dump power through its resistor banks to dissipate the excess power. It achieves this diversion using Pulse Width Modulation (PWM) switching from a duty cycle of 0%, which allows all the power to the battery bank, to a duty cycle of 100%, where all of the power is being dumped into the resistor bank and dissipated as heat. The point of transition where the duty cycle changes can be seen in Figure 5.1.

In Figure 5.1 the PWM controller is given a fixed voltage sequence to demonstrate the stages before, during and after the wind controller dumps power. This emulates the scenario where the batteries are undergoing a charging cycle from the diesel generator and the voltage is slowly rising towards the final voltage of 58 VDC limited by the generator. As stated previously the wind controller will dump all power with a bus voltage above 56.4 VDC and this can be seen to occur in the final stage of a generator charging cycle. Beyond this voltage the duty cycle stays at 100% until the charging cycle ends. Once it ends, the voltage of the battery bank drops immediately as it is loaded. The voltage drops as there is current being drawn from the battery bank and the drop is proportional to the internal resistance of the battery bank. This causes the PWM signal to revert back to 0% duty cycle and all available power is sent to the battery bank. The aim of this work is to try to ensure that the wind

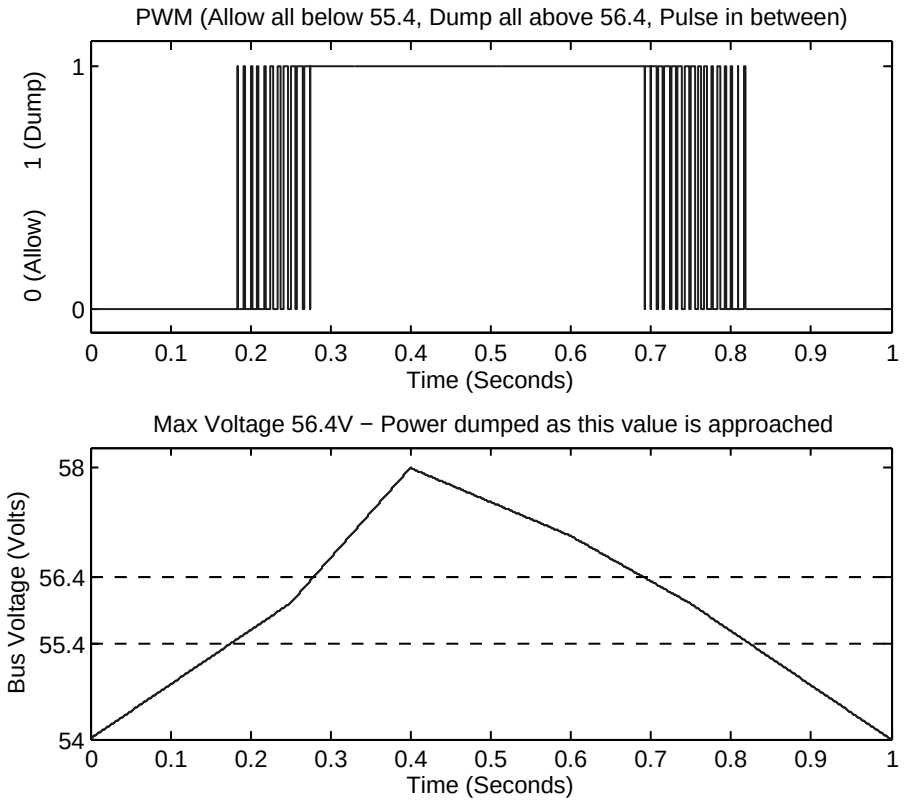

Figure 5.1: PWM diversion, PWM 1 ⇒ Dump all power, PWM 0 ⇒ Store all power from wind turbine. As the difference (region between dashed lines) between the bus voltage and the max voltage approaches zero, the turbine dumps increasing levels of power until the voltage exceeds 56.4 VDC after which all power is dumped

power is not dumped during times of high wind levels as significant amounts of potential power would be lost. The power dumped/stored is measured cumulatively and Simulink® operates fast enough to avoid any measurement problems [92] that can occur when measuring PWM signals with physical sensors. Data from the test HSRES, as discussed in Chapter four, demonstrates that the amount of power dumped is in excess of five percent during periods of moderate to high wind speeds with a 400 Ah battery bank.

In the simulated model the input to the wind turbine model is anemometer data acquired by the highest performing sensor on the Dublin City University campus. This anemometer was located at the most exposed region of the

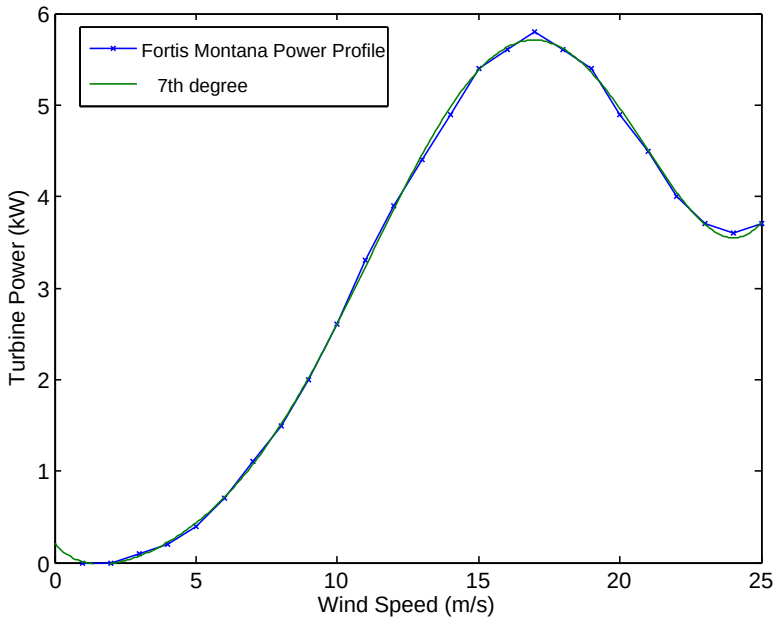

Figure 5.2: Fortis Montana wind turbine power profile which decreases after 17 m/s due to its furling mechanism with turns the turbine out of the wind to protect itself

campus and it had the highest level of data acquisition reliability. This data is captured by the remote anemometers at 1s intervals and averaged into 12 second data points before transmission. The HSRES model operates on a one second simulation interval and the wind data was interpolated to every one second to match the resolution that the model operates at. Piecewise constant interpolation was used which assigned the same wind value for the six seconds preceding and the six seconds after the sample. The wind speed, in m/s, is then converted to power in watts using a seventh order function which is a close polynomial fit to the manufacturers wind turbine curve [129]. Lower order functions also closely fit the power profile but the seventh order function minimised the residuals particularly at lower wind speeds. Residuals represent the differences between the data and the fit to the data at each value. The peak power output from the wind turbine occurs at 17 m/s after which point the output begins to decrease. The power decreases at higher wind speeds as the turbine has a furling mechanism to protect itself in high winds. This mechanism turns the turbine out of the wind to slow it down and protect it from rotating too quickly. The equation for this curve can be seen in equation

5.1 where 'u' is the wind speed and the power is in kW.

$$f(Power) = -8.4083 \times 10^{-8}u^7 + 7.8915 \times 10^{-6}u^6 - 0.00027472u^5 + 0.0044283u^4 - 0.035937u^3 + 0.18246u^2 - 0.38095u + 0.24257 \quad (5.1)$$

This equation is implemented in the 'Wind Turbine Power Profile' block in Figure 5.3. All of the components in the model output a current value which is controlled by the voltage from the battery bank which directly influences the bus voltage. The power and current values from the wind turbine are combined with a PWM signal which is generated from a 125 Hz sawtooth wave with a DC offset. The bus voltage is constantly subtracted from the max voltage of 56.4 VDC and the result of this is then subtracted from the sawtooth. The result of this subtraction is a negative number which is then subtracted (making the number positive) from the sawtooth wave. As long as the difference between the max voltage and the bus voltage is greater than one VDC, the result of subtracting that value from the saw tooth will yield a negative result.

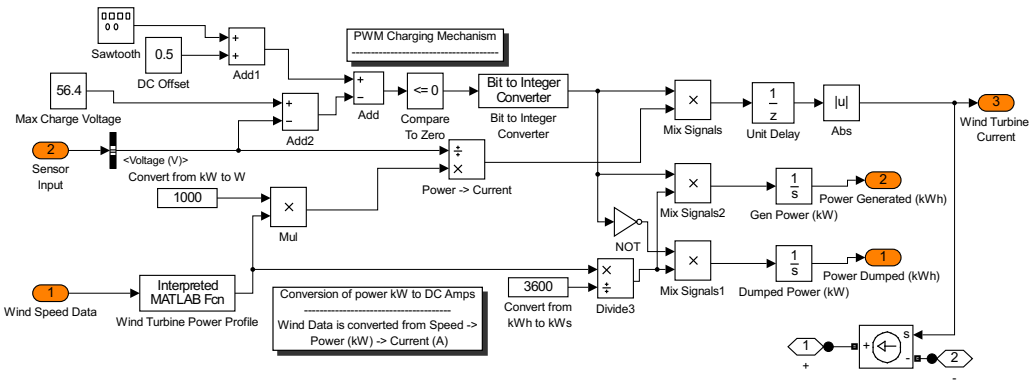

Figure 5.3: Simulink® wind turbine model and controller with PWM

The result is sent to the 'Compare to Zero' block where values below or equal to zero give a logical one and values above zero give a logical zero. The output of this wave is the PWM signal which dictates what portion of the power is being used and what is being diverted to the dump load. Looking back to Figure 5.1, if the voltage difference is one (or higher) then the compare to zero block

outputs a logical '1' which then feeds into three blocks. If the output is high (logical '1') then the 'Wind Turbine Current' will output a current source value which is calculated from the wind speed and bus voltage inputs. Additionally if the output is high, the cumulative power calculation 'Gen Power (kW)' for the generated power block also increments. The 'Dumped Power (kW)' cumulative calculation is inverted by a NOT gate and it only increments when the voltage difference between the maximum voltage and bus voltage is less than one. The power from the wind turbine minus any dumped power is output onto the DC bus of the model. The power generated and power dumped are kWh values used to measure the performance of the model.

5.3.2 Generator

The generator model is designed to represent a six kW 48 VDC generator. It is connected directly to the DC bus and its voltage is mainly influenced by the battery bank. The generator controller in its default configuration is unaware of any other power producing or consuming components on the bus and merely monitors the voltage to decide when to engage or disengage. The generator is capable of two stage charging where the battery bank is charged in constant current mode up to a voltage level of 54 VDC. Beyond this level the generator switches to constant voltage mode until a voltage of 58 VDC is reached. This voltage is recommended by the manufacturer as a suitable charging voltage during cycling [1]. As the battery voltage rises, during a charge cycle, the amount of current flowing into the battery bank falls and this current drops below five Amps as the voltage approaches 58 VDC. At this stage it is highly inefficient to be running the generator as it is severely under-loaded providing only 20% of its rated power (five A to battery bank and 20 A to the load). It is at this point that the generator is shut down to end the charging cycle and allow the battery bank and renewable energy source to supply the load.

The fuel consumption was measured using a differential (input/return) in-line flow meter which was polled every minute to obtain cumulative mL/minute values. The fuel consumption was measured over a full battery charging cycle to give a complete picture for the fuel consumption against DC current. Using

this data it was possible to get an accurate representation in the model as to what the fuel consumption for a given current was. This parameter is very useful as it allows the fuel consumption of different configurations to be accurately compared. Equation 5.2 describes the current to fuel ratio from the generator. This value is quite consistent and will not change dramatically unless there are mechanical changes applied to the generator or major changes in altitude which would necessitate a de-rating value.

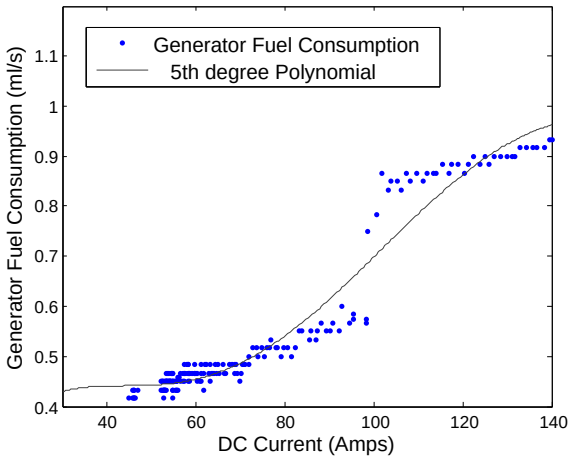

Figure 5.4: DC generator fuel consumption profile

The fuel consumption equation for the fuel profile was found by fitting a curve to the cumulative fuel and DC current data that was acquired during the fuel consumption testing of the generator. Other models apply a linear fit to the fuel consumption profile but they concede that this is not as accurate for variable speed machines [130]. This equation is used in the Simulink® model to represent how the fuel consumption changes in proportion to the load over time, see Figure 5.4. The fuel consumption can be found by substituting in the DC current for 'i' in equation 5.2.

$$\begin{aligned} Fuel(mL/s) = 1.5 \times 10^{-10} i^5 - 7.7 \times 10^{-8} i^4 + 1.4 \times 10^{-5} i^3 \\ -0.0011 i^2 + 0.037 i - 0.037 \end{aligned} \tag{5.2}$$

This equation is valid from 20 to 180 A outside of which the polynomial approximation diverges from the fuel profile. The current will not drop below 25 A for this model with a minimum of 20 A from the load and five A from the

battery bank when it is charged to 80% SOC. The model for the generator can be seen in Figure 5.5 where it takes current, voltage inputs and on/off signals from the control algorithm.

The generator model is only engaged when decided by the control algorithm described later in the chapter. Once the generator has been given an 'on' signal it can run in one of two modes depending on the bus voltage. The first mode is constant current mode which operates at the maximum generator current until a pre set voltage has been reached. The second mode is constant voltage mode which maintains a fixed voltage from the generator until the battery bank matches that voltage. In this case the voltage is set to 58 VDC and the current drops as the battery bank voltage rises to match this voltage. Once the battery bank voltage has risen to this level the charge cycle is over unless the control algorithm deems it necessary to end the cycle earlier. The fuel consumption profile block is connected to the output current values which is then converted from the mL output to litres for analysis. The current is continuously multiplied by the bus voltage to allow the cumulative power to be recorded so that it can be compared against the cumulative power from the other components in the system.

5.3.3 Battery Bank

The numerical model described in this work is designed around a common DC bus. Each component is connected in parallel to this bus but as described throughout this work, the voltage is mainly dictated by the battery bank. As stated in [38] which was published as part of this work, the performance and behaviour of each component is affected by the status of the battery bank. The voltage of the battery bank is supplied to each component and this influences the currents flowing out of the other elements of the model. The battery bank is represented using the generic battery module from Mathworks [8] which is supplied as part of the Simulink® environment which can be seen in Figure 5.6. This model is quite sophisticated in that it has the ability to represent four different battery types (Lead-Acid, Lithium-Ion, Nickel-Cadmium and Nickel-Metal-Hydride) along with the custom properties of each technology.

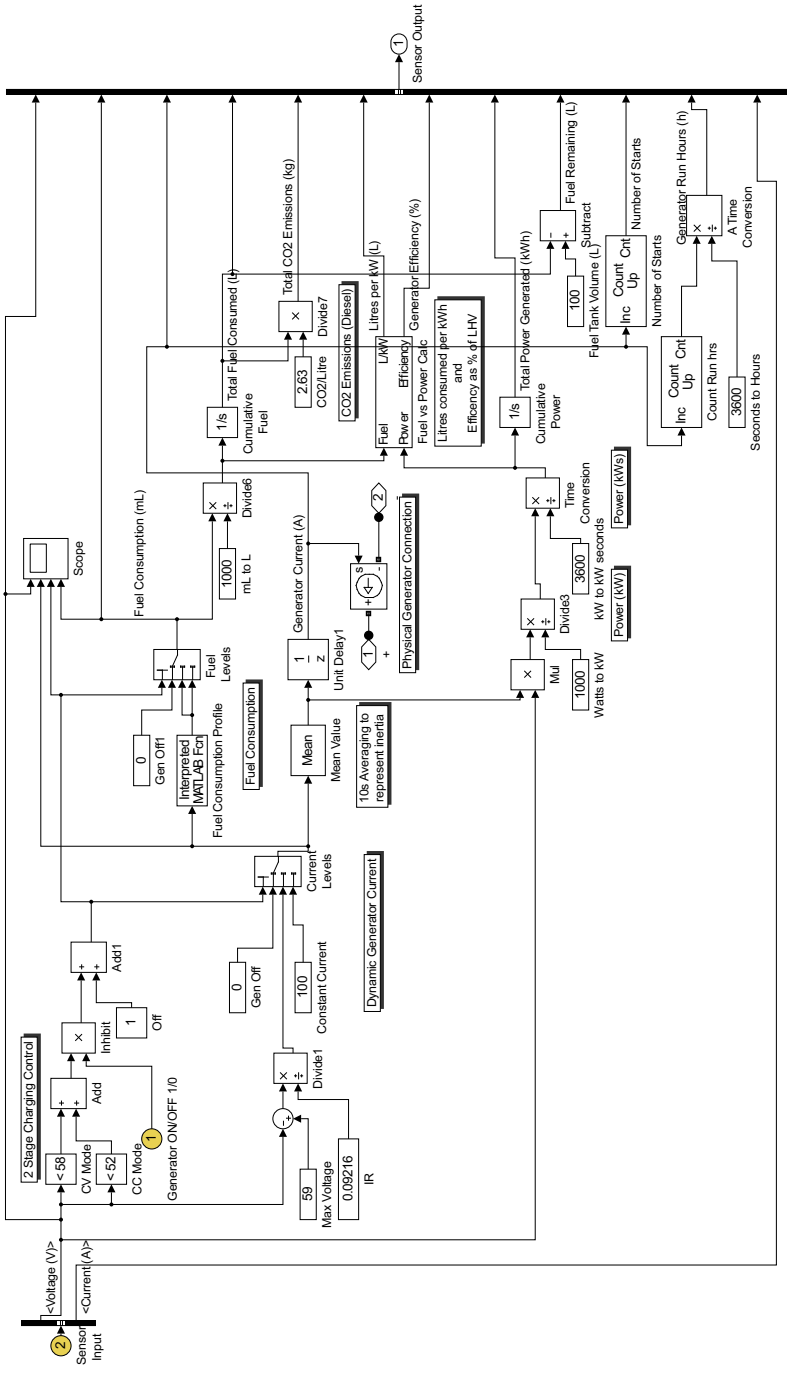

Figure 5.5: Simulink® generator model, controller two stage charging, emissions and run hours

Lead-Acid was chosen as the basis for this work but the charging system was restricted to cell voltages that were suited to AGM batteries. While the

charging voltages differed between AGM and Lead acid, there were a number of similarities in terms of internal resistance, charge profiles, and cycle life. The main property to be modified in the battery bank is the capacity in Amp hours (Ah). Manufacturers specify the capacity of their battery banks for a discharge rate ("C Rate") which is 10% of the battery's capacity (also known as the ten hour rate). In a system that is designed to supply a telecoms load of two kW maximum with a 48 VDC system, then an average load of approximately 40 A (2000 W/48 V $\approx$ 40 A) would be expected and thus a battery bank with a minimum capacity of 400 Ah would be appropriate for the application. This was also the size of the battery bank that was available for physical testing on the test site.

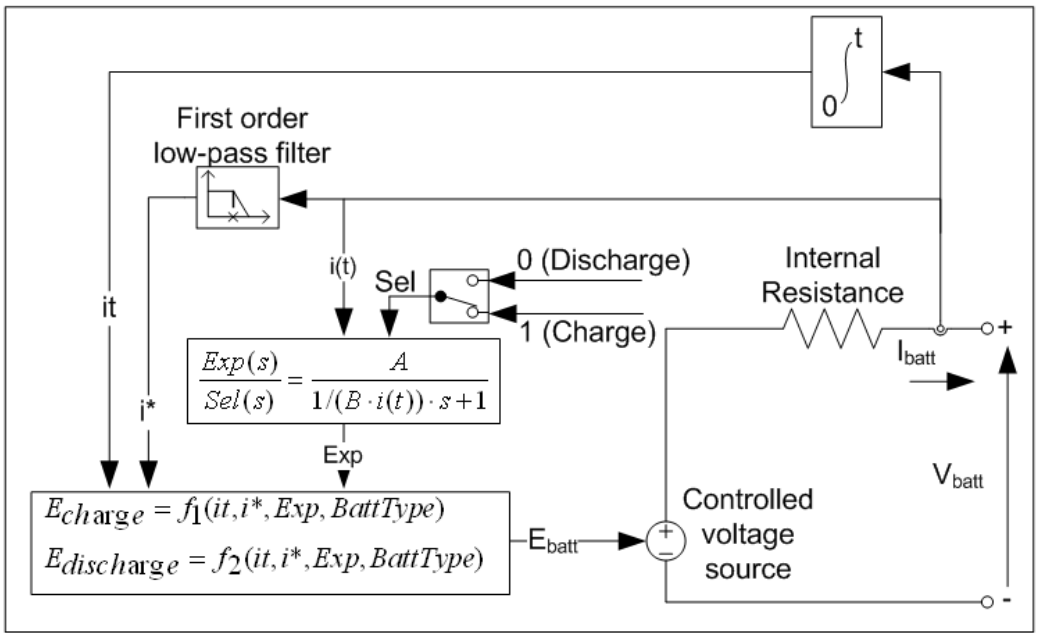

Figure 5.6: Simulink ® generic battery model [8]

One component that the model does not take into account is battery health in terms of sulfation and physical defects which can not develop from battery misuse. A typical lead acid battery can tolerate less than 1000 full cycles from 100% to 0% state of charge (SOC) but it can perform several thousand cycles if the depth of discharge is limited. The depth of discharge is limited to approximately 40% in this application but the algorithm can ignore this limit in cases where a large pressure change has been detected. In such a situation

the battery bank will be allowed to drop as low as 25% SOC in anticipation of a significant contribution of power from the wind turbine. The generic battery model has been used in other hybrid Simulink® systems such as [29] and also [114] to simulate hybrid energy systems.

5.3.4 Typical telecom load

The HSRES was designed to cater for average loads up to two kW. Loads that were much higher than this will cause the generator to run for longer periods of time which erodes the fuel saving advantage that a hybrid system has over a traditional 24/7 based generator system. The reason this advantage is reduced is that hybrid systems save fuel by using batteries to allow the generator to be turned off for a period of time. As this period of time is reduced, where the load becomes larger with respect to the battery bank size, a hybrid system will reach a point where it does not save any fuel compared to a similar sized AC generator running continuously.

As a result a single operator load was chosen as the most suitable load for the system.This type of load contains three 120° sector antenna transmitters and a point to point link to connect the site back to the core network. This will give a power consumption of between 800 W and 1.4 kW depending on the system load and power output. Rather than use a single average value for the telecoms load, 32 days of measurements were taken, overlaid and an average taken over a 24 hour period. This average gives a load which changes dynamically over a 24 hour period. The 32 day average, published [38] as part of this work, is approximated with it a 4th degree polynomial approximation can be seen in Figure 5.7. While a better approximation was potentially possible with the data available it was unnecessary to implement a better fit given that the load profiles fluctuated up to 0.1 kW above and below the mean. A higher approximation would have added an additional processing load that would not justify the incremental improvement in accuracy. This is the case as the standard deviation of the telecoms load, on different days, compared to the mean is up to 0.1 kW.

Equation 5.3 has been derived from this profile and used in the simulated model

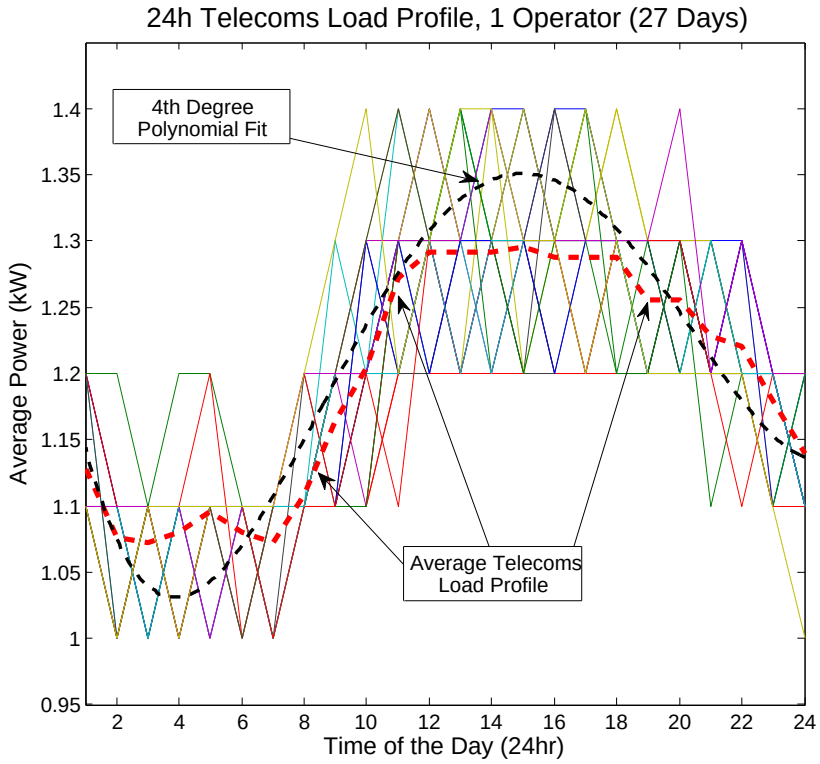

Figure 5.7: Telecoms load profile (1 month overlaid) with 4th degree polynomial approximation of the mean

of the HSRES. This equation accepts a time value 'n' which is an integer hour value ranging from 1.0 h to 24.0 h. The output is a varying kW value which is representative of a single telecoms operator.

$$Load(kW) = 1.346 \times 10^{-5} n^4 - 0.00082126 n^3 + 0.015426 n^2 - 0.085309 n + 1.2024 \tag{5.3}$$

The numerical model for the telecoms load can be seen in Figure 5.8. The model begins with a counter which resets every 24 hours to emulate the continuously changing telecoms load profile. The load begins at midnight and the input wind and pressure data also begins at midnight to ensure that all the information is synchronised. The output value from the counter is converted to a integer value between 1.0 and 24.0 to suit the input for the telecoms power profile block. This value is converted into a current value for transmission in

the DC bus and into a kWh value for comparison between other components.

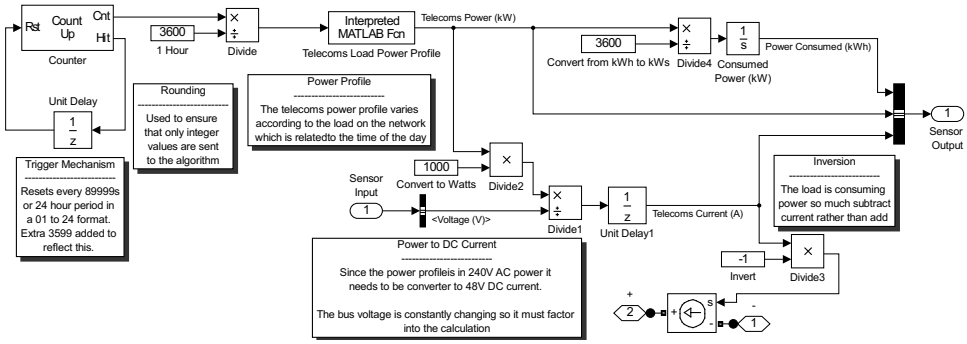

Figure 5.8: Numerical telecoms load model with dynamic time based load

This profile is based on an Irish mast location, other countries will have different power profile due to environmental and cultural differences. The environmental differences will occur as a result of cooling and lighting requirements while cultural differences result in different load profiles depending on the country. An example of a cultural difference was between an Irish usage profile and a usage profile acquired from remote site monitoring in Ghana. In Ghana the local phone usage patterns had a flat profile during the day with a large spike in the evening between 8 pm and 12 pm.

5.3.5 Wind prediction and generator mode algorithm

The wind prediction methodology is designed to alter the generator's charging regime by taking into account the anticipated wind conditions. The 'triggered subsystem' blocks in Figure 5.9 temporarily store data which allows the 'du/dt' block to take a derivative of the barometric pressure data every three hours. This differential is compared to zero to ensure that only a negative pressure change is taken into account as increasing pressure changes are associated with calm conditions as discussed in Chapter four. Equation 5.4 represents the three hour differential of barometric pressure where Δt is three hours, u(k) is the input value from the pressure data while y(k) is an impulse value when

the input changes otherwise it is zero.

$$y(k) = \frac{1}{\Delta t}(u(k) - u(k-1)) \tag{5.4}$$

This equation represents the internal operation of the du/dt block in the Simulink® model. It calculates the difference between the current value u(k) and the previous value u(k-1) with respect to the time step Δt. The simulation time step is one second so the differential calculation was delayed to run every 10,800 seconds (three hours) to correspond with the pressure tendency measurements in table 4.2 in Chapter four.

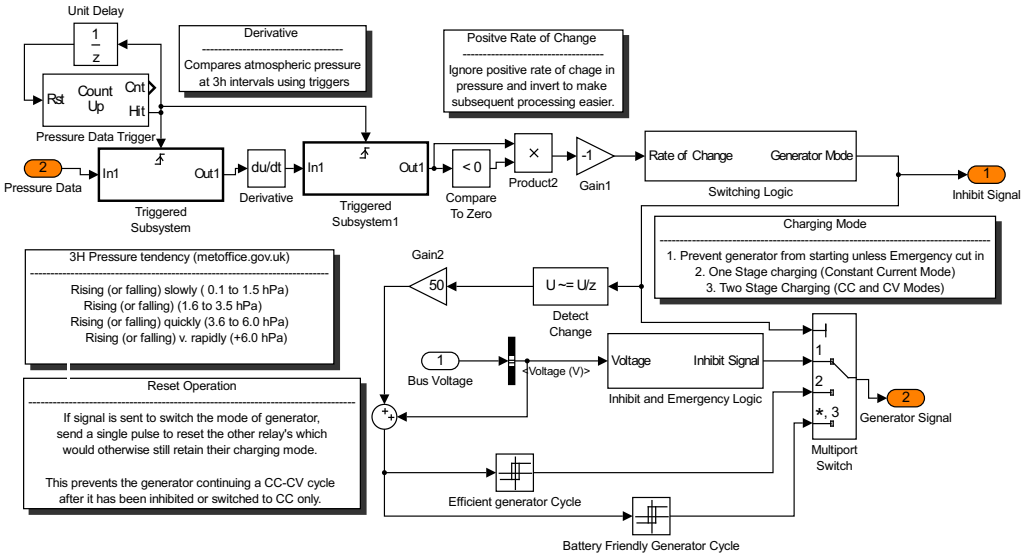

Figure 5.9: Wind prediction and generator mode algorithm

When the magnitude of the negative pressure change has been identified it is then classified in the 'switching logic' block in Figure 5.9. This classification is described in table 4.3 in Chapter four where the wind speed is divided into three categories. A signal of '1' immediately shuts down the generator as a significant increase in wind speed is expected. A signal of '2' keeps the generator in constant current mode which is only the first but most efficient stage of a charge cycle. A signal of '3', the most common signal, allows the generator to operate in its default configuration with two stage charging with operates within the voltage tolerances of AGM battery banks.

An extract from the sensor data can be seen in Figure 5.10. This Figure shows the wind speed, barometric pressure and output from the charging algorithm for the generator. It can be seen that during instances of rapidly decreasing pressure, e.g. at $t = 8 \times 10^5 s$, $t = 13 \times 10^5 s$ and $t = 14 \times 10^5 s$, there is a subsequent rapid increase in wind speed, see Figure 5.10 sub-plot 1. The signal sent to the generator control system can then be seen in Figure 5.10 sub-plot three. In this case, the generator has been signalled to immediately shut down due to the wind forecast.

Figure 5.10 demonstrates the method in operation, as negative pressure changes above specific magnitudes cause the battery charger settings change. Constant pressure has no effect on this system and this can be seen between $t = 9 \times 10^5 s$ and $t = 129 \times 10^5 s$ the pressure remains relatively constant and a signal of three has been maintained throughout this period. At $t = 3.7 \times 10^5 s$ a pressure change greater than or equal to two mb every three hours has been detected and a signal of two has been given and also at $t = 6.1 \times 10^5 s$, $t = 8.9 \times 10^5 s$. More dramatic changes with a pressure change of three mb every three hours were detected at $t = 8.3 \times 10^5 s$ and also at $t = 13 \times 10^5 s$ where a signal of one was given to immediately shut down the generator. Increases in pressure have been ignored as they have been observed to offer little consistency in terms of rapid changes followed by increases in wind speed. High pressure is generally associated with clear and calm weather with only moderate wind at best [97]. This data shows that rapid decreases in barometric pressure consistently results in an increase in wind speed a number of hours later and the system reacts accordingly.

5.4 Simulation results

The model overview can be seen in Figure 5.11 with inputs from the wind speed and barometric pressure data. By adopting the algorithm, described in the previous section, fuel savings of between one and two % were attained in moderate wind conditions where the average wind speed, at a height of ten meters, is between four and six m/s. To provide a comparison to the optimal situation, where the model perfectly predicts the wind speed, the future wind

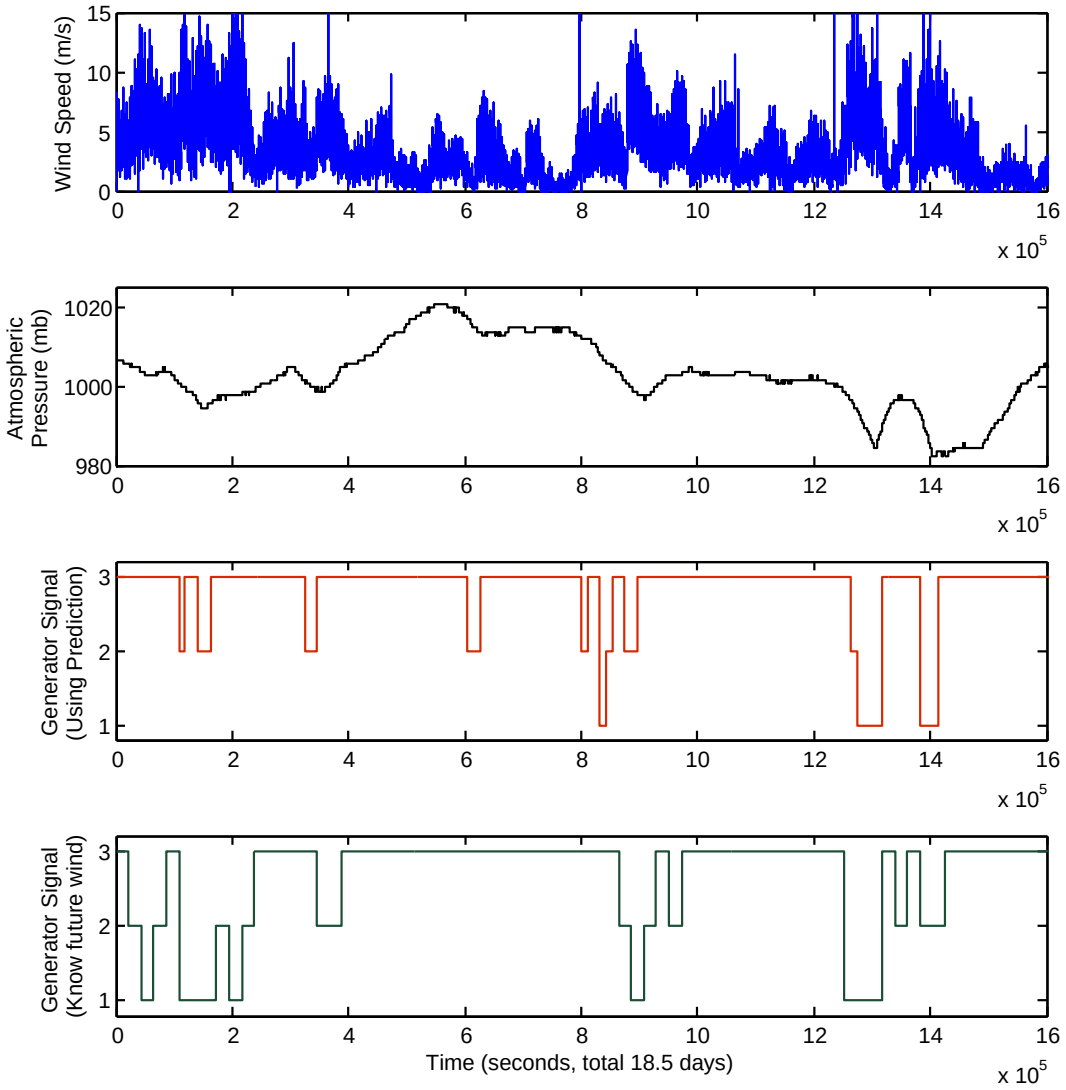

Figure 5.10: The effect of barometric pressure on the generator charging signal and wind speed

speed data was fed directly into the model. To avoid noise issues from the wind speed, the data was converted to six hour blocks of kWh values generated by the wind turbine. In this way, instead of the algorithm being controlled by barometric pressure it is controlled by the amount of kWh expected over the next six hours. Similar to the configuration for pressure in table 4.3, the system will operate normally with kWh values below two (Generator signal

'3'). It will enter constant current mode with kWh values between two and four (Generator signal '2'). For all kWh values above four kWh, the generator will be shut down immediately with a generator signal of '1'.

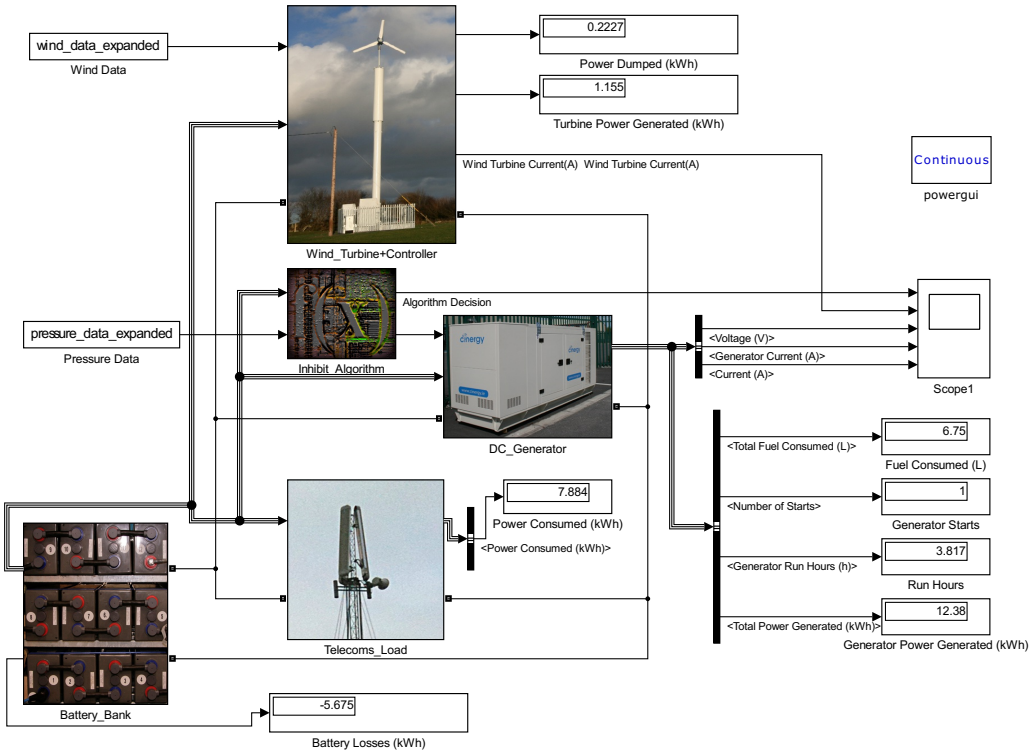

Figure 5.11: Overview of HSRES in Simulink®

The system model was run for three different scenarios with the results of each illustrated in Figure 5.12. One scenario was 'normal operation', the second implemented the control algorithm introduced in this work and the third was the ideal future wind scenario. All scenarios adopted a lower battery SOC boundary of 40% and a higher SOC boundary of approximately 85%. Scenario one, the default charging setting, is a charging regime chosen for optimal operation for a hybrid system undergoing continuous cycling with an AGM battery bank. This regime is optimal for two reasons. Firstly a lower SOC of 40% was chosen as a compromise between hours of battery operation and battery lifetime. An upper SOC of 85% was selected as the power the batteries can absorb decreases approaching and beyond this point resulting in the generator operating inefficiently. In addition to poor generator efficiency,

the efficiency of flooded lead acid batteries also decreases dramatically beyond 80% SOC with up to 30% less energy being stored as the bank reaches 100% SOC [41].As the batteries are not being charged correctly with the 85% SOC limit, they must undergo a full charge to 100% SOC at least once every four weeks [1].

The second and third scenarios use the same charging regime as scenario one but the algorithm has extra 'awareness' of the potential future power contribution from the wind turbine. Using the control system modification described earlier, during periods of decreasing barometric pressure above a certain rate, the generator will be restricted from charging the battery bank. It can be seen in Figure 5.12 that scenario two (modified charging) has a lower fuel consumption than scenario one. Scenario three (Future Knowledge Charging) has full awareness of the upcoming wind conditions so that it can test the effectiveness of second scenario. All three approaches are compared in Figure 5.12. When comparing the generator signal from the prediction scenario to the signal from the ideal scenario a difference is noticeable. It can be seen that the ideal scenario significantly outperforms the prediction model for the first 15% of the model run as the pressure changes are too small to trigger a response from the algorithm.

Focusing on a single battery bank size, 400Ah was used as the basis for a batch of testing in the Simulink® model, the HSRES was tested for four different groupings of equipment. The combinations included a DC generator, battery bank and wind turbine with a control system modification being the final combination. This run was simulated for a 500 hour operational time-frame using wind speed and barometric pressure as data inputs as seen in Figure 5.10. The total fuel consumed by the equipment over this period was recorded in table 5.1. The use of a battery bank immediately results in substantial fuel savings over a continuously operating generator. This type of saving is similar in magnitude to other commercial trials [131].

Using the costing data from [131] as a template, the savings made by adopting a hybrid charging strategy are not limited to fuel savings only. A diesel generator has a service interval of 250 hours of operation. This involves personnel physically visiting the generator to perform routine maintenance such

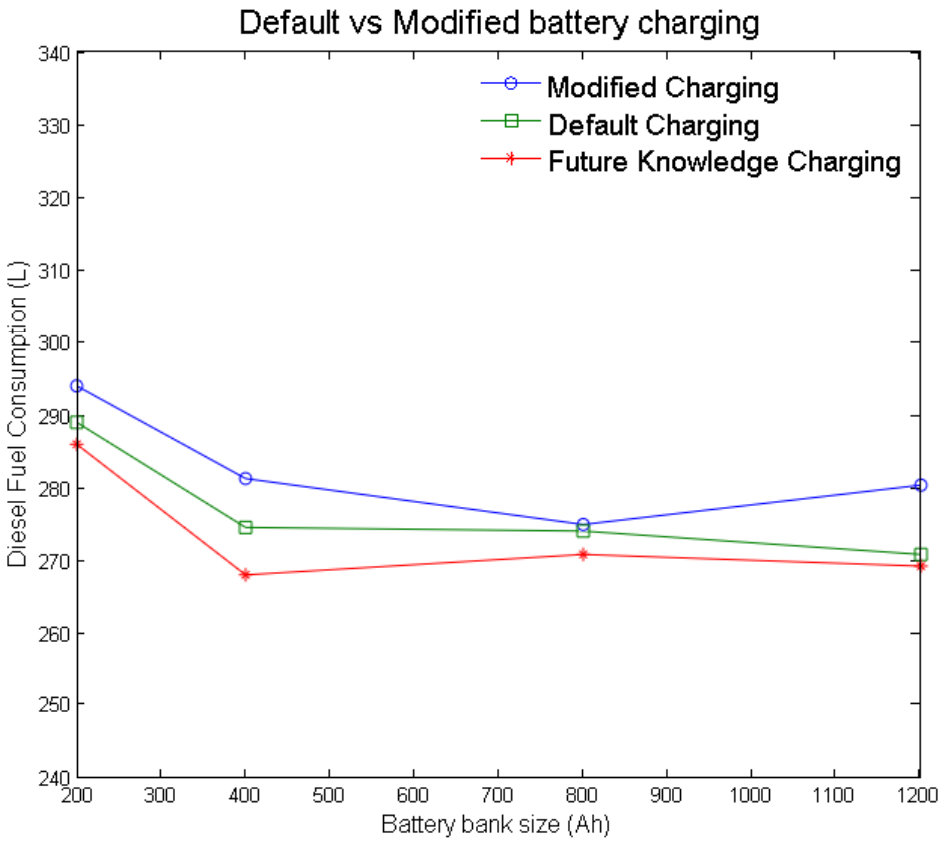

Figure 5.12: Fuel savings with (Modified Charging), savings with fuel savings as a result of future knowledge of wind conditions and without (Default Charging) the charging algorithm

as changing filters, oil and any other issues that need addressing. A cost of €250 was attributed to each visit so the control methodology used in this paper saves both fuel consumption and the amount of maintenance needed over the long term.

The area of wind-diesel-battery systems is widely researched and well understood so the prospects for improving energy efficiency within the constraints of existing technology are finite. While this algorithm can attain two to three percent fuel savings, the total (maximum saving) power dumped is as high as seven percent for small battery banks decreasing to as low as one percent for large battery banks. An ideal prediction scenario was tested here and it was found that with precise knowledge of upcoming wind conditions, fuel savings

Equipment Combination	**Fuel Consumed (Litres of Diesel)**	**Generator Run Hours**
Generator	698 L	500 h
Generator & Battery Bank	352 L	186 h
Generator & Battery Bank & Wind	281 L	148 h
Generator & Battery Bank & Wind & Control	274 L	143 h
Generator & Battery Bank & Wind & (Future Knowledge) Control	268 L	138 h

Table 5.1: Relative fuel cost of different energy configurations in 500h model run with 400 Ah battery bank

as high as 4.5% (see table 5.1) are feasible for a 400 Ah battery bank. The only downside to the ideal scenario is additional engine starts. Looking at Figure 5.12 it can be seen that the potential for fuel savings diminishes as the size of the battery bank increases.

Conservative settings, chosen to preserve battery health prevent the maximum saving from being achieved. Sustained periods of windy conditions will eventually cause the battery bank to reach capacity despite being predicted correctly leading to unavoidable portions of dumped power. New battery technologies, which are less sensitive to undercharging/over-charging, will facilitate double digit gains in efficiency as the algorithm can be more aggressive with its cut off limits. This aggressiveness would describe deeper battery discharges, higher charge rates, less equalisation charges and overall paying less attention to battery bank health. The cost of implementing such a prediction system is very low with the only requirements being a micro-controller and a pressure sensor. The costs of implementing a wind prediction mechanism into a battery charger would be quickly offset with the fuel and maintenance savings. The cumulative knock-on savings in a multitude of different areas as a result of saving fuel:

- Less run hours
- Physical maintenance required less frequently

- Extension of generator engine installation lifetime
- Lower instances of noise emissions into adjacent villages
- Heat generated in battery bank is lower
- Reduced fuel consumption
- Less power dumped from wind turbine
- Lower overall cost of electricity (COE)
- Lower CO_2, NO_x, SO_2, CO, PM_{10} (particulate matter) emissions

The savings can be attributed to two main parameters where certain reductions are as a result of the lower run time while others are as a result of the lower fuel consumption. Reduced run hours results in less frequent generator maintenance intervals and as its operational lifetime is in turn extended as a result of this. Lower run hours also means the generator is spending less time outputting low frequency noise pollution into the surrounding region. A generator cycle produces a significant amount of heat within the enclosure from both the engine and the battery bank. One of the main parameters that affects the lifetime of the battery bank is temperature and when the battery bank is spared of these higher temperatures its operating life time is extended. Reducing the amount of power dumped by the wind turbine will save fuel while simultaneously reducing the amount of time it takes for an operator to make a return on their initial investment on the turbine. When comparing the difference in cost between grid power and generator power it is useful to look at them in terms of cost of electricity (COE).

Equipment Combination	**CO_2**	**NO_x**	**SO_2**	**CO**	**PM_{10}**
Generator	1187.2kg	19.7kg	1.27kg	3.64kg	1.27kg
Generator & Battery Bank	598.74kg	9.98kg	0.64kg	1.84kg	0.64kg
Generator & Battery Bank & Wind	477.97kg	7.97kg	0.51kg	1.47kg	0.51kg
Generator & Battery Bank & Wind & Algorithm	466.07kg	7.77kg	0.50kg	1.43kg	0.50kg

Table 5.2: Relative emissions for different energy configurations in 500h based on an average engine efficiency of 25% [12] with 400 Ah battery bank

Lowering fuel consumption in turn leads to a reduction in emissions across the scale as demonstrated in table 5.2. International telecoms operators are continuously striving to reduce their carbon dioxide (CO_2) emissions yet there are other reductions with are less well publicised. Diesel is a dirty fuel when burnt and unless there are local environmental regulations specifying air quality there is no catalytic converter installed in a diesel generator to reduce its emissions. The dominant emissions other than CO_2 are oxides of nitrogen (NO_x), sulphur dioxide (SO_2), carbon monoxide (CO) and particulate matter (PM_{10}).

5.5 Summary

This chapter offers background information into hybrid wind-diesel system modelling taking place using both HOMER and Simulink® platforms. The model used for this work is broken down into its individual components with each the electrical performance and model characteristics of every major component described. The wind prediction methodology implementation in Simulink® is described and refers back to the extra detail on barometric pressure tendency in Chapter four.

The results demonstrating the performance of the system operating with and without the wind prediction methodology are compared at the end of the chapter. It was shown that if the battery charger has knowledge of upcoming wind conditions then its profile can be optimised to make fuel savings of one to two percent. The fuel saving also translates into reductions in emissions, run hours and noise. Additionally, if the system has full knowledge of upcoming wind conditions the fuel savings increase to as high as 4.5 % for the smaller battery banks. The fuel savings were found to diminish for larger battery banks as they repeatedly contained spare capacity irrespective of the algorithm performance.

There has been extensive research carried out in the areas of wind prediction and efficiency improvements for large (MW) scale wind turbine installations yet there is very little work done on improving the electrical efficiency of small

(kW) scale hybrid configurations. This work has drawn attention to the power being wasted by small wind turbines which has not been well documented up until this point. The work has also proposed a cost effective and viable method of reducing this wasted power to improve the overall system efficiency. The work has been intentionally published in an open access journal to allow companies around the world to learn from the observations made throughout this work.

Chapter 6

Conclusion

This work explored the concept of improving the fuel efficiency for off-grid hybrid energy systems in telecoms applications. The research focused on three major aspects which can be summarised as observation, interpretation and implementation. The system was initially observed using a variety of different remote monitoring systems which were constructed as part of this work. This data was very rich and valuable industrial measurement information which formed the basis of this study. The data, acquired by the data acquisition systems, was interpreted and a multitude of different sources of power wastage were identified.

A useful relationship between atmospheric pressure tendency and short term future wind conditions was identified. An algorithm was proposed to identify the trends in wind speed and allow the system to react accordingly. Once the data had been acquired and interpreted, the hybrid system was implemented in a numerical software model. This model represented the physical hybrid system and it facilitated the implementation of the wind prediction algorithm. Using the combination of the acquired data, the wind prediction algorithm and the software model, an approach for saving fuel in a hybrid energy system was proposed.

6.1 Remote monitoring of remote renewable energy installations

A comprehensive description of the components undergoing monitoring on telecoms sites in remote locations was carried out in Chapter two. A detailed analysis of the data acquired from these regions was undertaken in Chapter three with discussions describing what was happening in the data acquired. The data from the wind-diesel test site reveals that power is lost when the generator and wind turbine operate concurrently. This happens towards the final stages of a charging cycle when the battery bank is unable to accept much more charge. A portion of this (normally wasted) power can be saved with more effective generator scheduling. The optimal situation is that the generator is not running when there is enough wind to supply the load but this is not always avoidable.

6.2 Wind prediction

A number of different techniques for predicting wind speed have been discussed in Chapter four. Each of the techniques is generally suited to a different forecast horizon with time-scales that range from seconds to several weeks. These methods operate in an environment where inaccuracies in wind prediction can have severe financial implications for the wind farms which rely upon them. These costs easily justify the expense and time required to implement a prediction mechanism for a given location whether that be in terms of training time, computation time or algorithm complexity.

The implications of incorrectly predicting incoming wind conditions in a small scale HSRES is damage to battery health as these systems must store excess energy as they are off grid. In this case a low cost short term wind prediction methodology is proposed using barometric pressure as an input. The algorithm utilises a conservative configuration as priority was given to battery health over fuel savings. This difference can be observed when comparing the fuel savings from the ideal wind prediction scenario and the algorithm.

6.3 Modelling HSRES with predictive control

A numerical Simulink® model was developed to allow the HSRES to be tested using different configurations. The data obtained though remotely monitoring telecom sites and hybrid systems was used as a basis for the model. The model is capable of taking data inputs from anemometer and barometric pressure sensor data acquired as part of this work.

It has been shown that with the adoption of a charging algorithm based on changing barometric pressure, a fuel and run hour saving can be made. These savings reduce the amount of maintenance required for the generator and also the number of fuel deliveries to a remote location. These savings are more significant when applied to Telecom operators with broad portfolios of diesel powered off-grid base stations. The proposed method works effectively for geographical regions of continuously changing barometric pressure and frequently developing weather systems.

6.4 Future Work

- Validation of the hybrid model by comparing it to the physical hybrid system using an identical configuration
- Sensitivity analysis of the model to analyse how the output changes when altering individual inputs to the system
- Implement alternative predictions algorithms into the model to establish their viability as an alternative to the approach proposed in this work
- Propose methods of predicting solar irradiation and implement this approach into the model in place of wind
- Simulate and test alternative hybrid system with an AC bus
- Use fuel cells instead of a lead acid battery bank to investigate the potential fuel savings when battery health is not a system constraint
- Build a physical test platform in the lab to run the model
- Test real world implementation of the model in a physical system
- Develop battery model (Degradation, charging efficiency and sulfation)

Appendix A

Development tools, interfaces and system code

A.1 Prediction of solar insolation

Solar radiation is the most important form of energy as it influences all the weather conditions within the earth's atmosphere [97, P.23] and is of critical importance for PV-based renewable energy installations [132]. While there is a large resource available for yearly historical solar insolation information [6], it is more difficult to obtain predicted solar insolation information with the accuracy of a numerical model but with the simplicity of an analytical model. As a result analytical models such as time series implementations using on-site irradiation information or forecasts based on cloud motion vectors obtained from comparing different satellite images are only viable in a temporal range from 5 minutes up to 6 hours [133].

There are a number of models which aim to predict temporal solar radiation but it has been suggested that their simplified statistical assumptions about the data are not always correct [134]. Statistical models utilising artificial neural networks (ANN), numeric weather prediction (NWP) based models and satellite imagery are the core techniques used for the prediction of solar insolation [135].

A.1.1 Rationale for solar insolation prediction

In sunny climates the critical nature of power prediction from large commercial solar power plants is off-set by the relationship between air conditioning loads and short term solar insolation [136]. System operators in this case have identified solar PV as 'a great peaking resource' as it peaks at the same time of the day as the air conditioning loads. In the case of HSRES, the solar panels will reach their peak power production capacity but it will only be harvested if there is sufficient capacity in the battery bank to store the energy. Like the commercial systems, the cooling load in a HSRES in sunny climates will be higher during sunny periods which will match the power output from the solar panels during this time. This factor will use up some of the excess power being produced by the solar panels without having to rely on the battery bank to store all the energy generated.

A.2 Remote Monitoring

This section provides a reference to all the LabVIEW, Simulink® code and front panel interfaces that were built for acquiring data. This information was not pertinent in the main body of the text but the author felt it useful to include this information for the reader.

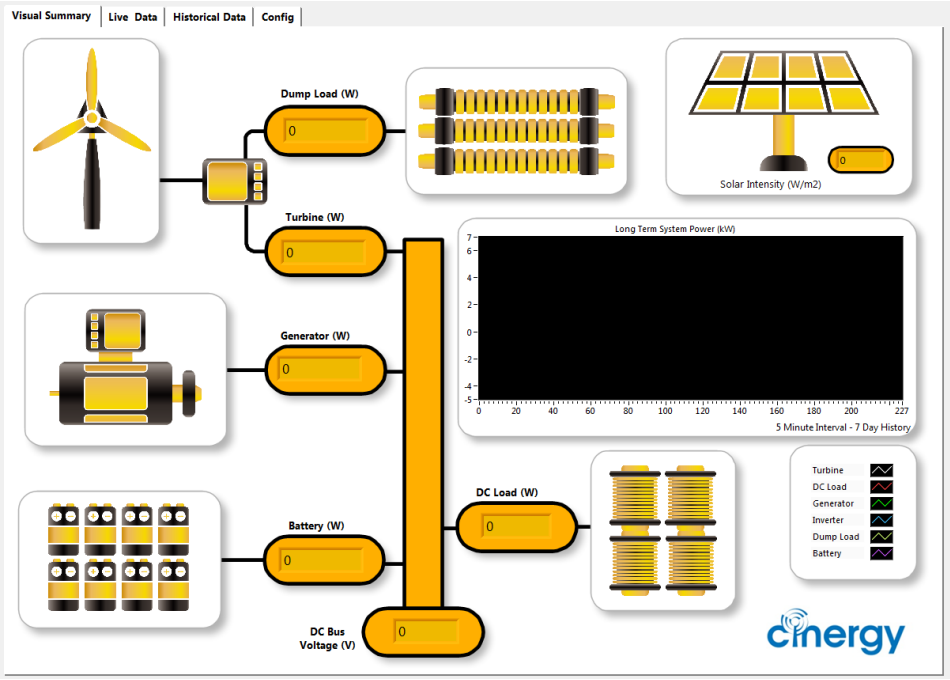

Figure A.1: LabVIEW front panel for the off grid hybrid system

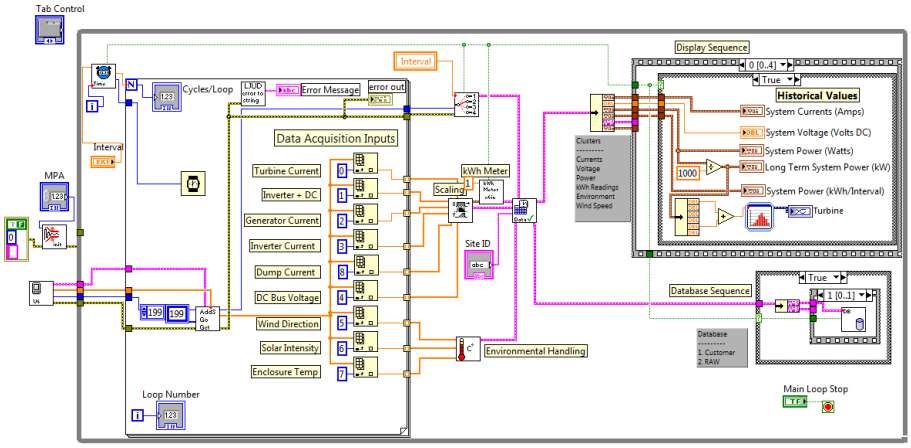

Figure A.2: LabVIEW code block diagram for the off grid hybrid system

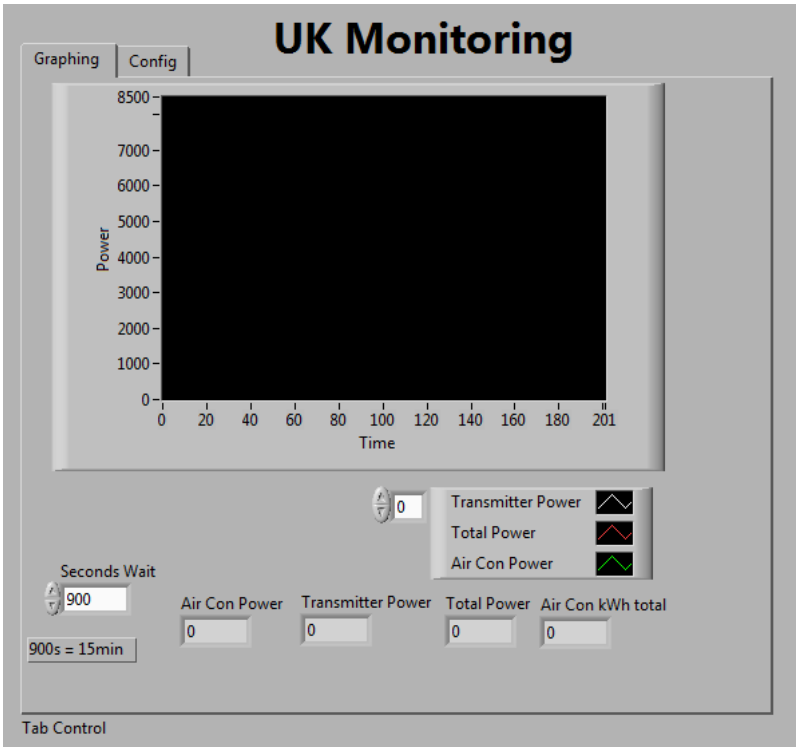

Figure A.3: LabVIEW front panel for monitoring remote sites

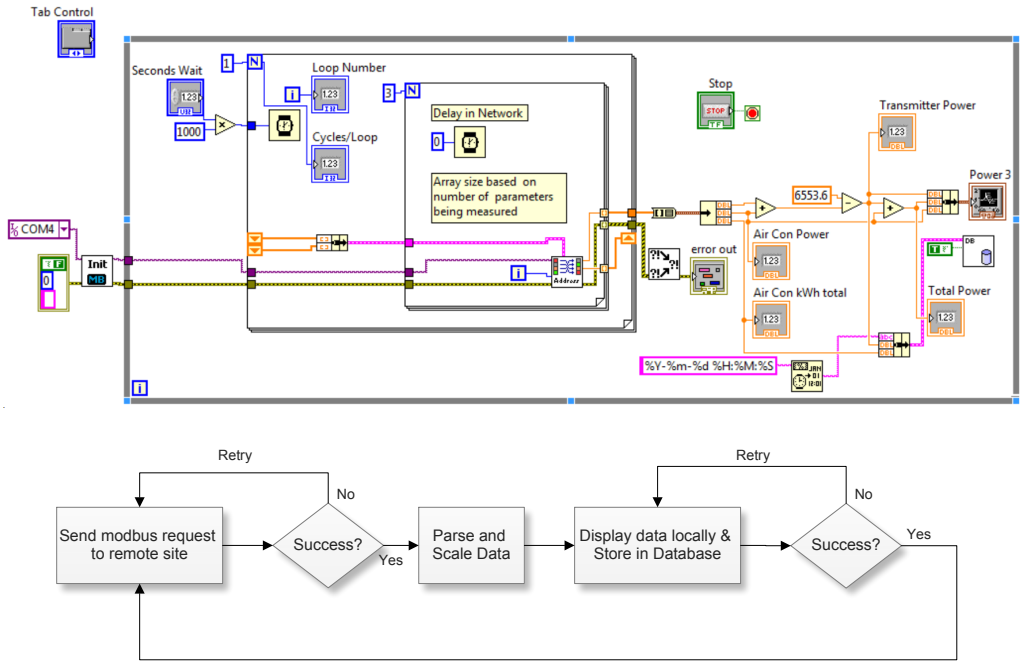

Figure A.4: LabVIEW code block diagram for remote site monitoring and flow chart describing this acquisition process

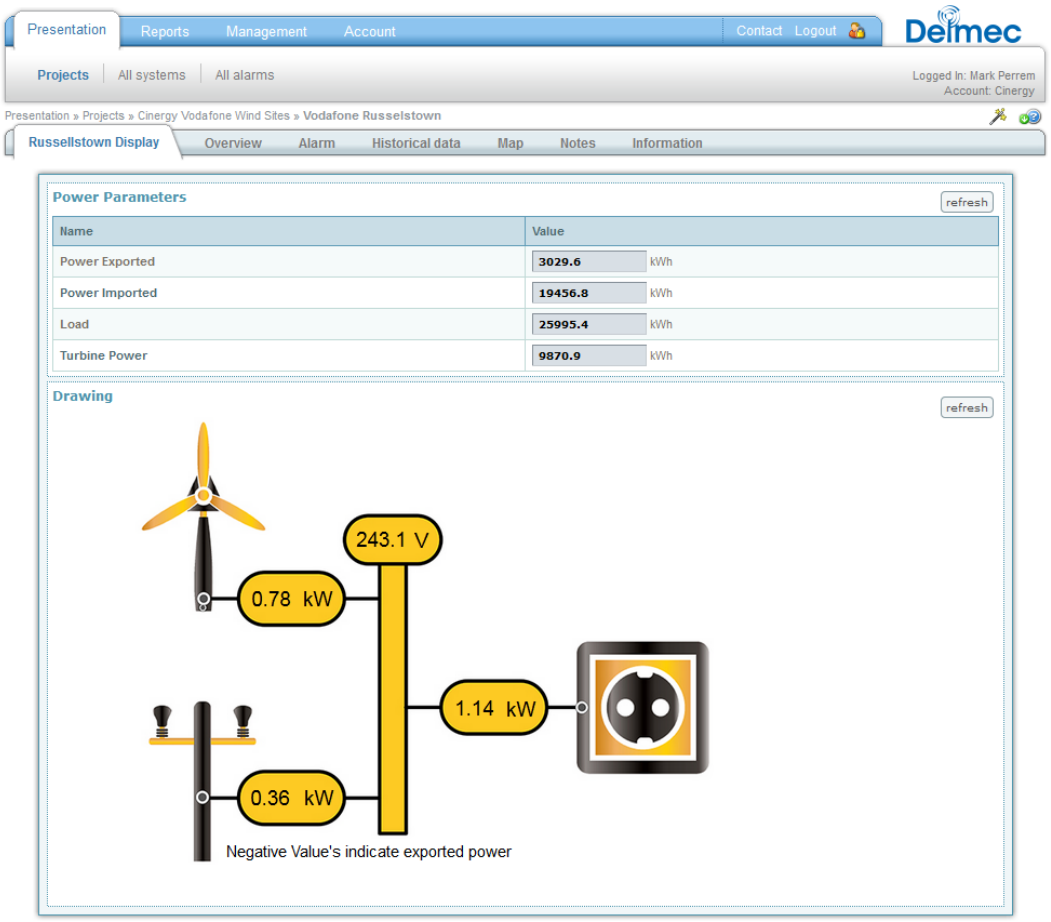

Figure A.5: Netbiter grid tied implementation in Russellstown, Carlow

Name	Value			Date logged
DC Current	15.2	Amps	Avg: 14.35 Amps Min: 13.40 Amps Max: 16.10 Amps	2013-07-23 12:52:00
DC Voltage	3.5	Volts	Avg: 3.47 Volts Min: 3.10 Volts Max: 3.80 Volts	2013-07-23 12:52:00
Fuel Level (Log)	2135.2	Litres	Avg: 2140.50 Litres Min: 2110.30 Litres Max: 2145.00 Litres	2013-07-23 11:00:00
Fuel Level Delta	-1	Litres	Yesterday: 0.000 Litres Today: -15.00 Litres	2013-07-23 11:00:00
Generator kWh	42069.9	kWh	Yesterday: 45.40 kWh Today: 21.00 kWh	2013-07-23 11:00:00
Indoor Temperature	27.4	C	Avg: 27.11 C Min: 26.30 C Max: 27.90 C	2013-07-23 11:00:00
Motion Sensor	1	0/1	Avg: 1.00 0/1 Min: 1.00 0/1 Max: 1.00 0/1	2013-07-23 11:00:00
Outdoor Temperature	29.2	C	Avg: 27.02 C Min: 24.50 C Max: 32.60 C	2013-07-23 11:00:00
Power L1 (Customer Tigo)	542	W	Avg: 548.30 W Min: 302.00 W Max: 680.00 W	2013-07-23 12:52:00
Power L1 (Generator)	686	W	Avg: 689.89 W Min: 582.40 W Max: 764.40 W	2013-07-23 12:52:00
Power L1 Vodafone	516	W	Avg: 519.54 W Min: 478.80 W Max: 571.70 W	2013-07-23 12:52:00
Power L2 (Customer Tigo)	286.5	W	Avg: 284.50 W Min: 154.00 W Max: 353.50 W	2013-07-23 12:52:00
Power L2 (Generator)	298.2	W	Avg: 515.11 W Min: 145.60 W Max: 821.80 W	2013-07-23 12:52:00
Power L3 (Customer Tigo)	270	W	Avg: 269.62 W Min: 144.00 W Max: 336.00 W	2013-07-23 12:52:00
Power L3 (Generator)	683.9	W	Avg: 689.94 W Min: 364.00 W Max: 857.50 W	2013-07-23 12:52:00
Solar Intensity	73.3	W/m2	Avg: 73.14 W/m2 Min: 72.70 W/m2 Max: 73.90 W/m2	2013-07-23 12:30:00

Figure A.6: Netbiter off-grid implementation in Ghana, Africa

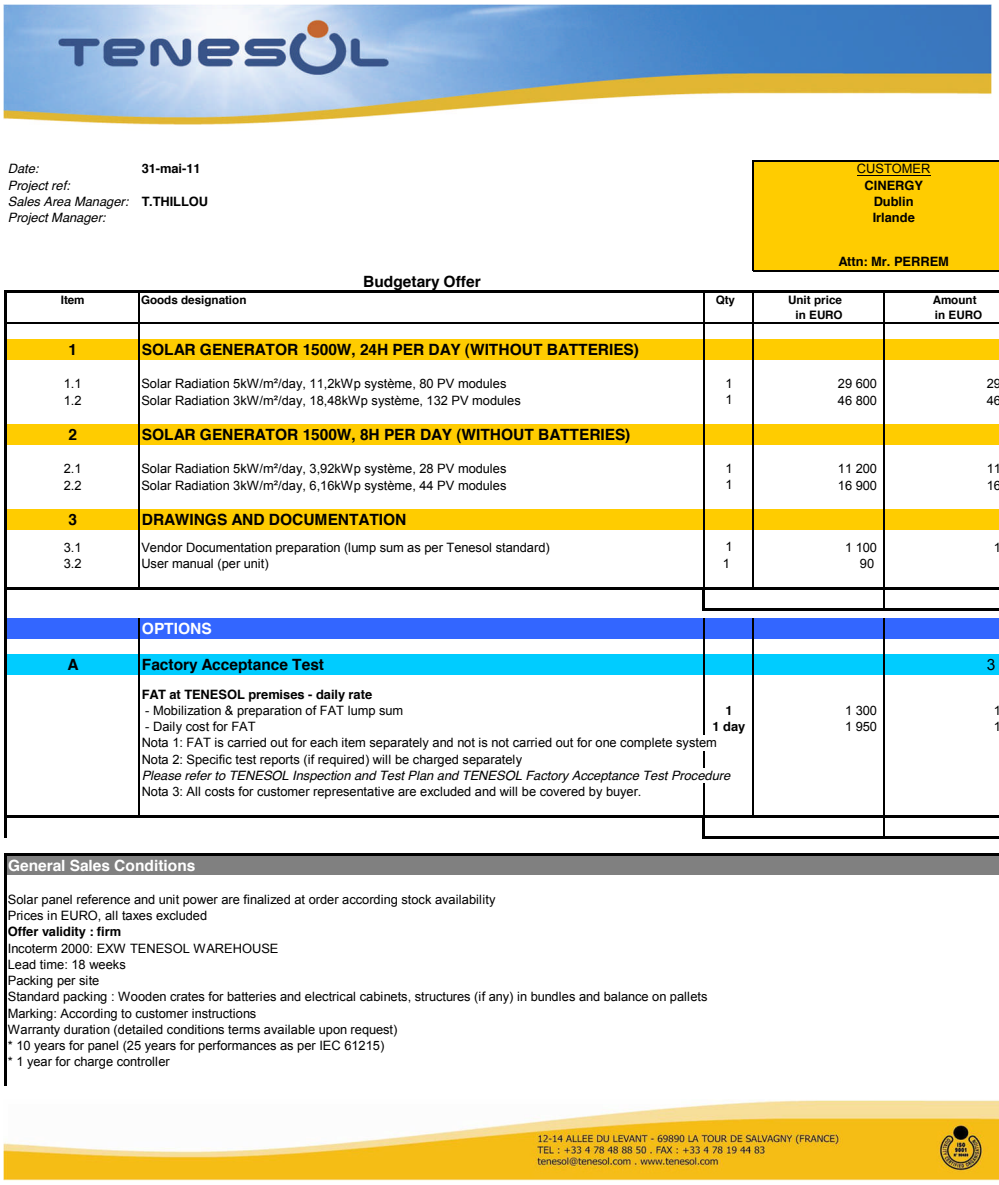

TENESOL

Date: **31-mai-11**
Project ref:
Sales Area Manager: **T.THILLOU**
Project Manager:

CUSTOMER
CINERGY
Dublin
Irlande

Attn: Mr. PERREM

Budgetary Offer

Item	Goods designation	Qty	Unit price in EURO	Amount in EURO
1	**SOLAR GENERATOR 1500W, 24H PER DAY (WITHOUT BATTERIES)**			
1.1	Solar Radiation 5kW/m²/day, 11,2kWp système, 80 PV modules	1	29 600	29 600
1.2	Solar Radiation 3kW/m²/day, 18,48kWp système, 132 PV modules	1	46 800	46 800
2	**SOLAR GENERATOR 1500W, 8H PER DAY (WITHOUT BATTERIES)**			
2.1	Solar Radiation 5kW/m²/day, 3,92kWp système, 28 PV modules	1	11 200	11 200
2.2	Solar Radiation 3kW/m²/day, 6,16kWp système, 44 PV modules	1	16 900	16 900
3	**DRAWINGS AND DOCUMENTATION**			
3.1	Vendor Documentation preparation (lump sum as per Tenesol standard)	1	1 100	1 100
3.2	User manual (per unit)	1	90	90
	OPTIONS			
A	**Factory Acceptance Test**			3 250
	FAT at TENESOL premises - daily rate			
	- Mobilization & preparation of FAT lump sum	**1**	1 300	1 300
	- Daily cost for FAT	**1 day**	1 950	1 950
	Nota 1: FAT is carried out for each item separately and not is not carried out for one complete system			
	Nota 2: Specific test reports (if required) will be charged separately			
	Please refer to TENESOL Inspection and Test Plan and TENESOL Factory Acceptance Test Procedure			
	Nota 3: All costs for customer representative are excluded and will be covered by buyer.			

General Sales Conditions

Solar panel reference and unit power are finalized at order according stock availability
Prices in EURO, all taxes excluded
Offer validity : firm
Incoterm 2000: EXW TENESOL WAREHOUSE
Lead time: 18 weeks
Packing per site
Standard packing : Wooden crates for batteries and electrical cabinets, structures (if any) in bundles and balance on pallets
Marking: According to customer instructions
Warranty duration (detailed conditions terms available upon request)
* 10 years for panel (25 years for performances as per IEC 61215)
* 1 year for charge controller

12-14 ALLEE DU LEVANT - 69890 LA TOUR DE SALVAGNY (FRANCE)
TEL : +33 4 78 48 88 50 . FAX : +33 4 78 19 44 83
tenesol@tenesol.com . www.tenesol.com

Figure A.7: Quotation for multiple types of solar arrays from Telesol

Bibliography

[1] Shenzhen Center Power Tech. Co. Ltd., "Vision Battery Specification CL400 2V 400Ah(10hr)," 2011.

[2] EXIDE GmbH, "Handbook for Gel VRLA Batteries Part 2," 2003.

[3] Exide Gmbh, "Handbook for Stationary Lead-Acid Batteries Part 1," 2011.

[4] S. N. Roy, "Energy logic: A road map to reducing energy consumption in telecom munications networks," *INTELEC 2008 - 2008 IEEE 30th International Telecommunications Energy Conference*, pp. 1–9, Sept. 2008.

[5] Mobile for Development, "Green Power for Mobile Interactive Replication Guide," tech. rep., GSMA, London, July 2011.

[6] M. Šúri, T. A. Huld, E. D. Dunlop, and H. A. Ossenbrink, "Potential of solar electricity generation in the European Union member states and candidate countries," *Solar energy*, vol. 81, no. 10, pp. 1295–1305, 2007.

[7] HK Renewable Energy, "Solar Photovoltaic Technology Outline," 2013.

[8] Mathworks, "Implement generic battery model - Simulink - MathWorks United Kingdom," 2012.

[9] D. Linden and T. Reddy, *Handbook of batteries*. McGraw-Hill, 2002.

[10] S. S. Soman, H. Zareipour, O. Malik, and P. Mandal, "A review of wind power and wind speed forecasting methods with different time horizons," in *North American Power Symposium 2010*, vol. 4, pp. 1–8, IEEE, Sept. 2010.

[11] M. Office, "Met Office: Marine forecasts glossary," 2012.

[12] K. Qian and P. Solanki, "A hybrid power system using wind and diesel generator: A case study at Masirah Island in Oman," *CIRED 2009. 20th International Conference and Exhibition on Electricity Distribution - Part 1*, no. 0586, pp. 8–11, 2009.

[13] M. Ombra, F. Di Noto, J. Jaffrain, S. Lansburg, and J. Brunarie, "Hybrid power systems deliver efficient energy management for off-grid BTS sites," in *Intelec 2012*, (Scottsdale, AZ), pp. 1–7, IEEE, Sept. 2012.

[14] H. Nordin and B. Lindemark, "System reliability, dimensioning and environmental impact of diesel engine generator sets used in telecom applications," in *21st International Telecommunications Energy Conference. INTELEC '99 (Cat. No.99CH37007)*, vol. 8528, p. 377, IEEE, 1999.

[15] L. Mahon, *Diesel generator handbook*. Butterworth-Heinemann, 1992.

[16] R. Edwards, V. MAHIEU, and J. GRIESEMANN, "Well-to-wheels analysis of future automotive fuels and powertrains in the European context," Tech. Rep. March, 2004.

[17] D. Saheb-Koussa, M. Haddadi, and M. Belhamel, "Economic and technical study of a hybrid system (windphotovoltaicdiesel) for rural electrification in Algeria," *Applied Energy*, vol. 86, pp. 1024–1030, July 2009.

[18] P. Nema, S. Rangnekar, and R. K. Nema, "Pre-feasibility study of PV-solar/Wind Hybrid Energy System for GSM type mobile telephony base station in Central India," in *Computer and Automation Engineering (ICCAE), 2010 The 2nd International Conference on*, vol. 5, pp. 152–156, IEEE, IEEE, 2010.

[19] M. Nejad and M. Radzi, "Hybrid renewable energy systems in remote areas of equatorial countries," in *Research and Development (SCOReD)*, pp. 11–16, 2012.

[20] G. Notton, V. Lazarov, Z. Zarkov, and L. Stoyanov, "Optimization of Hybrid Systems with Renewable Energy Sources : Trends for Research," in *2006 First International Symposium on Environment Identities and Mediterranean Area*, pp. 144–149, IEEE, IEEE, July 2006.

[21] J. Li, W. Wei, and J. Xiang, "A Simple Sizing Algorithm for Stand-Alone PV/Wind/Battery Hybrid Microgrids," *Energies*, pp. 5307–5323, 2012.

[22] O. Erdinc and M. Uzunoglu, "A new perspective in optimum sizing of hybrid renewable energy systems: Consideration of component performance degradation issue," *International Journal of Hydrogen Energy*, vol. 16, pp. 1412–1425, Apr. 2012.

[23] J. M. Lujano-Rojas, R. Dufo-López, and J. L. Bernal-Agustín, "Optimal sizing of small wind/battery systems considering the DC bus voltage stability effect on energy capture, wind speed variability, and load uncertainty," *Applied Energy*, vol. 93, pp. 404–412, May 2012.

[24] Y.-K. Wu and J.-S. Hong, "A literature review of wind forecasting technology in the world," in *2007 IEEE Lausanne Power Tech*, pp. 504–509, IEEE, July 2007.

[25] M. Muselli, G. Notton, and A. Louche, "Design of hybrid-photovoltaic power generator, with optimization of energy management," *Solar energy*, vol. 65, no. 3, pp. 143–157, 1999.

[26] J. Kaldellis, "Optimum hybrid photovoltaic-based solution for remote telecommunication stations," *Renewable Energy*, vol. 35, pp. 2307–2315, Oct. 2010.

[27] E. S. Takle and R. H. Shaw, "Complimentary nature of wind and solar energy at a continental mid-latitude station," *International Journal of Energy Research*, vol. 3, no. 2, pp. 103–112, 1979.

[28] S. Panickar, PS and Rahman, S and Islam and Pryor, "Adaptive control strategies in wind-diesel hybrid systems," *Murdoch University Energy Research Institute, Western Australia*, 2000.

[29] C. Kathirvel and K. Porkumaran, "Analysis and design of hybrid wind/diesel system with energy storage for rural application," *IPEC, 2010 Conference*, vol. 2, pp. 250–255, 2010.

[30] E. McKenna and T. L. Olsen, *Performance and Economics of a Wind-*

Diesel Hybrid Energy System: Naval Air Landing Field, San Clemente Island, California. Citeseer, 1999.

[31] Y. Hu and P. Solana, "Optimization of a hybrid diesel-wind generation plant with operational options," *Renewable Energy*, vol. 51, pp. 364–372, Mar. 2013.

[32] H. Sharma, S. Islam, and T. Pryor, "Dynamic Modelling and Simulation of a Hybrid Wind Diesel Remote Area Power System," *International Journal of Renewable Energy Engineering*, vol. 2, no. 1, pp. 123–128, 2000.

[33] R. Dufo-López, J. L. Bernal-Agustin, and J. L. Bernal-Agustín, "Multi-objective design of PV–wind–diesel–hydrogen–battery systems," *Renewable Energy*, vol. 33, pp. 2559–2572, Dec. 2008.

[34] N. a. Ahmed, M. Miyatake, and a. K. Al-Othman, "Power fluctuations suppression of stand-alone hybrid generation combining solar photovoltaic/wind turbine and fuel cell systems," *Energy Conversion and Management*, vol. 49, pp. 2711–2719, Oct. 2008.

[35] M. H. Nehrir, C. Wang, K. Strunz, H. Aki, R. Ramakumar, J. Bing, Z. Miao, and Z. Salameh, "A Review of Hybrid Renewable Alternative Energy Systems for Electric Power Generation," *October*, vol. 2, no. 4, pp. 392–403, 2011.

[36] P. Bajpai and V. Dash, "Hybrid renewable energy systems for power generation in stand-alone applications: A review," *Renewable and Sustainable Energy Reviews*, vol. 16, pp. 2926–2939, June 2012.

[37] L. Zhou, "Progress and problems in hydrogen storage methods," *Renewable and Sustainable Energy Reviews*, vol. 9, pp. 395–408, Aug. 2005.

[38] S. Phelan, P. Meehan, S. Krishnamurthy, and S. Daniels, "Smart energy management for off-grid hybrid sites in telecoms," in *Symposium on ICT and Energy Efficiency and Workshop on Information Theory and Security (CIICT 2012)*, (Stevenage, UK), pp. 15–21, Institution of Engineering and Technology, 2012.

[39] a.S. Ramadhas, S. Jayaraj, and C. Muraleedharan, "Characterization and effect of using rubber seed oil as fuel in the compression ignition engines," *Renewable Energy*, vol. 30, pp. 795–803, Apr. 2005.

[40] R. Malhotra, "Energy management & backup unit for telecom base stations," in *Telecommunications Energy Conference (INTELEC), 32nd International*, pp. 1–5, IEEE, 2010.

[41] J. Stevens and G. Corey, "A study of lead-acid battery efficiency near top-of-charge and the impact on PV system design," *Conference Record of the Twenty Fifth IEEE Photovoltaic Specialists Conference - 1996*, pp. 1485–1488, 1996.

[42] P. Akuon, "Optimized hybrid green power model for remote telecom sites," in *PowerAfrica 2012 Conference and Exposition Johannesburg, South Africa*, no. July, (Johannesburg), pp. 9–13, 2012.

[43] S. Chowdhury and S. Aziz, "Solar-diesel hybrid energy model for Base Transceiver Station (BTS) of mobile phone operators," in *Developments in Renewable Energy Technology (ICDRET)*, pp. 1–6, IEEE, 2012.

[44] C. Vetromile, A. Petraglia, A. D'Onofrio, M. Logorelli, G. Marsico, S. Curcuruto, and C. Lubritto, "New models for BTS energy savings strategies," in *Telecommunications Energy Conference (INTELEC), 32nd International*, pp. 0–3, IEEE, 2010.

[45] J. Dai, D. Das, and M. Pecht, "Risks to telecommunication equipment under free air cooling conditions and their mitigation," *Proceedings of MFPT: The Applied Systems Health Management Conference*, vol. 2020, pp. 1–14, 2011.

[46] J. VanZwol, "Outdoor Enclosures for Wireless Base Stations," 2012.

[47] X. Zhu and M. Genton, "Short-Term Wind Speed Forecasting for Power System Operations," *International Statistical Review*, vol. 80, pp. 2–23, 2012.

[48] A. Fabbri, T. GomezSanRoman, J. RivierAbbad, and V. MendezQuezada, "Assessment of the Cost Associated With

Wind Generation Prediction Errors in a Liberalized Electricity Market," *IEEE Transactions on Power Systems*, vol. 20, pp. 1440–1446, Aug. 2005.

[49] Mobile for Development, "Powering Telecoms : West Africa Market Analysis," tech. rep., GSMA, 2013.

[50] J. Rowley, "Editorial GSMA to step up off-grid green energy network conversions thanks to World Bank support — Public Policy," *GSMA*, 2012.

[51] Energy Agency, *Electricity Information 2012*. Electricity Information, OECD Publishing, July 2012.

[52] Renewables International, "German grid reaches record reliability in 2011 - 100% renewable," 2012.

[53] Los Angeles Times, "India power outage puts superpower dreams in a new light," 2012.

[54] C. Abbey and G. Joós, "A stochastic optimization approach to rating of energy storage systems in wind-diesel isolated grids," *IEEE Transactions on Power Systems*, vol. 24, no. 1, pp. 418–426, 2009.

[55] A. Cao-Paz and J. Marcos-Acevedo, "A multi-point sensor based on optical fiber for the measurement of electrolyte density in lead-acid batteries," *Sensors*, pp. 2587–2608, 2010.

[56] V. Pop, H. J. Bergveld, P. H. L. Notten, and P. P. L. Regtien, "State-of-the-art of battery state-of-charge determination," *Measurement Science and Technology*, vol. 16, pp. R93–R110, Dec. 2005.

[57] K. Zipp, "What Is The Best Battery For Your Solar Power System?," 2013.

[58] Rolls, "Battery User Manual - Flooded & AGM : Technical Support Desk," 2013.

[59] C. Lemoine, "Influence of float and charge voltage adjustment on the service life of AGM VRLA batteries depending on the conditions of use," *Journal of Power Sources*, vol. 144, pp. 322–328, 2005.

[60] A. Gee, F. Robinson, and R. Dunn, "Analysis of Battery Lifetime Extension in a Small-Scale Wind-Energy System Using Supercapacitors," *IEEE*, pp. 1–10, 2013.

[61] G. May, "Standby battery requirements for telecommunications power," *Journal of Power Sources*, vol. 158, pp. 1117–1123, Aug. 2006.

[62] G. Bonduelle and X. Muneret, "VRLA batteries in telecom application: AGM or gel?," *Telecommunications Energy Special Conference, 2000. TELESCON 2000. The Third International*, pp. 75–79, 2000.

[63] Rolls, "State of Charge & Charging - Flooded Lead Acid Batteries : Technical Support Desk," 2013.

[64] J. Brunarie and A. Billard, "Lithium-ion (Li-ion) battery technology evolves to serve an extended range of telecom applications," *... (INTELEC), 2011 IEEE ...*, 2011.

[65] B. Saha and K. Goebel, "Modeling Li-ion battery capacity depletion in a particle filtering framework," *Proceedings of the annual conference of the prognostics and health management society*, pp. 1–10, 2009.

[66] J. Andújar, F. Segura, E. Durán, and L. Rentería, "Optimal interface based on power electronics in distributed generation systems for fuel cells," *Renewable Energy*, vol. 36, pp. 2759–2770, May 2011.

[67] T. Elshatter, M. Eskander, and M. Elhagry, "Energy flow and management of a hybrid wind/PV/fuel cell generation system," *Energy Conversion and Management*, vol. 47, pp. 1264–1280, June 2006.

[68] O. Palizban, "Active and reactive power control for a hybrid system with photovoltaic panel, wind turbine, fuel cells, electrolyzer and super capacitor in off-grid mode," in *Control System, Computing and Engineering (ICCSCE)*, pp. 404–408, IEEE, 2011.

[69] L. Li, S. Kim, W. Wang, M. Vijayakumar, Z. Nie, B. Chen, J. Zhang, G. Xia, J. Hu, G. Graff, J. Liu, and Z. Yang, "A Stable Vanadium Redox-Flow Battery with High Energy Density for Large-Scale Energy Storage," *Advanced Energy Materials*, vol. 1, pp. 394–400, May 2011.

[70] D. Darcy and P. Gibson, "Zinc-Flow batteries for extended duration energy storage at cell towers," *INTELEC 2008 - 2008 IEEE 30th International Telecommunications Energy Conference*, pp. 1–4, Sept. 2008.

[71] Redflow, "Redflow Limited - Energy Storage Solutions," 2013.

[72] C. Nayar, "Control and interfacing of bi-directional inverters for off-grid and weak grid photovoltaic power systems," in *Power Engineering Society Summer Meeting, 2000. IEEE*, vol. 2, pp. 1280–1282, IEEE, 2000.

[73] E. Networks, "Connect a Micro-Generator : ESB Networks," Jan. 2007.

[74] L. Chiaraviglio, M. Mellia, and F. Neri, "Energy-Aware Backbone Networks: A Case Study," in *2009 IEEE International Conference on Communications Workshops*, pp. 1–5, IEEE, June 2009.

[75] Z. Li, F. Boyle, and A. Reynolds, "Domestic application of micro wind turbines in Ireland: Investigation of their economic viability," *Renewable Energy*, vol. 41, pp. 64–74, May 2012.

[76] T. Burton, N. Jenkins, D. Sharpe, and E. Bossanyi, *Wind Energy Handbook*. John Wiley & Sons, 2011.

[77] W. D. Lubitz, "Accuracy of vertically extrapolating meteorological tower wind speed measurements," in *Canadian Wind Energy Association Annual Conference Winnipeg, MB, Canada*, no. 519, 2006.

[78] G. Gualtieri and S. Secci, "Wind shear coefficients, roughness length and energy yield over coastal locations in Southern Italy," *Renewable Energy*, vol. 36, pp. 1081–1094, Mar. 2011.

[79] Met Éireann, "Met Éireann - Climate Data & Products," 2013.

[80] SEAI, "SEAI Wind Atlas Mapping," 2014.

[81] J. Manwell, J. McGowan, and A. Rogers, "Wind Energy Explained," *John Wiley&Sons Ltd, UK*, p. 577, Apr. 2002.

[82] N. Boccard, "Capacity factor of wind power realized values vs. estimates," *Energy Policy*, vol. 37, pp. 2679–2688, July 2009.

[83] M. Green and K. Emery, "Solar cell efficiency tables (version 39)," *Progress in ...*, no. version 39, pp. 12–20, 2012.

[84] A. Skoczek, T. Sample, and E. Dunlop, "The results of performance measurements of fieldaged crystalline silicon photovoltaic modules," *Progress in Photovoltaics: Research and Applications*, no. December 2008, pp. 227–240, 2009.

[85] A. Barhdadi and M. Bennis, "PVGIS approach for assessing the performances of the first PV grid-connected power plant in Morocco," *arXiv preprint arXiv:1208.4325*, pp. 337–344, 2012.

[86] Advantech, "UNO-2173A - Industrial PC," 2013.

[87] Labjack, "U6 Data Acquisition Device," 2013.

[88] Netbiter, "M2M Remote Monitoring Solutions," 2013.

[89] I. D. A. Modbus, "Modbus application protocol specification v1. 1a," *North Grafton, Massachusetts (www. modbus. org/specs. php)*, 2004.

[90] Libelium, "Waspmote - Wireless Sensor Networks 802.15.4 ZigBee Mote - Open Source Sensor Device — Libelium."

[91] J. Yang, S. Phelan, P. Meehan, and S. Daniels, "A distributed real time sensor network for enhancing energy efficiency through ICT," in *Symposium on ICT and Energy Efficiency and Workshop on Information Theory and Security (CIICT 2012)*, (Stevenage, UK), pp. 8–14, Institution of Engineering and Technology, 2012.

[92] N. J. Williams, E. E. V. Dyk, and F. J. Vorster, "Monitoring Solar Home Systems With Pulse Width Modulation Charge Control," *Journal of Solar Energy Engineering*, vol. 133, no. May, 2011.

[93] National Semiconductor, "LM35 Precision Centigrade Temperature Sensors Datasheet," 2000.

[94] LOGIC ENERGY, "LOGIC ENERGY :: Live Remote Monitoring & Data Loggers."

[95] SparkFun Electronics, "Barometric Pressure Sensor - BMP085 Breakout - SparkFun Electronics."

[96] Diesel Service and Supply., "Factors Affecting Power Generator Output Rating — Diesel Service."

[97] R. B. Stull and C. D. Ahrens, *Meteorology for scientists and engineers*. Earth Science Series, Brooks/Cole, 2000.

[98] J. P. Kossin and W. H. Schubert, "Mesovortices, Polygonal Flow Patterns, and Rapid Pressure Falls in Hurricane-Like Vortices," *Journal of the Atmospheric Sciences*, vol. 58, pp. 2196–2209, Aug. 2001.

[99] Wetterzentrale, "Wetterzentrale," 2013.

[100] D. Wheeler and C. Wilkinson, "From calm to storm: the origins of the Beaufort wind scale," *The Mariner's Mirror*, vol. 90, no. June 2013, pp. 37–41, 2004.

[101] A. M. Foley, P. G. Leahy, A. Marvuglia, and E. J. McKeogh, "Current methods and advances in forecasting of wind power generation," *Renewable Energy*, vol. 37, pp. 1–8, Jan. 2012.

[102] M. Black and G. Strbac, "Value of bulk energy storage for managing wind power fluctuations," *Energy conversion, ieee transactions on*, vol. 22, no. 1, pp. 197–205, 2007.

[103] C. W. Potter and M. Negnevitsky, "Very short-term wind forecasting for Tasmanian power generation," *Power Systems, IEEE Transactions on*, vol. 21, no. 2, pp. 965–972, 2006.

[104] T. Tanabe, T. Sato, R. Tanikawa, I. Aoki, T. Funabashi, and R. Yokoyama, "Generation Scheduling for wind power generation by storage battery system and meteorological forecast," in *Power and Energy Society General Meeting-Conversion and Delivery of Electrical Energy in the 21st Century*, pp. 1–7, IEEE, IEEE, July 2008.

[105] F. Cassola and M. Burlando, "Wind speed and wind energy forecast through Kalman filtering of Numerical Weather Prediction model output," *Applied Energy*, vol. 99, pp. 154–166, Nov. 2012.

[106] I. Colak, S. Sagiroglu, and M. Yesilbudak, "Data mining and wind power prediction: A literature review," *Renewable Energy*, vol. 46, pp. 241–247, Oct. 2012.

[107] C. Pérez-Llera, "Local short-term prediction of wind speed: a neural network analysis," *Proceedings of the iEMSs*, vol. 2, pp. 124–129, 2002.

[108] M. Monfared, H. Rastegar, and H. M. Kojabadi, "A new strategy for wind speed forecasting using artificial intelligent methods," *Renewable Energy*, vol. 34, pp. 845–848, Mar. 2009.

[109] J. Shi, J. Guo, and S. Zheng, "Evaluation of hybrid forecasting approaches for wind speed and power generation time series," *Renewable and Sustainable Energy Reviews*, vol. 16, pp. 3471–3480, June 2012.

[110] I. Damousis, M. Alexiadis, J. Theocharis, and P. Dokopoulos, "A Fuzzy Model for Wind Speed Prediction and Power Generation in Wind Parks Using Spatial Correlation," *IEEE Transactions on Energy Conversion*, vol. 19, pp. 352–361, June 2004.

[111] a. Tascikaraoglu, M. Uzunoglu, and B. Vural, "The assessment of the contribution of short-term wind power predictions to the efficiency of stand-alone hybrid systems," *Applied Energy*, vol. 94, pp. 156–165, June 2012.

[112] F. O. Hocaolu, O. N. Gerek, and M. Kurban, "A novel wind speed modeling approach using atmospheric pressure observations and hidden Markov models," *Journal of Wind Engineering and Industrial Aerodynamics*, vol. 98, pp. 472–481, Aug. 2010.

[113] H. Mori and Y. Umezawa, "Application of NBTree to selection of meteorological variables in wind speed prediction," in *2009 Transmission & Distribution Conference & Exposition: Asia and Pacific*, no. 2, pp. 1–4, IEEE, Oct. 2009.

[114] N.-K. K. C. Nair and N. Garimella, "Battery energy storage systems: Assessment for small-scale renewable energy integration," *Energy and Buildings*, vol. 42, pp. 2124–2130, Nov. 2010.

[115] P. Lilienthal, L. Flowers, and C. Rossmann, "HOMER: The hybrid optimization model for electric renewables," *Vol. Windpower'95-Proceedings AWEA*, pp. 475–480, 1995.

[116] M. Khan and M. Iqbal, "Pre-feasibility study of stand-alone hybrid energy systems for applications in Newfoundland," *Renewable Energy*, vol. 30, pp. 835–854, May 2005.

[117] D. Nelson, M. Nehrir, and C. Wang, "Unit sizing and cost analysis of stand-alone hybrid wind/PV/fuel cell power generation systems," *Renewable Energy*, vol. 31, pp. 1641–1656, Aug. 2006.

[118] GSMA, "HOMER Software: Training Guide for Renewable Energy Base Station Design — Mobile for Development," 2010.

[119] K. Kusakana and H. J. Vermaak, "Hybrid renewable power systems for mobile telephony base stations in developing countries," *Renewable Energy*, vol. 51, pp. 419–425, Mar. 2013.

[120] L. Tay and W. Keerthipala, "Performance analysis of a wind/diesel/battery hybrid power system," *Universities Power*, 2001.

[121] R. Sebastián and R. P. n. Alzola, "Effective active power control of a high penetration wind diesel system with a NiCd battery energy storage," *Renewable Energy*, vol. 35, pp. 952–965, May 2010.

[122] R. Sebastián and R. P. n. Alzola, "Simulation of an isolated Wind Diesel System with battery energy storage," *Electric Power Systems Research*, vol. 81, pp. 677–686, Feb. 2011.

[123] A. Agrawal, R. Wies, and R. Johnson, "Development of a Simulink Model to Study the Sensitivity Analysis of Fuel Cost on Wind with Diesel-Battery Hybrid Power Systems for Remote Locations," *aseanenergy.info*, 2011.

[124] a. Yasin, G. Napoli, M. Ferraro, A. Testa, and V. Antonucci, "Fuzzy logic based management of a stand-alone hybrid generator," *2011 Inter-*

national Conference on Clean Electrical Power (ICCEP), pp. 690–696, June 2011.

[125] M. Deshmukh and S. Deshmukh, "Modeling of hybrid renewable energy systems," *Renewable and Sustainable Energy Reviews*, vol. 12, pp. 235–249, Jan. 2008.

[126] T. Chan, "Transient analysis of integrated solar/diesel hybrid power system using MATLAB Simulink," Tech. Rep. 4, Victoria University, 2010.

[127] M. Muselli, G. Notton, P. Poggi, and A. Louche, "PV-hybrid power systems sizing incorporating battery storage : an analysis via simulation calculations," *Renewable Energy*, vol. 20, pp. 1–7, 2000.

[128] B. Panahandeh, J. Bard, A. Outzourhit, and D. Zejli, "Simulation of PVWind-hybrid systems combined with hydrogen storage for rural electrification," *International Journal of Hydrogen Energy*, vol. 36, pp. 4185–4197, Mar. 2011.

[129] F. Ltd and Fortis, "Montana Wind Turbine," Oct. 2012.

[130] HOMER Energy, "10336 - Modeling a variable speed generator in HOMER - Powered by Kayako Resolve Help Desk Software," 2010.

[131] J. Brunarie, "Fuel savings make a powerful case for hybrid diesel generator systems," 2011.

[132] A. Mellit and M. Benghanem, "Modelling of sizing the photovoltaic system parameters using artificial neural network," *Proceedings of 2003 IEEE Conference on Control Applications, 2003. CCA 2003.*, vol. 1, pp. 353–357, 2003.

[133] M. Egido and E. Lorenzo, "The sizing of stand alone PV-system: a review and a proposed new method," *Solar Energy Materials and Solar Cells*, vol. 26, pp. 51–69, 1992.

[134] a. Mellit, M. Benghanem, and S. Kalogirou, "An adaptive wavelet-network model for forecasting daily total solar-radiation," *Applied Energy*, vol. 83, pp. 705–722, July 2006.

[135] H. Diagne, M. David, P. Lauret, and J. Boland, "SOLAR IRRADIATION FORECASTING: STATE-OF-THE-ART AND PROPOSITION FOR FUTURE DEVELOPMENTS FOR SMALL-SCALE INSULAR GRIDS."

[136] J. Hill, "California Grid Hit Record Solar Peak," *Clean Technica*, 2012.